

Status of Thesis

Title of thesis

Sintered Bonding of the M3/II High Speed Steel and Cast Iron

I

WAN NURSHEILA WAN JUSOH

hereby allow my thesis to be placed at the Information Resource Center (IRC) of Universiti Teknologi PETRONAS (UTP) with the following conditions:

1. The thesis becomes the property of UTP
2. The IRC of UTP may make copies of the thesis for academic purposes only
3. This thesis is classified as

Confidential

Non-confidential

If this thesis is confidential, please state the reason:

The contents of the thesis will remain confidential for _____ years.

Remarks on disclosure:



Signature of Author



Signature of Supervisor

Permanent Address:

No.9, Jalan Bukit Jati 5c,
41000 Klang,
Selangor.

Name of Supervisor:

Dr. Othman Mamat

Date : 14 / 7 / 05

Date : 14 / 7 / 05

UNIVERSITI TEKNOLOGI PETRONAS

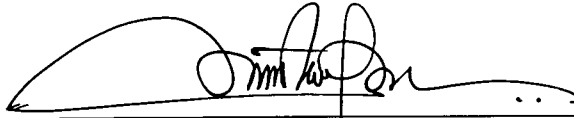
Approval by Supervisor

The undersigned certify that they have read, and recommend to The Postgraduate Studies Programme for acceptance, a thesis entitled "**Sintered Bonding of the M3/II High Speed Steel and Cast Iron**" submitted by (**Wan Nursheila Wan Jusoh**) for the fulfillment of the requirements for the degree of (Master of Science in Mechanical Engineering).

14/07/2005

Date

Signature :



Supervisor :

DR. OTHMAN MANAT.

Date :

14/07/05

UNIVERSITI TEKNOLOGI PETRONAS

Sintered Bonding of the M3/II High Speed Steel and Cast Iron

By

Wan Nursheila Wan Jusoh

A THESIS

SUBMITTED TO THE POSTGRADUATE STUDIES PROGRAMME

AS A REQUIREMENT FOR THE

DEGREE OF MASTER OF SCIENCE

MECHANICAL ENGINEERING

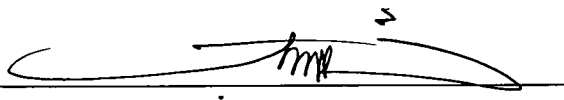
BANDAR SERI ISKANDAR,

PERAK,

July, 2005

Declaration

I hereby declare that the thesis is based on my original work except for quotations and citations which have been duly acknowledged. I also declare that it has not been previously or concurrently submitted for any other degree at UTP or other institutions.

Signature : 
Name : Wan Nurshella Wan Jusoh
Date : 14 / 7 / 05

Abstract

Powder metallurgy components are increasingly attractive in replacing cast materials for various applications. This occasionally requires the powder metallurgy parts to be joined to another material as integrated components. In this experimental work, the objective is to develop the powder metallurgy sintered bonding mechanism between premixed M3/II High Speed Steel powder(M3/II HSS) acting as cam lobe and the solid cast iron (as a shaft) which was formerly used for Proton Saga's 1.3 car camshaft. The base powder was characterized using Particle Size Analyzer in order to determine particle dimensions, X-ray Florescence (XRF) for elements composition, Scanning Electron Microscope (SEM) to observe the particles shape, X-ray Diffraction (XRD) for phase constitution existed in the powder, Differential Thermal Analysis (DTA) to determine the transformation temperatures experienced by the powder during the sintering process. Meanwhile the cast iron was analyzed using the Optical Microscope (OM) to observe the microstructure and SEM with Energy Dispersive X-ray attachment for the chemical composition. The powder was divided into 3 groups consisting of base M3/II HSS powder, M3/II HSS with addition of 5, 7, 8, 9, 10, 15wt.% copper and M3/II HSS with addition of 9wt.% copper and 1wt.% phosphorus addition. The elemental copper and phosphorus powders were added to the base powder to enhance the bonding mechanism. Prior to sintering, the powder was compacted at 350MPa and produced a green density of 5.0gcm^{-3} . The compacts were sintered at various temperatures of 800, 900, 1000 and 1100°C for 30 minutes in argon gas atmosphere. Metallographic analysis of the samples was examined using OM and SEM simultaneously. Results showed that the liquid phase had promoted the pore elimination, growth in the grain size and hardening the matrix. The decreasing of pores amount thereby increased the density up to 6.2gcm^{-3} with the maximum hardness of 619Hv. The presence of complex carbides such as MC and M_6C were detected on the sintered powder microstructures. Formation of expected migration layer caused by the liquid phase between the powder mixture and the cast iron was not found. It is due to the presence of chemically stable and physically tenacious oxide layer on the cast iron surface due to the chemical composition that impedes the liquid phase to produce an intimate contact with the cast iron even though polishing was done earlier on the cast iron.

Abstrak

Komponen metalurgi serbuk semakin menarik perhatian dalam menggantikan berbagai aplikasi besi tuangan. Dalam sesetengah situasi, ia memerlukan komponen metalurgi serbuk ini disambung ke bahan besi tuangan sebagai bahan integrasi. Objektif kajian ini adalah untuk menghasilkan 'sintered bonding' antara serbuk M3/II 'High Speed Steel'(M3/II HSS) bertindak sebagai 'cam lobe' dan besi tuangan daripada 'camshaft' kereta Proton Saga 1.3 (bertindak sebagai 'shaft'). Serbuk asas diperincikan kepada menggunakan Analisa Saiz Partikel untuk memperolehi saiz partikel serbuk, Mikroskop Imbansan Elektron (SEM) untuk memerhatikan bentuk-bentuk partikel, komposisi elemen di dalam serbuk dianalisa menggunakan kaedah Floresen X-ray (XRF), Pembelauan X-Ray (XRD) untuk mengetahui fasa yang wujud dalam serbuk asas dan suhu peralihan yang dialami oleh serbuk asas semasa proses penyinteran dikaji melalui Analisis Kebezaan Terma (DTA). Manakala besi tuangan dianalisa menggunakan Mikroskop Optik (OM) untuk pencerapan microstruktur dan SEM untuk mengetahui komposisi kimianya. Serbuk dibahagikan kepada 3 kumpulan yang terdiri daripada serbuk asas M3/II HSS, serbuk asas dengan penambahan 5, 6, 7, 8, 9, 10, 15wt.%serbuk kuprum dan serbuk asas dengan penambahan serbuk 9wt.%kuprum dan 1wt.% fosforus. Penambahan serbuk kuprum dan fosforus adalah untuk menggalakkan mekanisme 'sintered bonding'. Sebelum proses penyinteran, serbuk-serbuk ini dipadatkan pada tekanan 350MPa yang menghasilkan purata ketumpatan hijau sebanyak 5.0gsm^{-3} . Padatan hijau ini disinter dalam atmosfera gas argon selama 30 minit pada suhu 800, 900, 1000 dan 1100°C . Pemerhatian metalurgi ke atas sampel dilakukan menggunakan OM dan SEM. Kekerasan sampel pula diuji dengan penguji kekerasan Vickers. Keputusan menunjukkan fasa cecair daripada padatan serbuk telah mengurangkan kehadiran liang-liang udara, meningkatkan saiz butiran dan menguatkan matriks. Pengurangan liang-liang udara ini secara tidak langsung meningkatkan ketumpatan dan kekerasan hingga ke 6.2gsm^{-3} dan 619Hv. Microstruktur sampel menunjukkan kehadiran karbon kompleks seperti MC dan M_6C . Pembentukan lapisan migrasi anatara padatan serbuk dengan besi tuangan, hasil daripada fasa cecair tidak diperolehi. Ini disebabkan oleh kehadiran lapisan oksida yang stabil secara kimia dan fizikal dipermukaan besi tuangan kesan daripada komposisi kimianya yang menghalang lekatan fasa cecair walaupun permukaannya telah digilap.

Acknowledgements

I would like to take this opportunity to acknowledge a number of people who have been immensely helpful in making this thesis possible throughout the research conducted.

My highest gratitude to my supervisor Dr. Othman Mamat, who has always been there not only giving the assistance and guidance but also sharing his invaluable knowledge and experience in order to accomplish a better research work.

A special thanks to Dr. Patti Hussain from AMREC SIRIM for his willingness to be my external examiner and sharing his expertise in powder metallurgy. My sincerest gratitude to Dr. Faiz Ahmad, who is also my internal examiner for his constructive advice and ideas throughout the research.

My deepest appreciation to Mr. Imtias Amir Bahauddin, Mr. Muhd Anuar Muin and Mr. Shairul for their help and exceptional cooperation during the laboratory works together with the other Mechanical Department staffs headed by Assoc. Prof. Dr. Fakhruddin Hashim.

I am especially indebted to the postgraduate's office, for allowing me to undergo this postgraduate studies. Particular thanks to Assoc. Prof. Ir. Dr. Fadzil Nuruddin, Mrs. Haslina, Mrs. Norma, Mr. Fadil and Mrs. Shariza for their help in making this Master degree successful.

My warmest appreciation goes as well to my family Mama, Papa, Kakak, Abe, Jihan, Jimmy, Danny and Aisya for their assistance and unwavering loving support which always be the strength in my life. I am especially grateful to have a very supportive fellow postgraduate colleagues especially Kak Aniza, Fazira, Zaza and Kak Irma who always been the helping hands and enriched this project in many ways.

Not forgotten to my housemates Jihan, Arfah, Arieya, Adzni, Ekma, Fara, Widya, Asnur, Shidah, Ipah and Hana thanks for a wonderful friendship that we shared and accomplished together which I would cherish through out my life.

Finally, I owe a debt of gratitude to all those who helped me in one way or another in accomplishing this research. I am grateful to all who have assisted for their attention, constructive comments and suggestions in order to make this research successful.

Dedication

To My Mum and Dad

Table of Contents

Approval Page	ii
Title Page	iii
Declaration	iv
Abstract	v
Abstrak	vi
Acknowledgements	vii
Dedication	ix
Table of Contents	x
List of Tables	xiv
List of Figures	xv
CHAPTER ONE: INTRODUCTION	1
1.1 Sintered Bonding	1
1.2 Scope of Study and Objectives	3
1.3 Thesis Overview	5
CHAPTER TWO: LITERATURE REVIEW	6
2.1 Joining Techniques	6
2.1.1 Sintered Bonding	7
2.1.1.1 Solid State Sintered Bonding	8
2.1.1.2 Liquid State Sintered Bonding	9
2.1.2 Brazing	10
2.1.3 Fusion	10
2.2 Powder Metallurgy	11
2.2.1 Reason for Using Powder Metallurgy	12
2.2.2 Powder Metallurgy Applications	14
2.2.3 Metal Powder Production (Atomization)	14
2.2.3.1 Gas Atomization	15
2.2.3.2 Water Atomization	15
2.2.3.3 Centrifugal Atomization	16
2.3 Powder Characterization	17
2.3.1 Particle Size	17
2.3.2 Particle Shape	18
2.3.3 Particle Packing	19
2.4 Mechanical Alloying	21

2.5	Compaction	23
2.5.1	Particle Deformation	24
2.5.2	Compaction Technology	26
2.5.2.1	Warm Compaction	26
2.5.2.2	Powder Injection Moulding	26
2.6	Sintering	27
2.6.1	Basic Concepts of Sintering	27
2.6.2	Transport Mechanism	29
2.6.3	Pore Structure and Densification	30
2.6.4	Liquid Phase Sintering	32
2.6.4.1	Classic Sequence of Stages	34
2.6.5	Sintering Atmosphere	35
2.6.5.1	Hydrogen	36
2.6.5.2	Nitrogen	36
2.7	Iron and Steel Powders	36
2.7.1	High Speed Steel	37
2.7.2	High Speed Steel Alloying Elements	39
2.7.2.1	Molybdenum	40
2.7.2.2	Tungsten	40
2.7.2.3	Vanadium	41
2.7.2.4	Chromium	42
2.7.2.5	Carbon	42
2.7.2.6	Copper Addition	43
2.7.2.7	Phosphorus Addition	45
2.7.3	Complex Carbides	46
2.8	Camshaft	51
2.9	Summary of Literature Reviews	54
CHAPTER THREE: METHODOLOGY		55
3.1	Material	55
3.2	Material Characterization	55
3.2.1	Powder Particle Shape	56
3.2.2	Powder Particle Size	57
3.2.3	Composition	58
3.2.4	Phase Constitution	59
3.2.5	Thermal Analysis	60
3.3	Sample Preparation	60
3.3.1	Powder Sample	62
3.3.1.1	Weighing and Mixing	62
3.3.1.2	Compaction	63

3.3.1.3	Sintering	64
3.3.1.4	Sintered Density	65
3.3.1.5	Grinding and Polishing	65
3.3.1.6	Metallographic Examination	66
3.3.1.7	Microhardness	67
3.3.2	Cast Iron Sample	68
3.3.2.1	Machining	68
3.3.2.2	Polishing	68
3.3.2.3	Composition	68
3.3.2.4	Surface Roughness	69
3.2	Sintered Bonding	69
CHAPTER FOUR: RESULTS AND DISCUSSION		70
4.1	Powder Characterization	70
4.1.1	Powder Particle Shape	70
4.1.2	Powder Particle Size	72
4.1.3	Composition	73
4.1.4	Phase Constitution	74
4.1.5	Thermal Analysis	74
4.2	Sintering Evaluation	76
4.2.1	Sintered Density	77
4.2.1.1	M3/II HSS Base Powder	77
4.2.1.2	M3/II HSS with Cu Addition	78
4.2.1.3	M3/II HSS with 9wt.%Cu and 1wt.%P	79
4.2.2	Microhardness of Sintered Sample	80
4.2.2.1	M3/II HSS Base Powder	80
4.2.2.2	M3/II HSS Cu Addition	82
4.2.2.3	M3/II HSS with 9wt.%Cu and 1wt.%P	83
4.2.3	Microstructure Development of Sintered Powder	85
4.2.3.1	M3/II HSS Base Powder	85
4.2.3.2	M3/II HSS with Cu Addition	86
4.2.3.3	M3/II HSS with 9wt.%Cu and 1wt.%P	88
4.2.4	Scanning Electron Microscope Analysis	89

4.3	Cast Iron Characterization	94
4.3.1	Composition	94
4.3.2	Metallographic Examination	95
4.3.3	Surface Roughness	96
4.4	Sintered Bonding	97
	CHAPTER FIVE: CONCLUSION AND RECOMMENDATION	99
5.1	Conclusion	99
5.2	Recommendation	101
	REFERENCES	103
	PUBLICATION	107
	APPENDIX A: Pellet Preparation	
	APPENDIX B: Compaction Pressure Calculations	
	APPENDIX C: Particle Size Analysis Result	
	APPENDIX D: Certificate of Analysis (1) Copper (2) Phosphorus	
	APPENDIX E: X-RAY Florescence Result	
	APPENDIX F: X-Ray Diffraction Pattern	
	APPENDIX G: M2 High Speed Steel Phase Diagram	
	APPENDIX H: Sintered Density Calculations	
	APPENDIX I : Sintered Hardness Calculations	
	APPENDIX J : Fe-P and Cu-P Phase Diagram	
	APPENDIX K: Surface Roughness Result (1) Before Polishing Process (2) After Polishing Process	

List of Tables

2.1	Comparison of PM and competitive metalworking techniques	13
2.2	Complex carbides description	50
3.1	Details on the material background	55
4.1	Particle mesh size analysis for Cu	73
4.2	M3/II HSS composition from XRF analysis	73
4.3	Possible phases for DTA peaks	75
4.4	EDX composition of sintered M3/II HSS-9wt.%Cu-1wt.%P	93
4.5	CI elements composition	94

List of Figures

2.1	Mechanism of diffusion bonding	8
2.2	A sketch of four possible particle generation mechanisms associated with water atomization; cratering, splashing, stripping and bursting	16
2.3	A sketch of a liquid breakup and formation in spherical particles of a rotating electrode	17
2.4	An illustration of difficulty in measuring particles size. The number of possible increases as the particle shape becomes more complex	18
2.5	A schematic of homogeneity associated with stratified mixture and agglomerated mixture and a homogenous dispersed mixture	21
2.6	Data for the die compaction of a spherical bronze powder	24
2.7	A simplified view of the stages of metal powder compaction	25
2.8	The two sphere sintering model with the development of the interparticle bond during sintering, starting with a point contact	28
2.9	A schematic diagram of pore changes during sintering	31
2.10	Two possible grain boundary pores configuration during sintering(German, 1994)	32
2.11	Phase diagram for M2 type HSS	46
2.12	Camshaft	51
2.13	Cam and follower	52
3.1	Material characterization Flow	56
3.2	SEM and EDX	57
3.3	XRF Machine	58
3.4	XRD Machine	59

3.5	Process flow for powder sample preparation and evaluation	61
3.6	Weighing Machine	62
3.7	Ball Milling Machine	63
3.8	Auto Presser	63
3.9	Lynx Gas Furnace	64
3.10	Grinder and Polisher	65
3.11	Optical Microscope	66
3.12	Vickers Microhardness Machine	67
3.13	Abrasive Cutter	68
3.14	Surface Roughness profiler	69
4.1	Scanning Electron Micrograph of (a) M3/II HSS particle (1.04kX) (b) Copper particle (1.08kX) (c) Phosphorus particle (1.3kX) (d) M3/II HSS loose powder (300X) (e) Mixture of M3/II HSS with 9wt.%Cu and 1wt.%P(500X)	71
4.2	Particle Size distribution of M3/II HSS powder	72
4.3	DTA peaks of M3/II HSS base powder	75
4.4	TGA curve of M3/II HSS base powder	76
4.5	Sintered compacts in different atmosphere at 1100°C (a) Argon Gas (b) Furnace atmosphere	76
4.6	Densification of sintered M3/II HSS base powder	77
4.7	Densification of sintered M3/II HSS with Cu addition	78
4.8	Optical Micrograph of M3/II HSS with 9wt.%Cu.(Magnification 200X)	79

4.9	Densification of sintered M3/II HSS with 9wt.%Cu and 1wt.%P	80
4.10	Hardness Vickers of sintered M3/II HSS base powder	81
4.11	Scanning Electron Micrograph of sintered M3/II HSS surface.(Magnification 250X)	82
4.12	Hardness Vickers of M3/II HSS with Cu addition	82
4.13	Hardness Vickers of M3/II HSS with 9wt.%Cu and 1wt.%P	84
4.14	Optical Micrograph of Cu liquid phase at the grain boundaries.(Magnification 200X)	84
4.15	Optical Micrograph of sintered M3/II HSS base powder.(Magnification 200X)	86
4.16	Optical Micrograph of M3/II HSS addition of Cu in different composition.(Magnification 200X)	88
4.17	Optical Micrograph of sintered M3/II HSS with 9wt.%Cu and 1wt.%P. (Magnification 200X)	89
4.18	Scanning Electron Micrograph of M3/II-9wt.%-1wt.%Cu.(Magnification 1.3kX)	91
4.19	Back Scattered Micrograph of M3/II HSS with 9wt.%Cu and 1 wt.%P at 1100°C. (Magnification 350X)	93
4.20	Optical Micrograph of CI. (Magnification 200X)	96
4.21	Scanning Electron Micrograph of Sintered Bonding Attempt. (Magnification 350X)	98

CHAPTER ONE

INTRODUCTION

1.1 Sintered Bonding

Advances in material and manufacturing processes make powder metallurgy components increasingly attractive in replacing wrought or cast materials for various applications. This occasionally requires that powder metallurgy part to be joined to one another or with other materials as integrated components.

Bonding or welding of two materials will causes changes or deterioration of the microstructural and mechanical properties of the original materials in the joining region. Joining of two different materials leads to a much more complicated situation where each materiel's properties should be taken into account before the joining process can be done.

Variants of the bonding technique available, offering scope for joining many new materials and configuration such as laser welding, sintered bonding, brazing, electron beam welding and gas tungsten arc welding.

Cam and Kocak (1998) reported, among the various techniques available to join metal to metal as well as metal to ceramic especially in powder metallurgy, sintered bonding method seems to be the most promising. It is possible to join a wide range of materials in both like and dissimilar combination.

In addition, sintered bonding avoids undesirable structural transformations and the bonding strength is expected to be higher than that obtained with brazing or mechanical joining. Furthermore, for certain high-temperature applications, sintered bonding joining is the only technique which is suitable. These prime advantages have led to extensive use of this method in a wide range of industries extending from electronics, automotive, nuclear and also aerospace components.

Parmiagiani and Kosco (1999) defined sintered bonding or diffusion bonding as a solid state joining process involves introducing liquid phase with a melting temperature lower than the base material to be joined. This technique typically involves the use of materials that exhibit different expansion characteristic, due to either the admixed composition or density level of the green compacts as the components are sintered. Usually, the outer parts (ring) tend to shrink from the die sizes while the inner parts exhibit growth.

The subsequent bond results from the mechanical interlocking and potential alloy diffusion of the liquid phase. Similar results can be achieved if two parts placed in intimate contact allowing the liquid phase to infiltrate to the interface between the parts.

Although sintered bonding is a well established process for metal-metal joining, however little comprehensive information available on the joining powder metallurgy parts to the cast iron. Replacing the cast iron with the powder metal will lead to weight reduction than the conventional cast iron parts of the same geometry. Reduction of the weight is important especially in engines and transmission component as it increased the efficiency and lowering fuel consumption.

In previous development, Hitachi Powdered Metals (HPM) have used the sinter bonding techniques in their sintered rotors for Honda Civic Hybrid electric engine automobiles to join ring shaped and cylindrical green parts to each other. The powder metallurgy sinter bonded rotor core developed by Honda for the brushless electric motor of the new powertrain contribute to help cleaner environment by using only half the fuel required by its conventional petrol-engine predecessor (Capus,2003).

Leither (1990) reported manufacturers such as Nippon Piston Ring Ltd. from Japan has applied the sintered bonding technique in their valve train parts design with their new assembled camshaft (low alloy PM cams).

The new assembled camshaft (PM cams) will have a 30% to 40% weight saving over conventionally made chilled cast iron camshafts. The parts also have better tolerances, surface finished and most important it permits utilization of some material composition that cannot normally be processed by casting, forging or machining (Metal Powder Report,1983).

1.2 Scope of Study and Objectives

In the current casting technique, cam and camshaft conventionally manufactured as a whole as a unit particularly from grey cast iron or chilled cast iron. A major problem in casting technique is high porosity and inclusion level. Cast parts generally have rough surface and the material strength is inherently poor with high rejection rate and needs to rework or secondary process.

The assembled (cam lobe from powder metals) camshaft in other hand has created a revolution in valve parts design, which not only help to cut total engine weight, but also increase the efficiency. Cams that are manufacture by powder metallurgy (PM) marked advantages because of the reduction in accelerated masses, increase the torque and enable changes the cam lobe position for different profile and purposes. Cams which essentially PM iron compacts are slotted on to a steel shaft using bonding techniques such as sintered bonding that involved liquid phase sintering.

This research is based on producing PM cam lobe for the camshaft, which focuses on the M3/II High Speed Steel powder and cast iron materials properties and sintered bonding involved in PM.

The main objective of this research work is to develop sintered bonding mechanism between M3/II powder (acting as cam lobe) and the cast iron as the shaft. However, due to time constraints, only laboratory sample will be produced throughout this research.

The first part of this study focused on characterizing the available M3/II HSS (base material) properties such as the particle size, composition, phase existed, thermal properties, density, hardness and microstructure (particle distribution and shape). The results obtained will indicate the optimum condition in producing M3/II HSS green samples. It is important to choose best samples properties because it is related to the sintered bonding process later. The properties of cast iron such as the composition microstructure and surface roughness were also examined.

The second part of the research was aiming to determine sintered bonding process mechanism which involves introducing liquid phase by adding powders with lower melting temperature than the base material. An understanding of the fundamental principles involved in liquid phase sintering provides a better view in obtaining a good bonding strength as well as basis for more extensive application of this technology in fabricating high performance materials or components.

At the end of the research, a migration of liquid phase from the mixture powders of M3/II HSS-9wt.%Cu-1wt.%P expected to formed between the cast iron interface. The sintered bonding is characterized by its ability to form a strong bond between the materials.

Generally, there is still a lot of unexplored region in understanding joining mechanism between dissimilar materials such as PM and cast iron. This often is the reason of reluctance in replacing conventional engineering materials and techniques. This research would contribute in giving a better understanding on sintered bonding parameters to the students and researchers especially those in PM area. The findings can also be useful for automotive industries to utilize possibility of producing assembled camshaft in Malaysia.

1.3 Thesis Overview

In the study of this postgraduate research, the thesis is divided into a few chapters to explain the stages that have been done in order to reach the objectives. Chapter One starts with a brief introduction on the sintered bonding, current problem statements, the aim objectives and the research scope of study.

In Chapter Two there will be a literature review on the concept to be looked in depth which includes Joining Techniques, Powder Metallurgy Process, High Speed Steels and Cast Iron materials properties. Others researcher's findings and issues that interlinked with this research are also highlighted here.

Chapter Three shows how the principal described earlier are use in practice. This chapter covers the research methodology which involved the experimental works. The experimental works were divided into a few stages such as identifying the powders and cast iron properties, preparing the green sample (green compacts), sintering process and sintered bonding attempt.

Meanwhile in Chapter Four, details explanation on the results obtained from the conducted analysis and testing. Figures of micrographs and data are included to illustrate the process description which would able give a better understanding and clarify on certain issues. Relevant appendixes are also attached at the back.

Finally is the Conclusion and Recommendation in Chapter Five, where the important issues and results arising in this research are summarized and addressed to the original aim and objectives. Potential beneficial expansion and continuation of this research in future work is also recommend here.

CHAPTER TWO

LITERATURE REVIEW

2.1 Joining Techniques

In principle, a very wide range of processes can be used to join both similar and dissimilar materials, but it is often limited by economics as well as technical factors such as characteristic of the particular materials that have to be joined and the service condition that must be endured.

After fabrication, several components may need to be joined to form an assembly. The assembly might involve different materials that could not be combined in sintering. Joining is a comprehensive term used to denote all process that affix one part to another. Most welding processes require the application of heat with some controlled melting of the base material and or filler metal (fusion), while others rely on surface diffusion and or mechanical interlocking.

Permanent bonding is usually the goal expected for components joined using fasteners, such as bolts or screws. There are several variants, including joining porous materials (PM) to solid steels, porous material to porous materials and full density powder metallurgy steels to wrought steels.

Processes that form permanent joints either produce bonding directly between the component materials or make use of foreign materials introduced between mating surfaces.

Hamill Jr. (2000) reported, warpage, porosity, and alloy composition factors influence the selection of the joining process. At low porosity levels, below approximately 8%, no major difference exists between joining procedures for powder metallurgy and wrought materials. However, bonding porous powder metallurgy materials requires special care. Pores reduce thermal conductivity and can wick molten metal away from the interface being joined.

2.1.1 Sintered Bonding

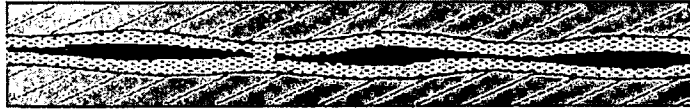
Sintered bonding is a unique technique since it can be applied to joining components during the sintering cycle. Sintered bonding involves the removal of joint interface or when two mating surfaces are bond induced by thermal activation (Humpston and Jacobson, 1993).

Diffusion happened through the migration of atoms across the interface. The diffusion bonding process is characterized by its ability to join materials with minimal deformation and absence of any identifiable bond line (Cam and Kocak, 1998).

In this process, the mating surfaces are brought into intimate, atomic scale contact so that an interface can be formed by interdiffusion and create a structural. Sintered bonding has permitted successful diffusion bonding of a wide range of similar and dissimilar metals including Copper, Ferum, Molybdenum, Titanium and Tungsten (Nicholas, 1998).

Cam and Kocak,(1998) also suggested that the holding times at elevated temperature can exceed 60 minutes, but this depends on the material types being bonded, the joint required and the remaining bonding parameters. Although the majority of bonding operations are performed under vacuum or in an inert gas atmosphere, certain bonds have also been produced in air.

The mechanism of sintered bonding is shown schematically in Fig 2.1. In order to form a bond it is necessary for the two metal surfaces to come into atomic contact and hence microasperities and surface contaminations must be removed before bonding (Cam and Kocak, 1998).



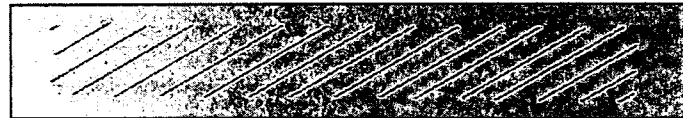
(a) Yielding and creep, leading to reduced voids and thinner contaminant layer



(b) Final yielding and creep, some voids remain with very thin contaminant layer



(c) Continued vacancy diffusion, eliminates oxides layer leaving few small voids



(d) Bonding is complete

Figure 2.1: Mechanism of diffusion bonding (Cam and Kocak, 1998)

2.1.1.1 Solid State Sintered Bonding

Diffusion bonding can be categorized into two main groups that is solid state and liquid state sintered bonding. Solid state sintered bonding is mainly carried out under vacuum or in protective gas such as argon with heat being applied by radiant, direct or indirect resistance heating. In the former, a low pressure usually 3 to 10MPa is used to avoid macrodeformation of the parts.

This type of process therefore requires a good finish on the mating surfaces since the contribution to bonding by plastic yielding is restricted. In addition, the surfaces should be as clean as possible to minimize surface contamination that may lead to process

failure. In hiping, much higher pressures (100 to 200MPa) are used and the surface finished are not critical. In case of metal to ceramic joints, it is possible to introduce single or multiple interlayers of other materials to assist in the bonding process and to modify post bond stress distribution (Parmigiani and Kosco, 1999).

In the case of the combination Fe-1.5wt.%Cu-0.7wt.%C as a inner ring and Fe-1.5wt.%Cu-1.0wt.%C as outer ring by Suzuki (1993), the 0.7wt.%carbon alloy expands more than 1.0 wt.%C alloy. This sinter fit method uses lower carbon alloy for the inner component. The parts produced by this process can be heat treated and steam-treated without any problem.

2.1.1.2 Liquid State Sintered Bonding

Liquid state sintered bonding in the other hand, is applicable only to dissimilar material combination or where dissimilar metal insert is used. The technology of liquid state diffusion has been applied successfully to respond to the demand for wear resistant metals.

Hamill Jr.(2000) reported that solid state diffusion process lead to a change of composition at the bond interface and the bonding temperature will lead a layer of liquid spread along the interface to form a joint at a temperature lower than the melting point of both parent metals.

Alloyed tool steel or high speed steel containing elements such as Chromium, Molybdenum, Tungsten, Vanadium or Cobalt are liquid state diffusion bonding with Copper, Phosphorus or Boron during the sinter process. An increase in density combined with diffusion across the boundary creates a strong bond (Suzuki, 1993).

2.1.2 Brazing

Brazing consists of introducing a filler metal which has a melting point below 427°C. During brazing only the filler metal melts and typically the melting points of the materials to be joined are well above the brazing temperature and capillary attraction draws the filler metal into the gap. The filler metal forms a strong joint by alloying with the base metals (Hamill Jr.2000).

The density of the joining parts affects the thermal expansion coefficient whereas the composition influences dimensional change, both of which can influence the gap distance. The best procedures utilizes a method of gap width control is by using a fixed diameter placed between the mating surfaces. The brazing alloy should be placed immediately adjacent to the joint to assists in capillary action and flow into the joint (Parmigiani and Kosco, 1999).

2.1.3 Fusion

In fusion joining techniques, electromagnetic accelerate particle beams such as electron, ion and neutral beams and special type beams (i.e. laser and plasma beams) with large output has been used as the heat source. Typical fusion processes such as Gas Tungsten Arc Welding (GTAW), Friction Welding (FW), and Laser Beam Welding (LBW).

Electron beams, which are easy to generate and offer relatively higher output, were the first high energy beams to be commercially applied. The disadvantages of using the electron beam is the requirement of a vacuum working chamber, since propagation range in air is extremely short.

The plasma arc technique is the only arc welding process which is capable of achieving the energy density required for penetration. An arc is formed between a tungsten electrode and the workpiece, which is constricted and intensified by a copper nozzle surrounding the electrode, giving a plasma arc of a columnar form. The combination of

high welding current and plasma gas flowrates results in deep penetration of the workpiece.

Laser is an attractive heat source as their potential to give extremely high energy density. In laser welding, when the laser beam impinges on the metal, it delivers its heat to the surface and further penetration beneath the surface relies on thermal conduction. The metal under the laser beam evaporate and a cavity is formed through the thickness of the workpiece. By moving this keyhole along the joint between two pieces of metal, a weld is made (Cam and Kocak, 1998).

Cam and Kocak, (1998) also reported that laser welding technique posses a dual handicap of high investment and low thermal efficiency but they have the great advantages of low distortion, greater accuracy and automation and avoid the need for vacuum working chamber in most cases.

All techniques involving melting produce a heat-affected zone near the weld with a reduced strength. The thermal stresses associated with the bond can cause distortion, cracking or accelerated corrosion in this zone. Stress-induced cracking is a common problem in joining powder metallurgy steels. The best practice is to use as high a sintered-density component as possible to ensure a strong weld. Lower carbon contents reduce cracking near the weld.

Parmigiani and Kosco (1999) mentioned that metal powders are used for joining, especially in forming welding rods, brazing compounds and laser weld fillers. In the latter area, a prealloyed spherical powders fills a gap and precise laser melting is performed to bond two components with minimized melting of the parent structures.

2.2 Powder Metallurgy

Powder metallurgy (PM) is a processing technique that involves the production of metal powders and conversion of these powders into useful engineered structures. Powder metallurgy takes a metal powder with specific attributes of size, shape and packing

(involve powder compaction in rigid dies) then convert it into a strong, precise and high performance shape. The steps include shaping and compaction of the powder and the subsequent thermal bonding of particles by sintering (German, 1994).

In most cases, as reported by Upadhyaya (2000) the powder will be metallic, although in many instances they are combined with other phases such as ceramic or polymer. An important characteristic of a powder is its relatively high surface area to volume ratio. The particles exhibit behavior that is intermediate between solid and liquid. Powders will flow under gravity to fill containers or die cavities, like liquids.

German (1994) reported that the production cost can be cut by using the PM because the sintered parts can be produced directly to the specified dimensions, reducing the amounts of machining required. Material usage is very much better, with scrap being almost negligible.

The production cost in PM are generally higher than in conventional casting or forging due mainly to the high price of the starting material and tooling. However, the high precision achieved in PM results in considerable savings on machining costs and hence on investments in machining operations.

2.2.1 Reason for Using Powder Metallurgy

Generally, PM techniques have advantages with respect to microstructure control, material use, product homogeneity and mass production. Powder metallurgy are widely use in applications, which rely on the economical production of complex parts. Component for automotive industry represent good examples of this area and their production is a large PM activity (German, 1998).

Both the precision and cost are very attractive in PM, while in casting, there are problems associated with segregation, machining and maintaining final tolerances. Prealloyed in

PM for example allow fabrication below the melting temperature. This eliminates segregation and other defects associated with casting.

There are also unique property or microstructure justifications that only can be fabricated by using PM approaches. Some examples include ceramic-metal composites, and cemented carbides. This inability to produce this unique microstructure by other techniques has contributed a large part to the growth of PM. The major growth and expansion will most likely come from further combinations of economic, captive and unique, low cost and high quality products. Table 2.1 shows the comparison between PM and other metalworking techniques (German, 1994).

Table 2.1: Comparison of PM and competitive metalworking techniques (German,1994)

Technique	Advantages Versus PM	Disadvantages Versus PM
Casting	Widely used technique; small to large part size range; low set up cost; low tooling cost	Not useful for many materials; flashing, parting line, pores; chemical segregation; single-use molds; recycle of sprues and runners
Cold forging	Faster production; higher strength; good surface finish	Lower precision; shorter tool life; limited materials
Hot forging	High mechanical properties; large, complex shapes; fast production; tailored properties	Flash and material waste; poor dimensional control; inclusion and blemish; rapid tool wear
Stamping	Flat, high precision; high production rates; large area parts; precise feature location	Single-level, thin shapes; limited materials; waste, edge roughness, small features prove difficult

2.2.2 Powder Metallurgy Applications

Maximum use of sintered powders structural parts is in structural applications mainly in the automotive, aerospace and defense industries. Some example includes wristwatch cases, laminated knife blades, automobile engine timing components, automotive gears, brake sensors, jet engines and biomedical implants. Many PM applications associated with automobile engines like valve seats, lifters, sensors, power steering pump, bearing, sprocket, camshaft and connecting rod (German, 1994).

Materials with improved wear or tribological characteristics in automotive valve train applications have been developed Upadhyaya, (2000). These include cam lobes, rocker arm tips, tappet shims and valve guides. Automotive applications are a dominant aspect of ferrous PM especially in engine applications such as pulley and sprockets for camshaft, crankshaft, water and injection pumps, crankshaft bearing caps, rotors and cam rings for hydraulic pumps while in transmission application it include synchronizer hubs and rings, gearshift lever for manual transmissions and planet carriers for automatic transmissions.

2.2.3 Metal Powder Production (Atomization)

Atomization techniques are the major technique in fabricates powder especially the metal powders. German (1994) reported that atomization involves the formation of powder from molten metal using a spray of droplets. Both elemental and prealloyed powders are can be formed by such processes.

2.2.3.1 Gas Atomization

It was called gas atomization because the use of air, nitrogen, helium or argon as a fluid for breaking up a molten metal stream. The liquid metal stream is disintegrated by rapid gas expansion out of a nozzle.

Gas atomization can be performed totally under inert condition, thereby maintaining the integrity of high alloy feedstock. The particle shape is spherical with a fairly wide size distribution. The main advantage of gas atomization process is in the powder homogeneity and the good packing properties available with the resulting spherical powder.

2.2.3.2 Water Atomization

Water atomization is the most common technique for producing elemental and alloy powders from metals which melt below 1600°C. High pressure water jets are directed by a single jet, multiple jets or an annular ring. The process is similar to gas atomization, except for the rapid quenching and differing fluid properties.

Due to rapid cooling, German (1994) described the powder shape is irregular and rough, with some oxidation. Microscopic examination of iron powder particles produced by water atomization reveals an irregular geometry.

Pressure is the main process control variable in this technique. Higher the water pressures result in higher water velocities and smaller particle sizes (see Fig.2.2 for water atomization particle generation)

In his previous report German (1985) recommended that, if oxide coating is detrimental, then it can be removed by heating in hydrogen after atomization. Since the reduction process causes particle bonding, subsequent milling might be required to maintain discrete particles.

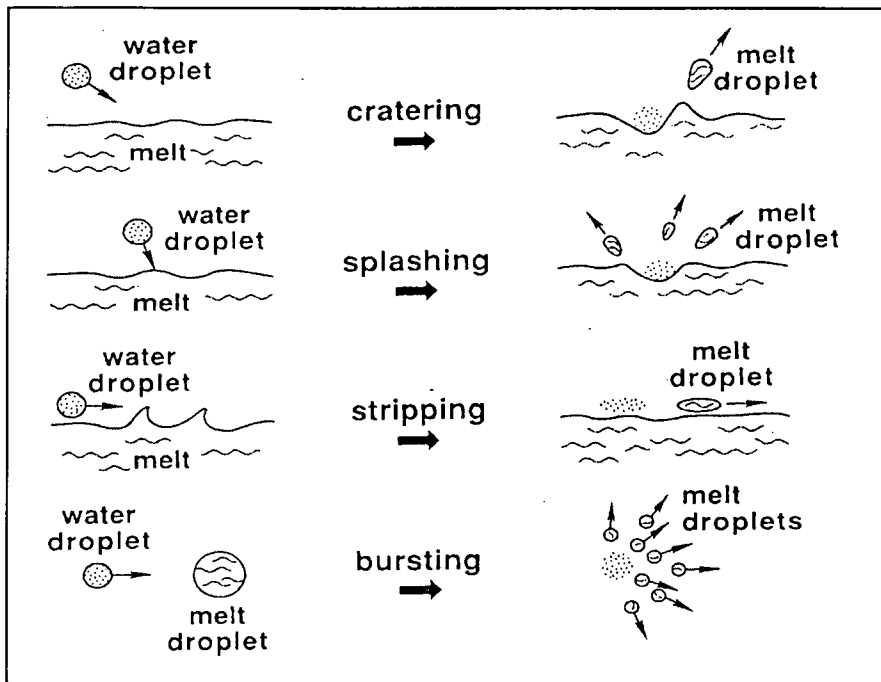


Figure 2.2: A sketch of four possible particle generation mechanisms associated with water atomization; cratering, splashing, stripping, and bursting (German, 1994).

2.2.3.3 Centrifugal Atomization

The centrifugal atomization was developed to overcome the difficulties in controlling the particle size and fabricating powders from reactive metals. The centrifugal force throws off the molten metal as a fine spray that solidifies into a powder particle.

The apparatus consists of a consumable electrode made from the desired material (powder). The electrode is melted at its end by either plasma arc or stationary tungsten electrode. The electrode rotation is driven by an external motor. As melting occurs, the electrode is fed into the chamber via an external mechanism.

Electrical contact with the electrode is made outside the chamber using a contact brush. Like gas atomization, centrifugal atomization is often performed under an inert gas blanket to protect the powder from oxidation. The droplet formation event on a rotating substrate are diagrammed in Fig 2.3.

The liquid forms as a sheet that extends beyond the lip of the solid (anode). The benefits of this technique are the powder cleanliness, spherical shape (high packing density and easy flow) and uniform particle size (German, 1994).

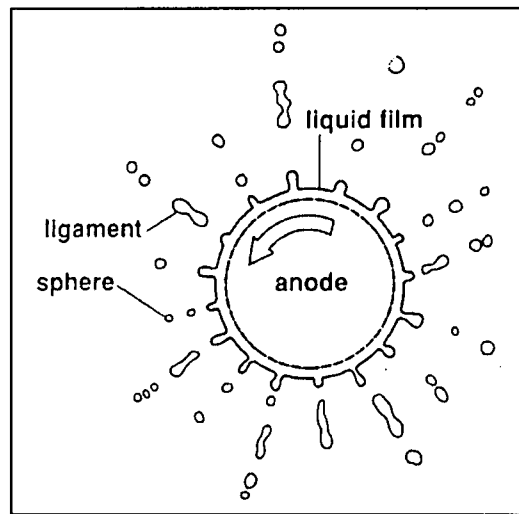


Figure 2.3: A sketch of a liquid break up and formation in spherical particles of a rotating electrode (German, 1994).

2.3 Powder Characterization

2.3.1. Particle Size

Particle size is a determination of the dimensions of particle. Inter-particle friction has a considerable influence over apparent density, and this effect becomes more significant as the particle size decreases (Hamill Jr., 2000).

German, (1994) reported that, the size of a particle depends on the measurement technique, specific parameter being measured and particle shape. The basis for analysis can be any of the obvious geometric value, such as surface area, projected area, maximum dimension, minimum cross sectional area, or volume. Considering a plate or flake shape particle as shown in Fig 2.4 (b), at least two parameters are needed to fully describe the sizes that are diameter and width.

For rounded shape Fig 2.4 (a), the size can be described in terms of the horizontal width, equivalent spherical volume and diameter of a sphere. In the other hand there is great difficulty in defining a single particle size for irregular shaped powder. Since the size depends on the attributions measured, it is common to find disagreement between the particle size distributions obtained by many different instruments such as microscopy, screening, sedimentation, light scattering and electrical zone sensing.

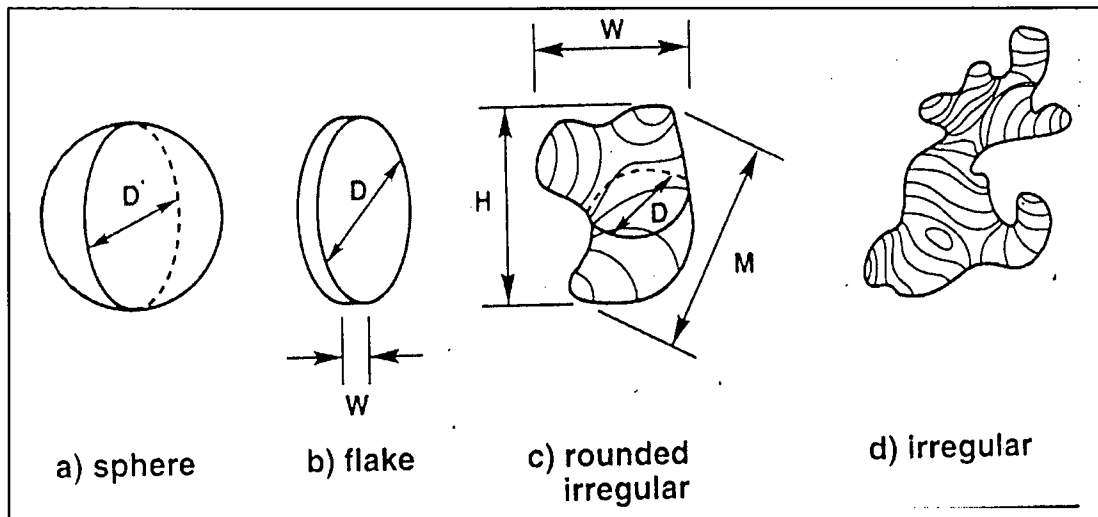


Figure 2.4: An illustration of difficulty in measuring particle size. The number of possible increases as the particle shape becomes more complex (German,1994).

2.3.2 Particle Shape

Particle shape influences packing, flow and compressibility, which provide information on the powder fabrication route. Particle shape varies with size and manufacturing technique (German, 1998).

Greater the surface roughness or the more irregular the particle shape, the lower the packing density, higher the angle of repose, and slower the powder flow. High density is normally associated with smooth spherical particles with hard surfaces. The use of vibration or lubricants can help attain a high packing density, but problems may arise with agglomeration or size segregation. (German, 1998).

The apparent density of such irregular particles (loose powder) is found to be significantly lower than the packing density of spherical particles. The apparent density of a PM powder is one of its most important characteristics in order to avoid material wastage and possible production problems.

However, Smith and Midha (1997) reported that, particles with irregular geometries are in fact the type of particles which constitute the majority metal powder consumed by PM industry. A typical example of irregular particle is the water atomized iron powder that used in automobile structural parts.

It is also reported that, the green strength from mechanical interlocking is enhanced by an irregular particle shape. Consequently, a rounded but irregular particle shape often results in the optimal green strength.

A tumbling action proves effective in smoothing the surface asperities on a rough powder and for distributing a coating on the powder. It is also effective in deagglomerating and smoothing the powder surface. Consequently, the packing densities will increase significantly (German, 1994).

2.3.3 Particle Packing

Years of empirical research indicate that powder densities are dependent upon a number of factors relating to particle shape and size (Hamill Jr. 2000). Particle packing is important in most forming processes. The packing density dictates the die fill, binder content and shrinkage in sintering. Interparticle friction can arise from irregularities on the particle surface.

The greater surface roughness or more irregular the particle shape, the lower the packing density. For particles of the same size but different shapes, the packing density will decrease as the shape departs from spherical (German, 1994).

German (1994) also added that, small particles are selected to fit the interstices between large particles without forcing the large particles apart. In turn, even smaller particles can be selected to fit into the remaining pores, giving a corresponding improvement in packing density.

Eventually, the small particles will fill all of the spaces between the large particles. Further additions will force the large particles apart and no improve the packing density. In contrast, starting with the small particles, clusters of small particles and their associated voids can be removed and replaced by large particles. The benefits of replacing small particles with large particles continue until a concentration where the large particles contact one another.

Moreover, the packing density will increase with the homogeneity of mixture. Depending on handling practice, randomly mixed systems will range between unmixed and fully mixed and typically exhibit some inhomogeneities that degrade actual packing from the ideal. Analogous to the behavior of spheres, a density increase is associated with blending different particle size of similar shapes. However, a major difference between spherical and nonspherical particles is that the initial packing is generally higher for spheres (German, 1994).

The greater surface roughness, shape irregularity, or particle aspect ratio, then the lower the inherent packing density. Thus, although the relative density gain is similar for spherical and nonspherical particles, the starting density for nonspherical particles is lower.

2.4 Mechanical Alloying

Mixing and blending are necessary to prepare unique particle size distribution, combine powders to generate new alloys during sintering, add lubricants for compaction and to prepare a powder binder mixture for shaping.

A major reason for blending powders is to remove segregation, typically induced by vibration in transport. The segregation of particle based on size, with larger particle on top, leading to uneven compaction and sintering.

Mixing processes variables include particles sizes, mixer type, mixer size, relative powder volume in the mixer, speed of mixing, shear and time of mixing. Environmental factor such as humidity also influence mixing (German, 1994).

Agglomeration (as shown in Fig. 2.5) which is known to decrease packing density, is a common phenomenon in fine powders caused by cohesion forces which increase with increasing particle specific area (German,1994).

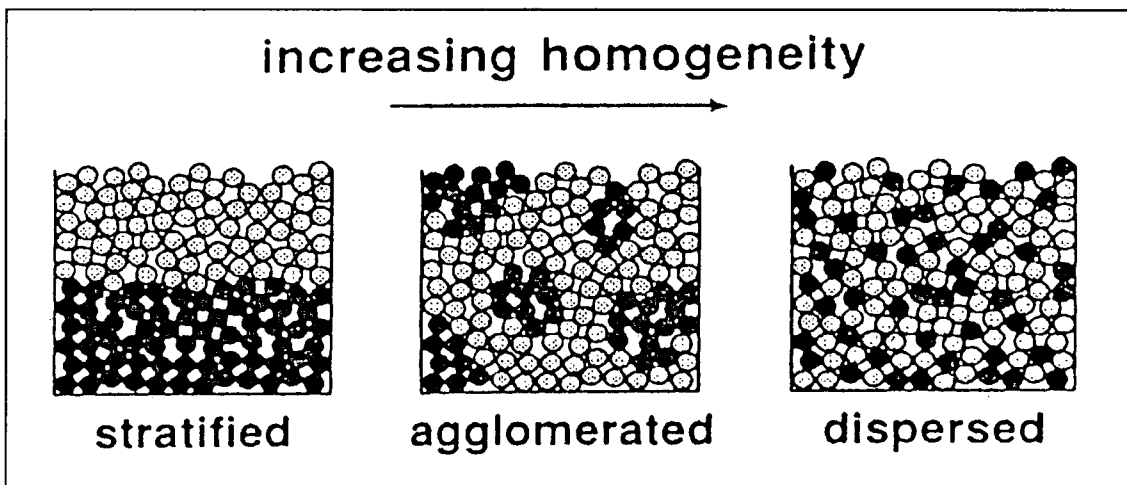


Figure 2.5: A schematic of a homogeneity associated with stratified mixture, an agglomerated mixture and a homogenous dispersed mixture (German, 1994).

One way to overcome these obstacles mentioned by Kauly (1997) is by adding a wetting agent which reduces surface tension and friction between particles. Liu et. al., (2001) reported that powders with homogenous distribution of reinforcement particles will exhibit superior mechanical properties.

In the early stage, (up to about 2 hour milling time) as mentioned by Amador and Toralba (2003), apparent density decrease due to the worst packaging properties of powders that get flattened shape by plastic deformation. Powder particle are deformed into thin layers, perpendicular to the direction in which the powder particles were flattened by milling ball. In this stage, particle size is smaller than the as-received powders.

On the other hand, during the second stage, cold welding events enter in the process while plastic deformation continues with decreasing dominance along this period but the fracture mechanism still going on in this period. The third stage is characterized by equilibrium between fracture and cold welding mechanism where plastic deformation plays a negligible role (Liu et. al, 2001).

Convective mixing refers to a transfer of adjacent powder groups from one location to another. The screw cuts off small group of particles from the lower surface and transports them to elsewhere in the batch. Shear mixing occurs by continual division and flow of the powder over slip planes.

The volume of powder in the mixer determines the mixing efficiency. As the mixer becomes filled with powder, the relative motion of powder is inhibited. Optimum powder volumes are between 20 and 40% of the mixer capacity (German, 1994).

The rotation speed also has a large effect on mixing efficiency. A slow rotation will prolong the time necessary to obtain adequate mixing and extensive free-fall of the powder in the mixer will cause preferential size settling and impact grinding, but rapid rotation will impart a centrifugal force to the powder, which interferes with flow.

density by contact enlargement through plastic deformation. Thus, the pressure causes localized deformation at the contacts, giving work (strain) hardening and allowing new contacts to form as the gaps between particles collapse.

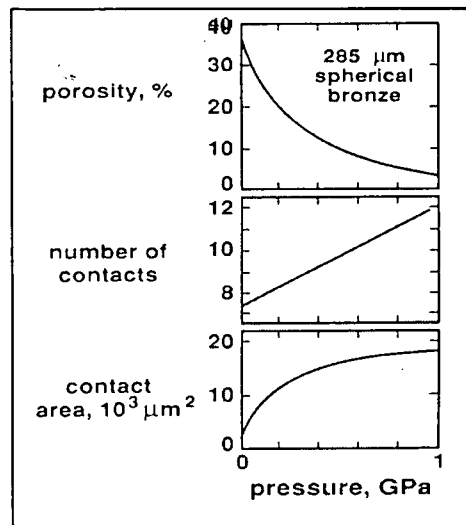


Figure 2.6: Data for the die compaction of a spherical bronze powder (German,1994)

From the experimental result on the effects of compacting pressure to the linear shrinkage, from which one can see that the higher the compacting pressure is, the smaller the linear shrinkage will be. This is because that the porosity in the green compact will reduce with the increased of the compacting pressure.

2.5.1 Particle Deformation

When ferrous powder is compressed, the particles slide past one another, deform, bond and harden. The greater the compaction pressure, the harder the particles become, thereby resisting further densification.

Compaction initially deforms the particles at their contacting points and results in welding at those contacts. The higher pressure applied, the higher density achieved. Powder characteristic have a large effect on compaction. As the pressure increase, the green density increases, but the gain density with higher pressures progressively decays.

This is because of the work hardening. At the atomic level, the dislocation move and become entangled, making further atomic motion difficult. Particle deformation during compaction cause particle hardening which increase hardness but decrease ductile (Liu et. al., 2001).

At the beginning of a compaction cycle (see Fig. 2.7), the powder has a density approximately equal to the apparent density. Void exist between the particles and even with vibration, the highest obtainable density is only the tap density. As the pressure is applied, the first response is rearrangement of the particles filling the large pores, giving a higher packing coordination.

During deformation, cold welding at the interparticle contacts contributes to the development of strength in the compact. The strength after pressing, but before sintering is termed the green strength (German,1994).

At low pressures, plastic flow is localized to particle contacts. As the pressure increases, homogeneous plastic flow spreads from the contacts and the entire particle becomes work hardened. The large pores are eliminated first and the particle packing increases to further distribute the load (German, 1994)

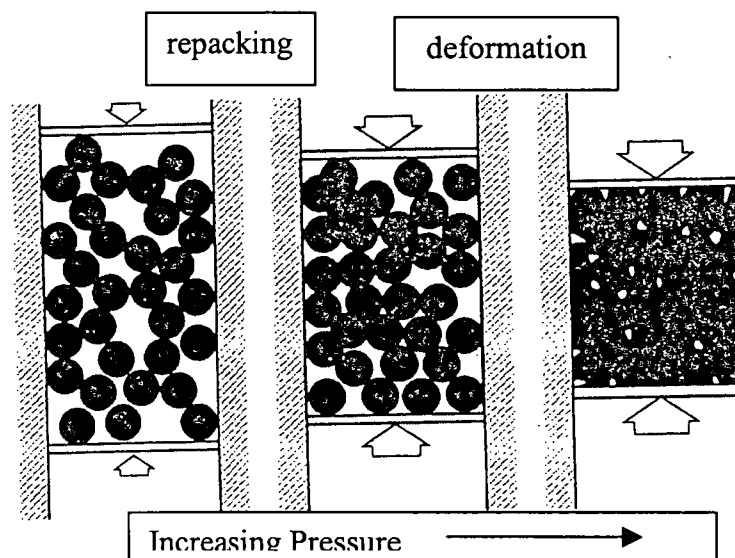


Fig 2.7: A simplified view of the stages of metal powder compaction (German, 1994).

2.5.2 Compaction Technology

2.5.2.1 Warm Compaction

In warm compaction, both powder and the tooling are heated in warm compaction, giving a slight softening of the iron that produces a higher green density. A typical temperature for the powder and tooling might be 150°C, and compaction pressures are usually in the range of 700 MPa.

Usually, a polymer is added to glue the particles together. The polymer-coated powder is more costly than typical die-compaction grades, unless a simple lubricant such as stearate is admixed with the powder. Heating of the die and punches requires modifications to the compaction press and a heater is required in the powder feed mechanisms.

Close temperature control is necessary, since product uniformity suffers if the polymer is too hot. After cooling to room temperature, the warm compacted powder is stronger because chilling the polymer adds strength to the compact.

Final properties of the sintered compacts are slightly improved over conventional compaction, due to the higher green density usually increases by 0.15gcm^{-3} . The major role of warm compaction is in lowering the pressure required for attaining density over 7.0gcm^{-3} . Unfortunately, if warm compaction is performed at too high temperature, then polymer degradation leads to lower sintered properties. Thus, precise temperature and process control are required to fully realize the benefits possible via warm compaction (German, 1994).

2.5.2.2 Powder Injection Molding

Powder injection molding (PIM) builds on the shaping flexibility, but relies on high particle content to form complex metallic shapes. The process begins by mixing selected powders and binders. The particles are small to aid in sintering densification, and often

have average sizes below $20\mu\text{m}$ with near spherical shapes. The binders are thermoplastic mixtures of waxes, polymers, oils, lubricants and surfactants. The powder-binder mixture is granulated and injected molded into the desired shape (German, 1994).

After molding, the binder is removed and the remaining powder structure sintered. The product may then be further densified, heat treated or machined. The sintered compact has the shape and precision of an injection molded plastic, but is capable of performance levels unattainable with polymers.

2.6 Sintering

Sintering is the bonding together of particles at high temperatures. It can occur at temperature below the melting point by solid-state atomic transport events, but in many instances involves the formation of a liquid phase. On a microstructural scale the bonding occurs as cohesive necks grow at the particle contacts (German, 1985).

A first function of the sintering is to remove the lubricants and other polymer additions used for shaping, pressing or bonding the particles. Heat will melt the polymer and then breaks down its molecular bonds, forming small molecules that evaporate out of the compact.

2.6.1 Basic Concepts of Sintering

Consider two spherical particles in contact (German, 1994) such as shown in Fig. 2.8. In powder compacts there are many such contacts on each particle. The bonds between contacting particles enlarge and merge as sintering progresses. At each contact, a grain boundary grows to replace the solid vapor interface.

The initial stage of sintering is characterized by rapid growth of the interparticle neck. In the intermediate stage, the pore structure becomes smoother and has an interconnected, cylinder nature as the compact properties are developed. It is common for grain growth

to occur in the latter portion of the intermediate stage of sintering, giving a larger average grain size with fewer grains. That is accompanied by possible pore isolation and a slower sintering rate.

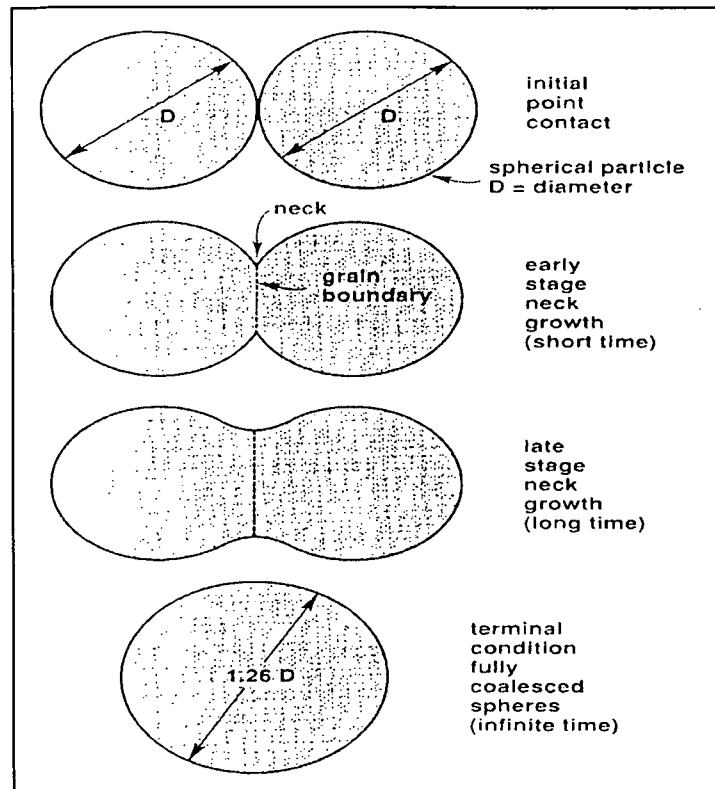


Figure 2.8: Two spherical particles sintering model with the development of the interparticle bond during sintering (German, 1994).

The open pore network becomes geometrically unstable when the porosity has shrunk to approximately 8% (92% of theoretical density). At that point, the cylindrical pores collapse into spherical pores, which are not as effective in slowing grain growth. The appearance of isolated pores indicated the final stage of sintering and slow densification. Gas in the pores will limit the end-point density; accordingly, vacuum sintering can produce high final densities as long as the metal does not evaporate.

The initial stage generally corresponds to a microstructure with large curvature gradients. Both the neck size ratio and shrinkage are small and the grain size is no larger than the

to occur in the latter portion of the intermediate stage of sintering, giving a larger average grain size with fewer grains. That is accompanied by possible pore isolation and a slower sintering rate.

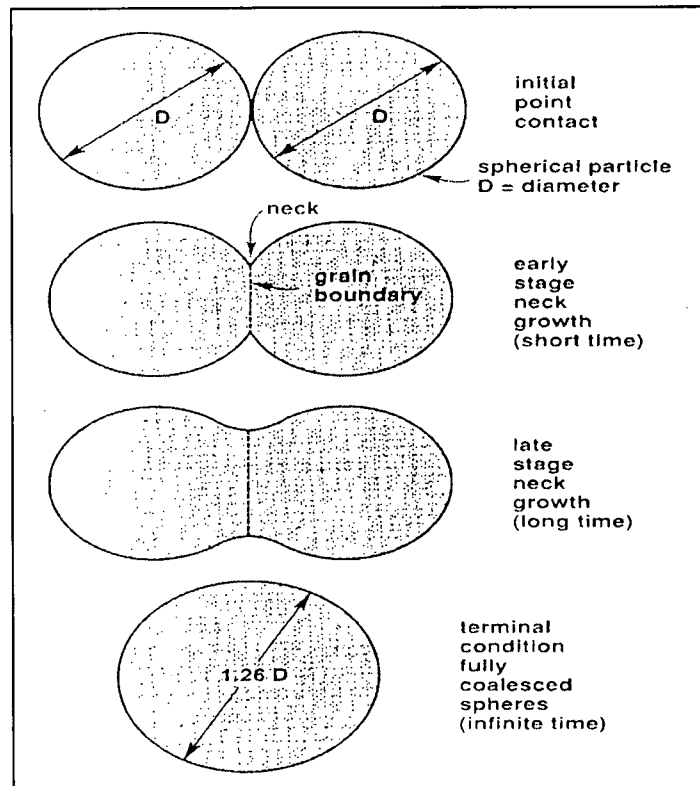


Figure 2.8: Two spherical particles sintering model with the development of the interparticle bond during sintering (German, 1994).

The open pore network becomes geometrically unstable when the porosity has shrunk to approximately 8% (92% of theoretical density). At that point, the cylindrical pores collapse into spherical pores, which are not as effective in slowing grain growth. The appearance of isolated pores indicated the final stage of sintering and slow densification. Gas in the pores will limit the end-point density; accordingly, vacuum sintering can produce high final densities as long as the metal does not evaporate.

The initial stage generally corresponds to a microstructure with large curvature gradients. Both the neck size ratio and shrinkage are small and the grain size is no larger than the

initial particle size. In the intermediate stage, pores are smoother and the density is between 70 and 92% of theoretical. Grain growth occurs late in the intermediate stage, so the grain size is larger than the initial particle size. In the final stage of sintering, the pores are spherical, closed and grain growth is evident (German, 1994).

Upadhyaya (2000) reported that heating of the 'green' compacts is carried out in a protective atmosphere within a furnace at a temperature below the melting point of the base metal, which is generally 75% of the absolute melting temperature.

Particles sinter by atomic motions that eliminate the high surface energy associated with powder. The surface energy per unit volume depends in the inverse of the particle diameter. Typically the surface energy is assessed by the surface area. Thus, smaller particles with high specific surface areas have more energy and sinter faster.

Zhang and German (2001) reported in the early stage of sintering, chemical gradients play the major role in promoting densification, dominating the effect of surface energy. Later, when the chemical gradients level off and iron transforms, other factors, such as grain size, dominate the sintering rate

For metal powders, the diffusion mechanisms are usually over the surfaces, along the grain boundaries, or through the crystalline lattice. Sintering is faster at higher temperatures, because of the increased number of active atoms and available sites (German, 1994).

2.6.2 Transport Mechanism

Transport mechanism determines how mass flows in response to the driving forces. The two classes of transport mechanism are surface transport and bulk transport. Surface transport involves neck growth without a change in particle spacing (no shrinkage or densification) due to mass flow originating and terminating at the particle surface.

Surface diffusion and evaporation condensation are the two most important contributors during surface transport controlled sintering. Surface diffusion dominates the low temperatures sintering of many metals, including iron (Bolton et. al, 1991).

Plastic flow is usually most important during the heating period, especially for compacted powders where the initial dislocation is large. Viscous flow is also possible for metals with liquid phases on the grain boundaries.

Grain boundary diffusion is fairly important to densification for most crystalline materials, and appears to dominate the densification of many common metals. Both surface and bulk transport processes give neck growth, the main difference is in density (or shrinkage) during sintering (German, 1994).

2.6.3 Pore Structure and Densification

German (1994) reported the voids between particles initially contain lubricants, binder and contamination. As heating occurs, these species evaporate and leaving pores between the particles. A conceptual sketch of the pore structure changes with sintering is given in Fig. 2.9. The point contact between particles will grow into necks. After the initial stage, the grain boundary and pore configuration control the sintering rate.

At the beginning of the intermediate stage, the pore geometry is highly convoluted and the pores are located at grain boundary intersections. The continued sintering process, will lead the pore to a cylindrical shape where densification occurs by decreasing the pore radius.

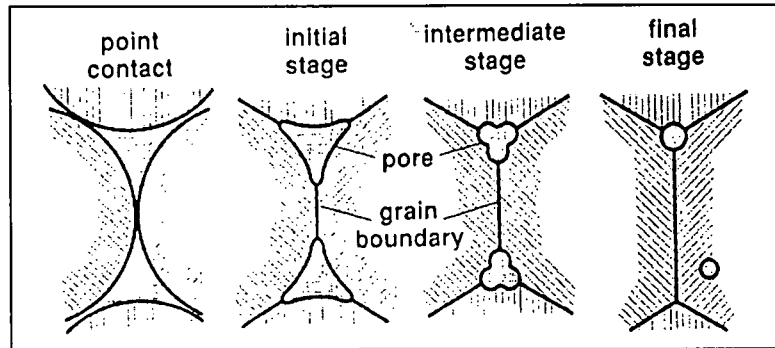


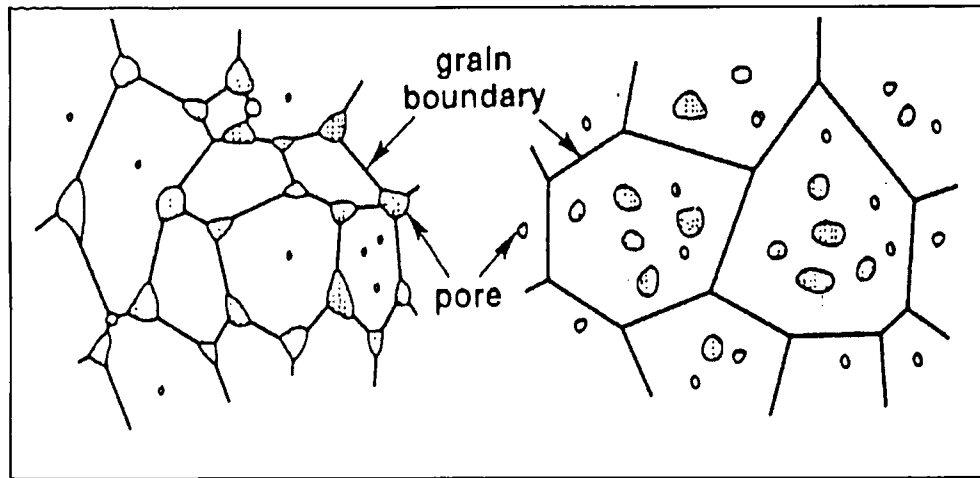
Figure 2.9: A schematic diagram of pore changes during sintering, starting with point contacts (German, 1994)

In the latter state of sintering, interaction between pores and grain boundaries can take three forms; the pores can retard grain growth, the pores can be dragged by the moving grain boundaries during grain growth or the grain boundaries can break away from the pores, leaving them isolated in the grain interior.

At low temperatures, the rates of grain growth is small, pores remain attached and impede it. Under the tension of a moving grain boundary, pores move by volume diffusion, surface diffusion or evaporation-condensation across the pore.

In a high temperature condition, the rate of grain growth increases to a point where the boundaries break away from the pores. As illustrated in the Fig. 2.10, pores can occupy sites on the grain edges or inside the grains. The system energy is lower for the pore occupying the grain edge, because the pore reduces the total grain boundary area and energy.

If the pore and boundary become separated, the system energy is increased in proportion to the amount of newly created interfacial area. As a consequence, the pore has a binding energy to the grain boundary which increases as the porosity. Hence, at the beginning of the intermediate stage, little separation of boundaries from pores is expected. As densification proceeds, the slower mobility of the pores coupled with the diminishing pinning force allows breakaway.



(a) Densification

(b) No densification

Figure 2.10: Two possible grain boundary pore configuration during sintering (German, 1994).

Separation of the pores from the boundaries limits the final density possible by sintering. Consequently, it is important to minimize breakaway by careful temperature control. The combination of a large pore size and a large grain size leads to breakaway during grain growth.

Early in sintering, the large pores are immobile and pin the grain boundaries, maintaining a small grain size. Late in sintering, there are fewer pores that are small due to shrinkage and the grain are relatively large. In this situation separation can be avoided if the pores are sufficiently mobile to migrate with the boundaries. Thus sintering requires precise manipulator of the initial powder microstructure and heating cycle, since several factors can inhibit final pore elimination (German, 1994).

2.6.4 Liquid Phase Sintering

Liquid phase sintering is defined as a thermal treatment (sintering) involving both liquid and solid phases such that the sintered compact has improved interparticle bonding and increased strength. A major distinction among pressureless sintering technique is between solid state and liquid phase techniques (German, 1985).

Hoyle (1988) mentioned, there are two basic ways to obtain the liquid phase during sintering. The use of mixed powders of differing chemistries is the most common technique. The liquid can result from melting of one component or formation of a eutectic. Furthermore, the liquid may be transient or persistent during sintering depending on the solubility relationship.

Alternatively, a prealloyed powder can be heated to a temperature between liquidus and solidus temperatures. The resulting mixture of liquid and solid phases leads to supersolidus sintering. Beyond these common forms of liquid phase sintering, there are several other techniques.

The requirements of liquid phase sintering Narasimhan (2001) reported that there should be a liquid at the sintering temperature, solubility of one element or phase is greater than the other, the melting temperature of the main phase is much higher than the other and liquid wets the surface of the solid phase.

Recent research done by Sustarsic et.al. (2003) reported that the densification of green compacts proceeds by the so called liquid-phase sintering process. A significant difference exists between the sintering cemented carbide (WC-Co) and high speed steel, in spite of the fact that the final densification occurs in the presence of a liquid in both cases.

As the liquid volume fraction increases, Liu et.al. (2000) reported that the liquid viscosity decreases at higher temperatures, rapid sintering takes place, but dimensional precision decreases. Consequently, temperature (which controls the solid-liquid ratio) becomes the main determinant of sintered density and dimensional precision.

Suganuma and Kazuoka, (1981) found that the mechanical properties, with the exception of hardness, were drastically improved by liquid phase sintering in both the as-sintered and heat-treated conditions. This improvement was more marked in the case of a higher green density. The loss in sintered density due to expansion caused by the liquid phase more than offset by better microstructure.

2.6.4.1 Classic sequence of stages

The classic liquid phase sintering system divided in four overlapping stages. Initially, the mixed powders are heated to a temperature where liquids formed. Prior to liquid formation, a solid solution can form by diffusion (German, 1985).

The changes prior to liquid formation are significant for systems exhibiting large melting point differences and large solubility differences. The formation of liquid promote densification due to atom capillary force exerted by the wetting liquid on the solid particles. The elimination of porosity occurs as the system minimizes surface energy and compact viscosity.

As a consequence German (1985) added, the densification rate continuously increases. The amounts of densification attained by rearrangement is dependent on the amount of liquid, contact angle, finer particles and give better rearrangement. Full density (zero porosity) is possible by rearrangement if enough liquid is formed. It is estimated that 35% of volume liquid is needed to obtain full density by rearrangement processes.

However, rearrangement processes can be totally inhibited by a high green density. The particle contacts resulting from compaction form solid state bonds during heating, thereby eliminating rearrangement.

The next stage of classic liquid phase sintering is termed solution-precipitation. A general attribute of solution reprecipitation processes is microstructural coarsening. The coarsening is due to a distribution in grain sizes. The solubility of grain in its surrounding liquid varies inversely with the grain size, small grains have a higher solubility than coarse grains. The difference in solubilities established a concentration gradient in the liquid. Material is transported from the small grains to the large grains by diffusion. The net result is a progressive growth of the larger grains, giving fewer grains with wider spacing.

Solution-precipitation not only contributes to grain coarsening, but also to densification. The grain shape can be altered by diffusion to allow tighter packing of the grains. This process of grain shape accommodation leads to pore elimination. The amount of liquid affects solution-precipitation in terms of both the diffusion distance and amount of grain shape accommodation. Both solubility of solid in the liquid and diffusive transport are necessary criteria.

The last stage of classic liquid phase sintering is referred to as solid state controlled sintering. Densification is slow in this stage because of the existence of a solid skeleton. Processes dominant in the final stage because of the existence throughout the entire liquid phase sintering cycle. However, because of the slow nature, solid state sintering is not of significance until late sintering cycle. The rigidity of the solid skeleton inhibits all rearrangement events, although microstructural coarsening continues by diffusion (German, 1985).

2.6.5 Sintering Atmosphere

The sintering atmosphere performs several roles but the most important one is to protect the compact from attack by air at high temperatures. The atmosphere helps in removing lubricants or binders, transferring heat to the compact, extracting surface oxides, controlling the final carbon content and adjusting impurity level such as the nitrogen content.

Bolton et.al. (1991) reported, several atmosphere conditions are possible inside a sintering furnace, ranging from oxidizing (carbon dioxide or oxygen), neutral (argon, helium or vacuum), reducing (hydrogen or carbon monoxide), nitriding (nitrogen), carburizing are not necessarily mutually exclusive.

Some differences in microstructures were produced by the addition of extra carbon before sintering and when either vacuum or nitrogen atmosphere sintering was used.

Although pre-deoxidation annealing of water-atomised powders is performed, high alloyed HSS powder are coated to some extent on the surface with oxides of alloying

elements with a high affinity for oxygen like Cr, V and W and sintering must be carried out in vacuum or protecting/reducing (N_2+H_2) atmosphere (Sustarsic et.al., 2003).

2.6.5.1 Hydrogen

Pure hydrogen is explosive, very light and exhibits a high thermal conductivity. Its reactivity with oxygen helps in the sintering of alloys containing elements that form stable oxides. The most common examples are stainless steels, where chromium is usually present in the alloy at concentration from 12-20% to prevent rusting in service.

Chromium provides protection by forming a stable surface oxide, too thin to see, but tenacious enough to prevent corrosive attack. However, this attribute makes sintering difficult. Instead of sintering the iron or chromium in the stainless steel, the oxide is being sintered if not removed. The oxides of chromium Cr_2O_3 , requires temperatures over the melting point of stainless steel. Thus, reacting hydrogen with the oxide to form water vapor that is swept away in the furnace. In this situation, pure hydrogen is preferred, in spite of concerns over reactivity, flammability and cost.

2.6.5.2 Nitrogen

Nitrogen is essentially neutral or even beneficial for many ferrous alloys since residual nitrogen in the steel increases strength. Some common compositions of nitrogen are between 80-97% with addition of hydrocarbon, alcohol, moisture, hydrogen, carbon monoxide or methane to control the final carbon level (German, 1994)

2.7 Iron and Steel Powders

Ferrous PM can be understood by intersection of various technological characteristic. It is best applied to strong, stiff, low-cost and tough structures that have a low weight sensitivity and the shape is complex. The application are less concerned with corrosion, oxidation, wear and more concerned with surface finish, shape complexity and good mechanical properties at a low manufacturing cost.

Pure iron exists in two crystal forms at atmospheric pressure, one body-centered cubic (bcc) in α -ferrite phase which remains stable from low temperature up to 910°C, when it transforms to face centered cubic (fcc) in γ -austenite phase.

Ferrite phase consists of an interstitial solid solution of carbon in bcc iron. An interstitial type of solid solution rather than substitutional forms because the difference in radius between two atomic species. The solubility of carbon in α -iron is very limited. The maximum solubility is 0.025% at 727°C and decrease to about 0.008% at room temperature.

Shackelford (2000) reported that this will restrict solubility due to the size of the interstitial spaces in the lattice compared with the size of a carbon atom. In α -ferrite, the latter interstitial holes are only about 0.38Å in diameter. Therefore, the iron cannot accommodate carbon interstitially without producing a significant lattice disturbance.

Austenite phase in steels consists of an interstitial solid solution of carbon in fcc iron. Austenite can exist from a temperature of 727 to 1495 °C and can dissolve up to 2% carbon at 1148°C. This amounts approximately 80 times the weight percent of carbon that soluble in α -iron. This is because of the larger interstitial void than in bcc form. In the austenite state, steel is nonmagnetic and relatively soft or ductile.

Delta (δ), this phase consists of solid solution of carbon in bcc iron. It has essentially the same crystal structure as α -iron, except that it exists above temperature of 1400°C. The maximum solubility of carbon in δ -iron is 0.10% (Shackelford, 2000).

2.7.1 High Speed Steel

High Speed Steels (HSS) takes its name from its capacity to retain a high level of hardness when cutting metals (and other materials) at high speed. Nowadays, sintered HSS are no longer used primarily as cutting material. However, Ruiz-Navas et.al. (2003)

reported, their name has remained as their early development when these materials were used exclusively for cutting and machining of metals, wood, polymers and others .

Wright et.al. (1998) reported, even though in many high speed cutting applications, they are being replaced by new, superior ceramic materials such as cemented carbides and Sialons. High speed steel are strongly competitive because of their simultaneously high hardness and toughness. Meanwhile Smith and Midha (1997) added, it could reach high temperature till 400 and 600 °C without losing hardness and maintain their sharp edge in good condition during cutting operations.

In spite of this, Zhang and German, (2001) mentioned that sintered HSS are established in application such as dies for pressing and extrusion processes, in high performance components like structural, antiwear, bearing materials (slide bearing, aircraft jet bearing, valve-seat inserts) and for space-vehicle components. High speed steel are excellent for parts exposed to wear, fatigue and corrosion where compressive strength, fracture toughness and thermal stability are required.

Production of the conventional HSS involves melting, casting, hot working and heat treatment. In molten stage, HSS may be considered to be reasonably homogenous, although it is possible for some carbide to remain out of solution during melting. Once solidification has started, the material never again assumes a single-phase condition

In the solidified material, the important constituent are the matrix, which is treated as normal alloy steel hardenable by heat treatment to a high hardness level, and the carbides which are always present in an undissolved condition and which impart the wear resistant properties to the steel (Hoyle, 1988).

In recent years, however, there have been important developments in the use of PM techniques in HSS. In the case of PM, the segregation pattern is minimized, and a more uniform distribution of carbides is possible.

Maki et.al.(2003) reported that, powder HSS has been overcome chipping failure at sharp edges of a compacting punch that often occurs due to the banded structure of carbides, coarse carbides and inclusions in the conventional wrought HSS. The new powder HSS compacting punches have more uniform carbide distribution and finer grain size.

Generally, Swift and Booker (1997) reported that PM techniques have advantages with respect to microstructure control, material use, product homogeneity and mass production. Powder metallurgy are widely used in applications which rely on the economical production of complex parts. Component for automotive industry represent good examples of this area and involved with a large number of PM activities.

Automotive design engineers have been adapting HSS powder part in order to design vehicles with greater reliability at lower cost. High speed steel powder enables parts to be produced to net or near net shape with the required alloy design. In case of sintered parts application, it would be most effective to provide them with high strength and fine accuracy economically. The main objective in HSS technology and production is to produce tools that satisfactory in performance and can be produced at a reasonable cost.

2.7.2 High Speed Steel Alloying Elements

High Speed Steel are characterized by high carbon content, sometimes up to 1.5% and major additions of strong carbide forming elements. High speed steels are ferrous based alloys of the Fe-C-X multicomponent system where X represents a group of alloying elements comprising mainly such as chromium, molybdenum, tungsten and vanadium (Boccalini and Goldenstein, 2001).

2.7.2.1 Molybdenum

Suganuma and Kazuoka, (1981) reported Molybdenum (Mo) not only increases the hardness of sintered mass by strengthening the matrix and enhancing the hardenability but also improves the slidability by forming a hardened compound carbide with $(\text{Fe.Cr.Mo.})_3\text{C}$ as the main component.

The addition of 0.2% Mo to medium carbon steel delays the transformation to such extent where the bainitic structure is usually formed even at temperature as high as 600 °C. Mo is also considered to contribute to improve in anti wear and anti scuffing properties.

They also found that side austenite containing about 6% Mo is in equilibrium with the liquid phase. Only after all carbide has been consumed, the formation of the liquid phase cease, leading to processes involving only solidification of the melt and a homogeneous distribution of molybdenum within the matrix grain (Suganuma and Kazuoka, 1981).

Fe-1.5wt.%Mo-0.1.2wt.%C steels prepared by the premix and prealloyed processes after sintering at 1160°C in hydrogen for 1 hour showed that the high hardness obtained after elemental processing may be suitable for wear applications since the steels acted like a composite. According to Udayyaya, the development Fe-1.5wt.%Mo prealloyed steels containing 0.2%C, 0.4%C and 6%C was to find better performance surface-hardening PM steels (Upadhyaya, 2000).

2.7.2.2 Tungsten

Tungsten (W) is widely used in tool steel because the tool will maintain its hardness even at red heat. W produces a fine, dense structure and adds both toughness and hardness. Its effect is similar to molybdenum, except that it must be added in greater quantity.

Llwellyn and Hudel (1998) reported that W has the highest melting point of all metals, and at temperatures over 1650°C has the highest tensile strength. The metal oxidizes in

air and must be protected at elevated temperatures. It has excellent corrosion resistance and is attacked only slightly by most mineral acids.

The precipitation of tungsten carbide (WC) is very similar to molybdenum carbide (Mo_2C). The morphology of the precipitate in each is the same, although the size and density of the precipitates are different. The particle density is less in the W steels, presumably due to lower diffusivity of the larger W atom in ferrite. The W steel is softer because the tungsten carbide particles are larger and further apart (Sustarsic et. al, 2003).

2.7.2.3 Vanadium

All HSS contain between 1% to 5%V and as the vanadium (V) content is increased, the carbon is generally increased by at least 0.1% for each additional 1%V. Vanadium is a very strong carbide-forming element and produces extremely hard particles of V_4C_3 (MC type complex carbide). Vanadium carbide improves the abrasion resistance of the high speed steel and is also beneficial as a grain refining agent

Vanadium carbide has been formed by heating V_2O_5 or V_2O_3 with carbon for two hours at 1800°C in 1-10 torr in carbon dioxides. Vanadium oxide (V_2O_5) react with carbon at 435°C , and the oxygen treatments or by the reaction of vanadium metal or hydride with carbon. Loss of vanadium at high temperatures and low carbon content presents a difficulty, but nearly saturated vanadium carbide can be heated to 2000°C without loss of vanadium (Llwellyn and Hudel, 1998).

Boccalini and Goldenstein (2001) found that irregular M_2C eutectic is chiefly promoted by low cooling rate or high vanadium content and the complex regular M_2C eutectic by high cooling rate or low vanadium content. The effect of higher vanadium content is decrease to the volume fraction of M_2C carbide in M_2C eutectic, thus increasing the difficulty of keeping M_2C carbide as the leading phase in the eutectic, and an irregular structure then arises.

2.7.2.4 Chromium

The chromium content of most grades of HSS is about 4wt%. Chromium forms carbides such as $M_{23}C_6$ and M_7C_3 but these carbides dissolve fairly readily and are taken into solution at the normal solution treatment temperatures employed for these steels around 1200 to 1300°C (Llewellyn and Hudel, 1998).

Chromium (Cr) is therefore added as a hardenability agent and promotes the formation of martensite. In addition, Cr is also beneficial in improving the scaling resistance of these steels at the high temperatures generated during machining operations. Cr is considered to contribute to improve anti-wear, anti-scuffing properties, and reducing oxidation and the content of it is limited to form 2.5-25%.

Steels with 0.1%C can accommodate up to about 13.5% Cr at 1050°C and still remain austenitic with face centered cubic structure. As the Cr content in the steel increased within this range, the hardenability also increases very substantially such that large section sizes can be through hardened to martensite on cooling to room temperature.

Above 5%, Cr promotes austenite retention to an unacceptable extent and upsets the stoichiometric balance as the effective carbon content would be too low (Smith, 1993).

2.7.2.5 Carbon

A high carbon content is required in order to produce a hard martensitic matrix and also to form primary carbides. However, the amount of carbon that can be accommodated in HSS is limited.

Carbon (C) is the most constituent in regard to the hardening operation by being solid dissolved in the matrix. The increasing C content lowers the solidus temperature. This means that the higher the C content, the closer the solidus temperature will approach the upper limit of the heat treatment range.

Another important role of C is producing the required amount and type of carbide to give the required abrasion resistance. These insoluble carbides do not enter into solution during the heat treatment and thus do not take part in the martensite hardening process.

However, Suganuma et.al. (1982) reported that if addition of C is less than 1.5%, the hardness of the matrix and the amount of the steadite are unsatisfactory, while the addition of more than 3.5wt.%C promotes the coarsening and the network growth of the matrix, carbide and steadite at the crystalline boundaries. This will make the slidability characteristics are greatly impaired and the attacking property to a piece to be coupled is increased.

The changes of C content will effect on the densification of the materials. By adjusting the C content of the material to be sintered, as sintered densities could be increased.

2.7.2.6 Copper Addition

Copper (Cu) is a well known an alloying element because it is an easily processed element (its oxygen potential is significantly less than iron). The effect of the Cu is based on hardening the matrix.

The work done by Ruiz-Navas, (2003) showed that although the sintered density decreases with increasing Cu content, the hardness increases continuously with the increasing Cu content. The increasing hardness can be assumed that the Cu is dissolved completely in the matrix. Penetration between the iron particles, result of pure capillary forces and penetration along the grain boundaries.

The rate of cooling from sintering to room temperature has a significant effect on the final properties. Rapid cooling gives high tensile strength and hardness, but lower elongation. Upadhayaya (2000) also found that the response to ageing after furnace cooling decreased as the Cu concentration in iron increased.

Olevsky et.al.,(2000) indicated that sintering in the temperature range of 300 to 500°C led to an increase of the tensile strength but decreased the microhardness. This effect was due to a simultaneous strengthening of bonds particles on one hand, and the recrystallization and softening of the individual particles on the other hand.

Upadhyaya, (2000) reported that the addition of both Cu and C to iron powder offers greater strength and more hardness than the addition of either alone. Upadhyaya also found that C impedes Cu melt wetting of the iron grain boundaries by increasing the dihedral angle between solid iron and liquid Cu. The presence of C in the austenite reduces the tendency of Cu to cause undesirable growth during sintering.

Dimensional change from the sintered to heat treated condition was reported to be expansion ranging from 0.03 to 0.16wt.%, which increased with both C and Cu contents. At 1-2wt.% of Cu, this change was relatively stable with regard to composition (Ruiz-Navas et.al., 2003).

During sintering dimensional changes take place which are highly influenced by the amount of Cu. The dimensional growth increases with an increases with an increasing Cu in iron. The addition of minor amounts of Cu is around (1-2.5%), therefore common to compensate for the shrinkage of plain iron compacts during sintering.

Copper growth can be decreased by changing the sintering temperature, sintering time or heating rate within practical limits. Other methods involve C or phosphorus addition and a decrease in the particle size of iron and Cu powders.

The rate of wear with Cu addition when sliding dry against iron is less than nickel by the factor 5. This indicates the slight tendency of Cu-iron pairings to adhere and the good emergency running properties of Cu which are associated with this (Ruiz-Navas et.al., 2003).

2.7.2.7 Phosphorus Addition

Iron (Fe) has a greater thermodynamic affinity for phosphorus than Cu, based on calculations involving the formation free energies for iron and Cu phosphides. The development of sintered steels containing phosphorus (P) had discovered that small amount of phosphorus in sintered Fe added as ferrophosphorus increased its strength considering without impairing the ductility (Jandeska, 1982).

Phosphorus is a very strong solid solution hardener in ferrite phase, second in intensity only to the interstitial elements such as C and nitrogen. It has also extremely high diffusivity as compared to other substitutional elements.

Generally, iron powder that mixed with ferro-phosphorus, Fe₃P and when the mixture is sintered at 1120°C phosphorus diffuses into the iron forming a liquid phase which assists liquid phase sintering. The P powders will solidly solved into the matrix during sintering, this is to activate the sintering and enable the sintering at a lower temperature and enhance the density through liquid phase (Narasimham, 2001).

The increasing of P content will increase strength but also increase loss of ductility. The addition of P is insufficient if it is less than 0.2% because too much liquid phase being produced. This will embrittling the crystalline boundaries and lowering the slidability characteristic. Hence, homogeneity in PM grains should be more easily attained with P than slower diffusing elements such as Cu, Ni or Mo (Jandeska, 1982).

A major drawback with the use of phosphorus in Fe reported by Narasimham (2001) is the relatively higher shrinkage of parts after sintering. It is natural to add Cu to Fe-P system to counteract the shrinkage because addition of Cu which normally produces growth.

2.7.3 Complex carbides

Badisch and Mitterer (2003) reported, HSS are highly alloyed and used in many applications where high wear resistance is needed. These steels could be considered as being a composite material where large primary carbides are dispersed in a martensitic matrix containing a much finer dispersion of small secondary carbides.

Extensive investigations into the relationships between alloy composition and sinterability have been carried out for a number of standard HSS grades by Wright et.al (1998) which had demonstrated that the optimum sintering temperature is located within an austenite+carbide(s)+liquid phase region .

Figure 2.11 shows the basic composition of M2 with 6%W, 5%Mo, 4%Cr and 2%V. The AB line on this diagram represents the normal C content of the steel as specified by Thyssen (Narasimham, 2001).

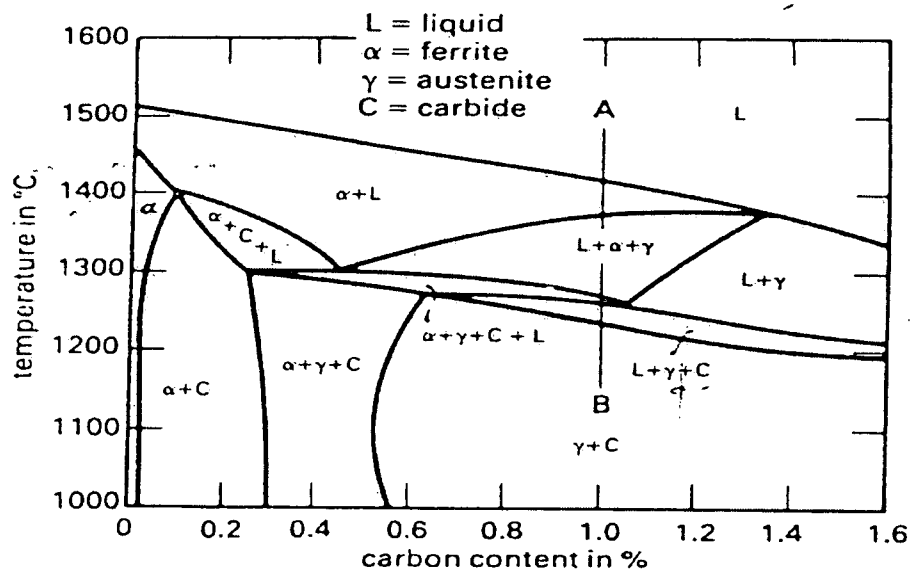


Figure 2.11: Phase diagram for M2 HSS (Narasimham,2001)

The sinterability of water atomized HSS powders is determined by the temperature interval separating the phase boundaries that define this austenite+carbide(s)+liquid phase region. Both solidus and liquidus gradients vary with the composition (Hoyle, 1988).

Referring to investigation done by Wright et.al.(1998), the densification for M2 alloy was initiated on the solidus at 1230 to 1240°C. The optimum sintering temperature, assessed on the basis of grain size and carbide size and shape was at 1255°C.

According to Porter and Easterling (1997), the solution of M_6C carbides begins about 1150°C and continues until the solidus is reached. On the other hand, MC carbide is extremely stable and little solution is achieved, even at temperatures close to the solidus.

Complex structure examinations were performed on HSS of different grades obtained using metallurgy and produced by application of PM. Transmission electron microscopy and X-ray diffraction studies established the type of primary carbides and the amount of retained austenite.

Bochnowski et. al. (2003), used the scanning electron microscopy examinations to calculate the volume fraction of primary carbides. Energy filtering was used to study the secondary carbides of nanometer size.

In M2 HSS, at 1200°C sintering temperature, the microstructures composed typically are the martensite plus retained austenite, together with M_6C . The latter appear as small spherical carbide particles within the grain or as big angular carbides at the prior austenite grain boundaries.

Liu et. al. (2000), reported at 1210°C, angular carbides at the grain boundaries became bigger, the small spherical carbides inside the grains were reduced and the grain size increased. There was no evidence of spherical carbide (inside the grains), and the

carbides. The Energy Dispersive X-ray (EDX) results showed that most of the carbides are rich mainly in Fe, W and Mo which should be M_6C .

Admixing of different hard or soft particulate phases to basic high-alloyed HSS powder is possible. The formed powder mixtures can obtain fine carbides, oxides, sulphides or fluorides (for example NbC, TiC, Al_2O_3 , MnS and CaF_2) enabling the synthesis of a special composite or gradient material with target properties for a precise defined application (e.g. improved wear resistance, higher thermal or corrosion resistance, better machinability and self lubricity) (Sustarsic et.al., 2003).

Conversely, the slightly superior sinterability of M3/II HSS powders (sintering window $\sim 10K$) compared with M2 was attributed by a slight expansion of the $(\gamma + M_6C + MC + L)$ region that occurs on increasing the vanadium content to 3wt%. Alloy of M3/II HSS contains increased amounts of C (an austenite stabilizer) and vanadium (a ferrite stabilizer) and because of its ferrite stabilizing properties, vanadium would be expected to constrict the critical $(\gamma + M_6C + MC + L)$ region (Wright et. al., 1998).

The boundary film which remained after sintering was composed of a continuous layer of iron-rich phosphide and contained particles of MC and M_6C carbides. The phosphide layer formed at prior austenite grain boundaries in M3/II HSS samples retained a similar composition at higher sintering temperatures and herringboned phosphide eutectic structures were found even at moderately high sintering temperatures well below those at which full density was achieved.

The actual eutectic structure also contained large angular M_6C carbides and more rounded vanadium-rich MC carbides, where both types of carbide had obviously grown. The carbides formed in association with any phosphide phase also differed from those found in normal high speed steels. The M_6C carbides, for instance, contained significant quantities of phosphorus whereas the vanadium rich MC-type carbides found in M3/II HSS steel eutectic did not contain phosphorus but did contain a higher than expected vanadium content.

The M3/II HSS alloys elemental composition of the M_6C carbides changed very little with either C addition or with the change from vacuum to nitrogen atmosphere sintering. In the other hand, the vanadium rich MC carbides appeared to become enriched in vanadium and depleted in both molybdenum and tungsten by the nitrogen atmosphere according to Bolton et. al.(1991).

MC carbides were also present as isolated carbides particles within the prior austenite grain boundaries. Energy Dispersive X-ray analysis of MC carbide confirmed the existence of essentially different MC carbides at different sintering temperature. MC carbides formed below the solidus temperature were essentially rich in both Fe and vanadium, but also contained detectable quantities of titanium (Bolton and Gant, 1996).

Bolton and Gant, (1996) also reported that the structure of sintered M3/II HSS typically composed of a martensitic matrix, plus retained austenite, together with both M_6C and MC type carbides, both as rounded carbide particles within the grains and as angular or continuous carbides at prior austenite grain boundaries.

Coarse M_6C eutectic grain boundary carbides and rod like M_2C carbides were produced by over sintering at excessively high sintering temperatures. Table 2.2 characterized the different types of complex carbides normally found in HSS.

Table 2.2: Complex carbides description (Othman,1998).

Carbide Types	Description
*M ₆ C	Nominal composition is FeW ₃ C/Fe ₄ W ₂ C or Fe ₃ Mo ₃ C/Fe ₄ Mo ₂ C in form of complex fcc. W and Mo are interchangeable. Cr and V can dissolve in as a substitution for Fe and Co. Hardness of this carbide is around 1200Hv. This carbide forms during cooling after sintering. This due to the fact that it is almost completely dissolved at the sintering temperature either in solid solution or in the liquid phase. This carbide tends to be blocky and coarsens rapidly if the sintering temperature is too high. It is not deleterious to impact strength in the same way as M ₂ C carbides.
*MC	A vanadium-rich monocarbide in form of fcc with compositions ranged from VC to V ₄ C ₃ . Hardness is around 1800Hv. Vanadium could be replaced with Fe, Cr, Nb or Ti to form other kinds of MC carbides with different properties. It is also capable of dissolving limited amount of W and Mo. This carbide exists in two forms: the first forms are blocky carbides formed during atomization , and in the second form thin grain boundary film type carbide formed during the solidification of the liquid phase during sintering.
*M ₂ C ₆	It is formed by W or Mo as W ₂ C or Mo ₂ C in form of hexagonal closed pack carbides. Both are usually decomposed on cooling and do not occur in room temperature within HSS because the M ₂ C will transform to M ₆ C + MC upon cooling. Hardness is about 1900Hv. This carbide may form in a limited number of alloys during both atomization and sintering. It is particularly deleterious as exists in the form of colonies of thin plates, which form either as grain boundary networks or lie even within grains, thus catastrophically reducing impact strength.
*M ₂₃ C ₆	An example of this carbide is Cr ₂₃ C ₆ . it is a fcc carbide and capable of dissolving some Fe, W, Mo and V. Hardness is around 1400Hv.
M ₃ C	This is Fe ₃ C,cementite. Hardness is about 800 Hv. It can also be

found in other carbon-contained steels.

*M refers to a metallic element which forms a carbide. In general the carbide are complex. For example the M_6C carbide found in an M2 type high speed steel has been reported to consists of 36 wt% Fe, 2 wt% C, 35 wt% W, 20 wt% Mo, 4wt% Cr and 3 wt%V.

2.8 Camshafts

A camshaft is simply a shaft on which cams are mounted. The camshaft is mounted in bearings in the lower part of the cylinder block in most in-line engines. In a few engines it is located on the cylinder head.

A camshaft is responsible for opening the valves. Camshaft has a number of cams along the length, two cams for each cylinder, one to operate the inlet valve and the other the exhaust valve. In addition, the camshaft has an eccentric to operate the fuel pump and a gear to drive the ignition distributor and oil pump. Figure 2.12 shows the camshaft and cams (cam lobes) location.

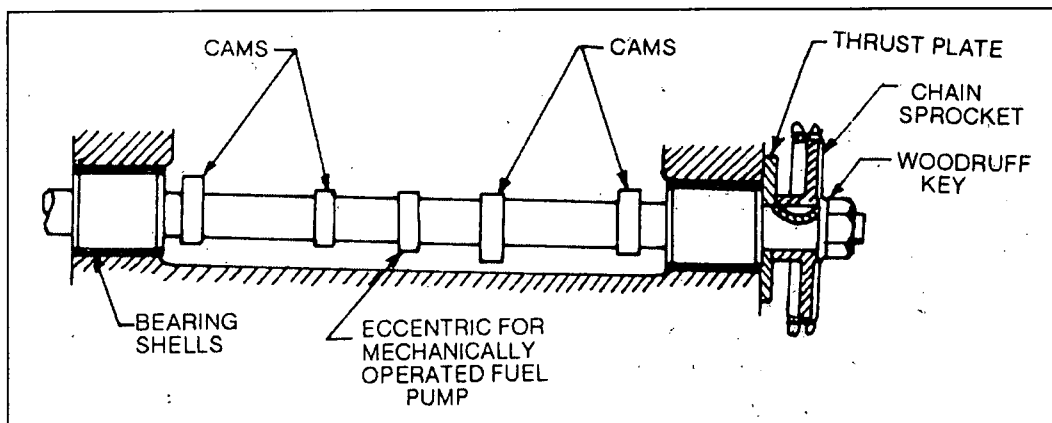


Figure 2.12: Camshaft (Gupta,2001)

A cam is a device that changes rotary motion of the camshaft into linear motion of the follower or lifter. The cam has high spot or lobe. The follower riding on the cams will move away from or toward the camshaft as the cam rotates (see Fig.2.13).

The purpose of the cams and their shaft is to actuate and control the opening and closing intervals of the inlet and the exhaust poppet valves relative to each piston position along its respective stroke.

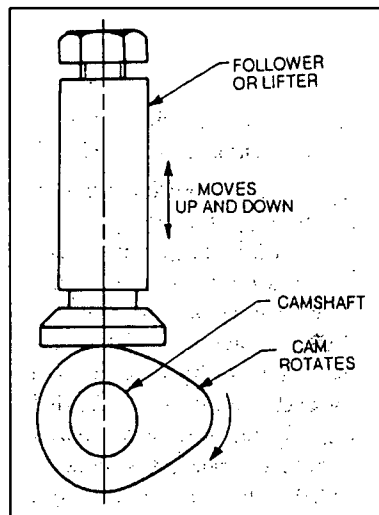


Figure 2.13: Cam and follower (Gupta,2001)

The term cast iron, like the term steel, identifies a large family of ferrous alloys. Cast irons are multicomponent ferrous alloys. It is also regarded as the most complex alloy, caused by its wide range of composition and the variety of structures that can be obtained.

Conventional camshaft reported by Shigley and Mischke (2001) is produced through sand casting technique. Sand casting is the basic low-cost process, and economically for production in large quantities with practically no limit to the size, shape or complexity of the part produced.

In sand casting, the cast is made by pouring molten metal into sand molds. A pattern is constructed of metal or wood, is used to form the cavity into which the molten metal is poured. Recesses or holes in the casting are produced by sand cores introduced into the mould (Michalski et.al., 2000).

Michalski et. al. (2000) also reported that ductile or nodular cast iron is the most widely used camshaft materials. This is because it has a very low cost, easily cast in large quantities, and easy to machine. The principal nodular graphite is to increase the toughness as well as increased the strength in tension.

However, nodular iron has a compressive strength higher than the tensile strength although the difference is not very high. Ductile iron is made by adding MgFeSi to the melt and since magnesium boils at this temperature, it is necessary to alloy it with other elements before it is introduced.

The resultant alloy is composed of pearlite, ferrite and graphite and under certain condition than pearlite may decompose into graphite and ferrite. The resulting product then contains all ferrite and graphite. The graphite in the form of thin flakes distributed evenly throughout the structure and darken the materials (Key to Steel, 2003).

The formation of stable or metastable eutectic is a function of many factors including the nucleation potential of the liquid, chemical composition, and cooling rate. A high graphitization potential will result in Fe with graphite as the rich C phase, while a low graphitization potential will result in Fe with iron carbide.

Graphite in cast iron is such an obvious and dominating phase. The amount, distribution and shape of the graphite phase have always been regarded as the governing factor in cast iron solidification. The sharp pointed graphite flakes contribute to characteristic brittleness in gray iron (Key to Steel, 2003).

Shigley and Mischke (2001) mentioned that casting quality issues that commonly occurred are such as high porosity and inclusion, extensive flat surfaces are prone to sand expansion defects, rough grainy surface, shrinkage and distortion during cooling, moulding sand must be carefully conditioned and controlled and materials strength is inherently poor.

The nodular iron castings are widely used for machines tool bodies, automotive cylinder blocks, heads, housings, camshafts, fly-wheels, pipes and pipe fittings (Shigley and Mischke, 2001).

2.9 Summary of the Literature Reviews

This chapter has extensively covered the scientific explanation with regards to joining techniques available in PM especially sintered bonding, PM characterization and process parameters, high speed steels, cast iron material properties and also a brief explanation on camshaft mechanism and applications. This literature review will provide a foundation and guidance in completing the following steps involves in this research.

CHAPTER THREE

METHODOLOGY

3.1 Material

Three powder types were used namely M3/II HSS, Cu, P and solid cast iron camshaft (CI). The cast iron was taken from the actual camshaft from Proton's car model 1.3 Saga. The suppliers of powder and CI used are given in the Table 3.1.

Table 3.1: Details on the material background

Material	Manufacturer
M3/II Powder	Hoganas Ltd. (UK)
Cu Powder	Alfa Aesar (USA)
P Powder	Alfa Aesar (USA)
Solid CI Camshaft	Proton

3.1 Material Characterization

Material characterization is important in order to know the composition of each element, as it will influence the material properties of the sample and prototype produced. Figure 3.1 shows the material characterization flow involved in the experiment.

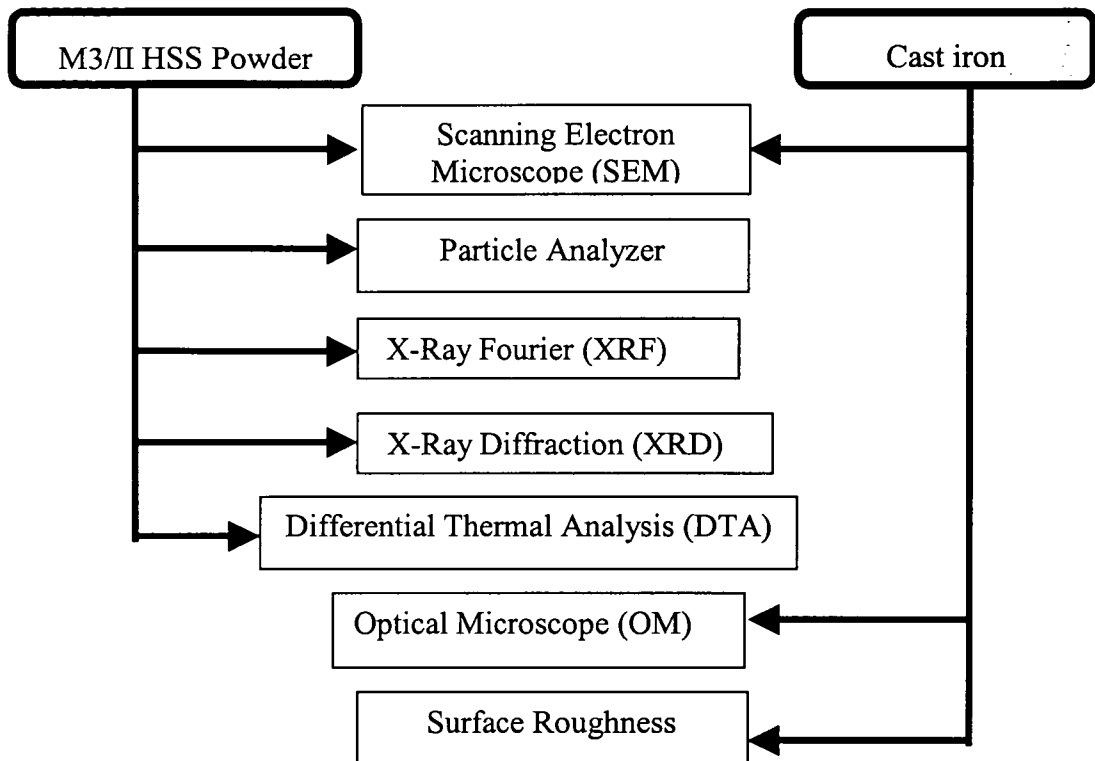


Figure 3.1: Material characterization flow involved in the study

3.2.1 Powder Particle Shape

The particle shape was identified using Scanning Electron Microscope (SEM) Leo Model. The powder was dispersed on the double sided carbon tape and placed on the stage inside the chamber using the holder. The analysis was done under vacuum atmosphere. High magnifications of relevant powder particles micrographs were produced.

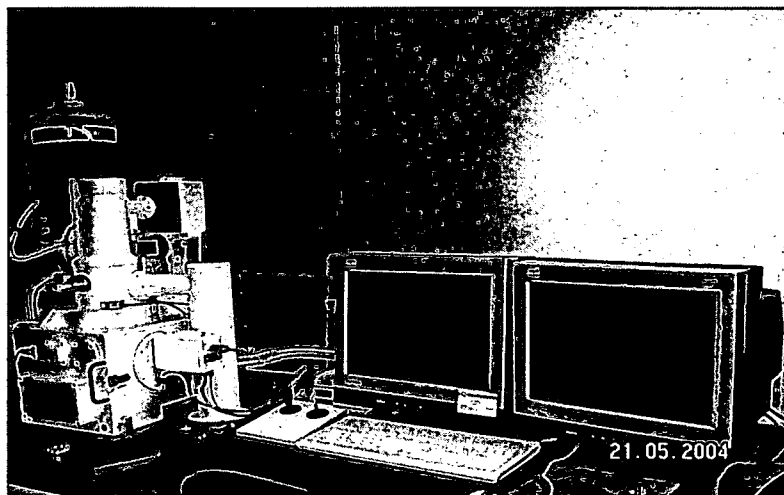


Figure 3.2: SEM and EDX

3.2.2 Powder Particle Size

Powder particle size is a determination of the dimensions of a powder particle. It is important to know the particle size as the driving force for agglomeration becomes larger as the particle size increase.

Particle size analysis for M3/II HSS powder was done using the Honeywell Microtac X100 particle size analyzer. This analysis is based on light scattering. Size determination is based on a discontinuity in the fluid stream due to the presence of the particles. The particles were soaked in distilled water and then dispersed in front of a light (laser) detector system. The data relating to particle size are collected using a photodiode detector array. The angle of light scattering varies inversely with the particle diameter. A computer then analyzed the intensity versus angle data, which will determine the particle size distribution.

Cu and P powders, size were obtained from the Material Safety Data Sheet (MSDS) given by the supplier.

3.2.3 Composition

The chemical compositions of M3/II HSS powder and CI were analyzed quantitatively and qualitatively using the EDX (attached to the SEM as shown in Fig.3.2). The procedures for EDX are similar to SEM except it use a higher electron capacity and the liquid nitrogen to cool down the probe during analysis.

XRF is another method of obtaining the materials proportion and identify the major elements in the M3/II HSS base powder. The M3/II HSS was compacted using hand press at 100kN to produce a cylindrical compacts with 40mm diameter and 5mm thickness (size of holder). Then it is placed in side the machine using the standard holder. The Bruker S4 Pioneer XRF (see Fig. 3.3) machine was used in this study.

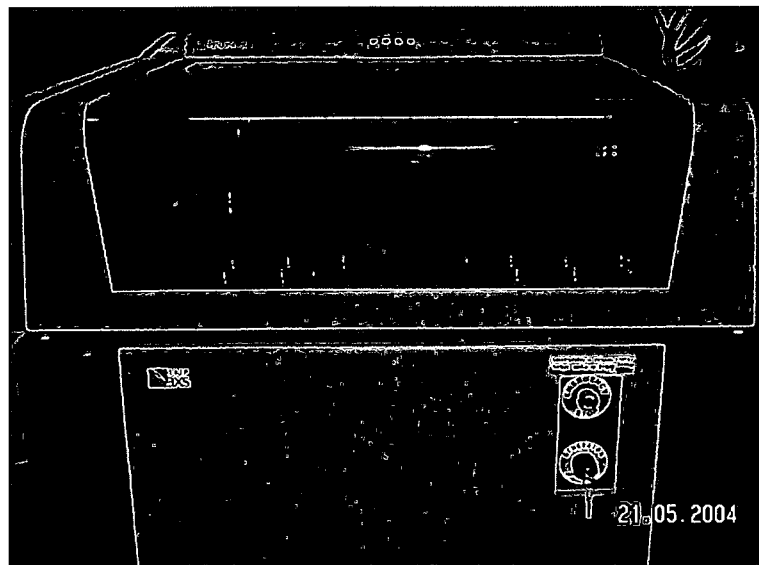


Figure 3.3: XRF Machine

3.2.4 Phase Constitution

The atomic structure and phase of the materials will affect the inherent sintering rates. The phase constitution in the M3/II HSS and solid CI were examined using X-ray diffraction (XRD) Model Bruker as shown in Fig. 3.4.

The M3/II HSS powder was placed onto the holder. Then it was pressed and swiped slowly to remove excess particles as well as to make a uniform layer. The analysis start at 5° and end at 80° with diffraction step at 0.040° , each angle was held for 5 seconds.

Rotating of the beam changes the angle of incoming radiation and produces different sets of spots and eventually produces a complete diffraction pattern that is used to determine the distances and angles within the lattice. The result will show the different diffraction line and concentration referring to the phase.



Figure 3.4: XRD Machine

3.2.5 Thermal Analysis

Thermal analysis is important in order to get the qualitative and quantitative analysis. Differential Thermal Analysis measurement is a standard method of determining transformation temperatures of materials. Differential Thermal Analysis plot provides the information on exothermic and endothermic reactions taking place in the sample. Accurate interpretation of the measurements is essential to indicate the location of equilibrium phase diagram boundaries (Boettinger and Kattner, 2002).

For M3/II HSS, the smearing effect of the particular, the DTA heat flow at different heating and cooling rates is demonstrated for various solidification path features. The DTA peak during melting, often selected as liquidus temperature experimentally.

Differential Thermal Analysis curves calculated for freezing with dendritic growth due to supercooling quantify the errors associated with of the determination of the liquidus temperature on cooling. The analysis was done in Argon gas atmosphere with 40 ml/min flow using DTA Setaram Model. The heating rate is 5°C/min and heated from 600°C to 1200°C.

Thermogravimetric Analysis (TGA) was done in conjunction with the DTA. Thermogravimetric Analysis is a branch of thermal analysis that examines the mass change of a sample as function of temperature. Thermogravimetric Analysis able to characterize the decomposition of materials (weight loss) detected from the DTA (Metler Toledo, 2005)

3.3 Sample Preparation

Three batches of sample were prepared that are the M3/II HSS alone, M3/II HSS with Cu and M3/II HSS with 9wt.%Cu and 1wt.%P. The process flows for powder and cast iron sample preparation are as indicated in Fig. 3.5

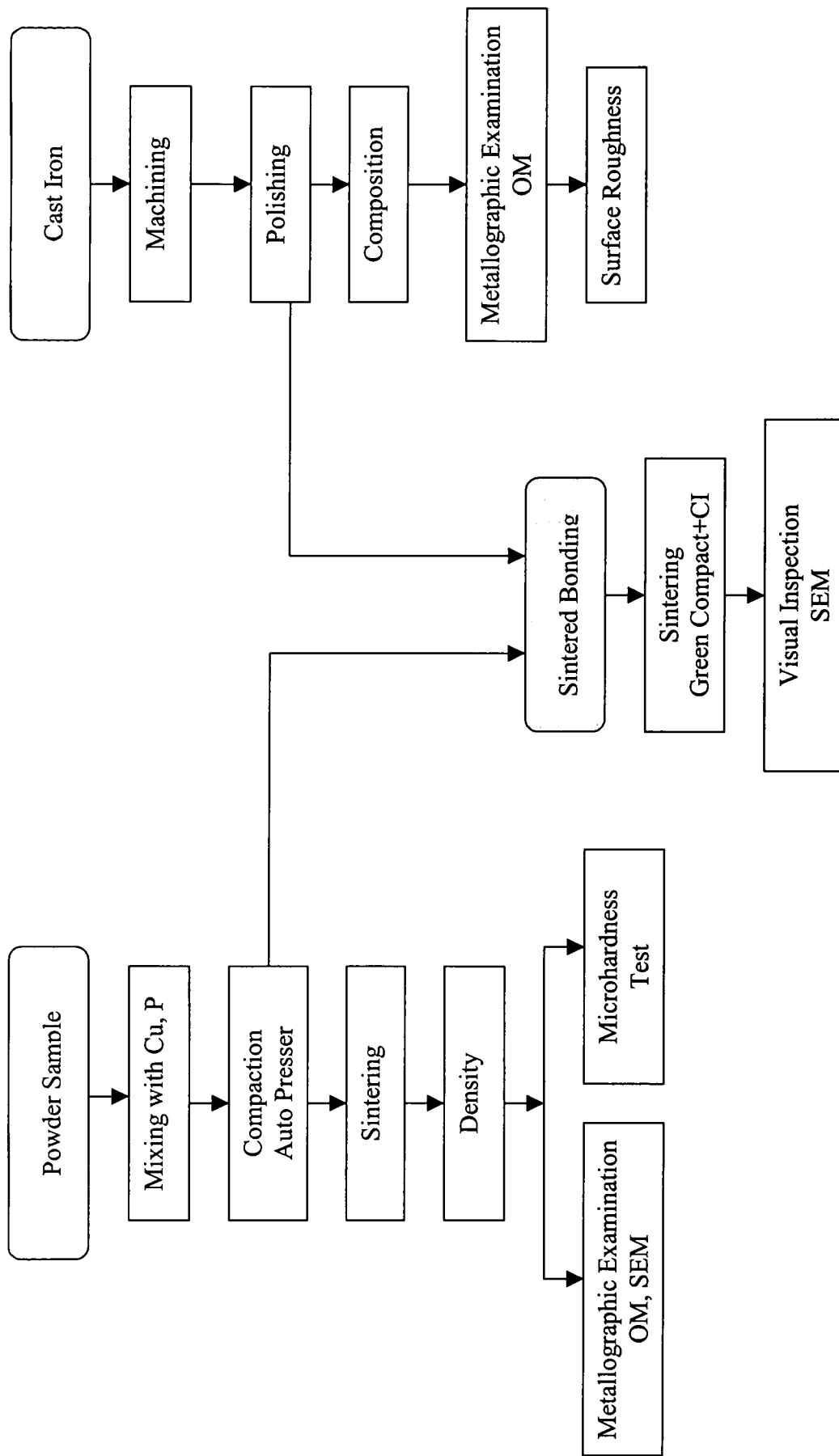


Figure 3.5: Process flow for powder sample preparation and evaluation.

3.3.1 Powder Sample

3.3.1.1 Weighing and Mixing

The powder were divided into three batches that consists of M3/II HSS, M3/II HSS-(5, 7, 8, 9, 10, 15 wt/%)Cu and M3/II HSS-9wt.%Cu-1wt.%P. The measurement was done using the Metler Toledo (500g) weighing machine (as shown in Fig. 3.6).

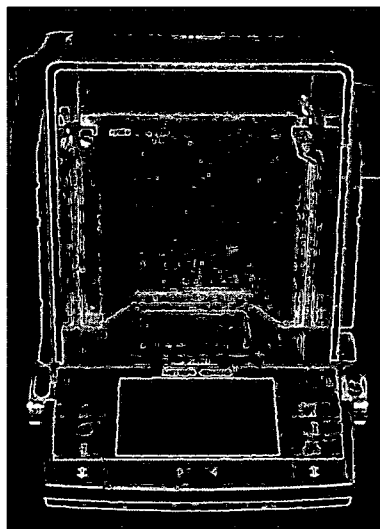


Figure 3.6: Weighing Machine

In order to get a uniform distribution of each element, the mixing process was done in a ball mill model U.S. Stoneware. The mixture powder was put in the bowl with a few ball mills and the milling process done for 30 minutes for each composition. Binder was not added during this the mixing process (refer to Appx. A for pellet preparation).

Rotation of the jar will carry the balls to the top of the jar before falling back down the jar side. The objective of milling is to mixing and blending the mixture uniformly in order to get a homogenous distribution of elements (El-Eskandarany, 2000). Figure 3.7 shows the ball milling machine.



Figure 3.7: Ball Milling Machine

3.3.1.2 Compaction

The prepared powders mixtures were cold compressed for using the Auto Presser Model Carver (Fig. 3.8) to form simple cylinders ($\text{Ø}13\text{mm} \times 4\text{mm}$) with pressures of 350 MPa. The pressure was held for 2 minutes for each compaction. After each compaction, punches are cleaned using soft cloth to avoid any powder left inside (refer Appx. B for compaction pressure calculations)

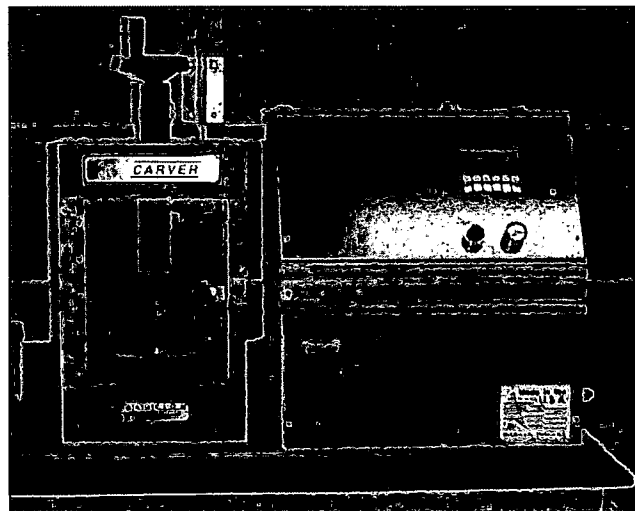


Figure 3.8: Auto Presser

3.3.1.3 Sintering

Sintering is the process whereby powder compacts are heated so that adjacent particles fuse together, thus resulting in a solid article with improved mechanical strength compared to the powder compact. The evolution of compact strength starts with the sintering process. Theoretically, the strength properties are assessed accounting for hardening due to the growth of the particle necks during sintering and softening due to the increase of the temperature.

The base M3/II HSS powder was sintered in furnace atmosphere and gas atmosphere in order to see the differences between the two sintering environment. The process was done using a Lynx Model furnace (see Fig. 3.9) in argon atmosphere. Sintering the green compacts were performed at 800, 900, 1000 and 1100°C. Heating and cooling condition were identical for all samples. The heating rate was kept at 5°C min⁻¹ followed by a natural furnace cool after the sample being held for 30 minutes. After sintering, weight loss and shrinkage of the samples were determined. Due to high affinity for oxygen by Cr, V and W the sintering for the mixed powder must be carried out in the controlled atmosphere (Sustarsic, 2003).

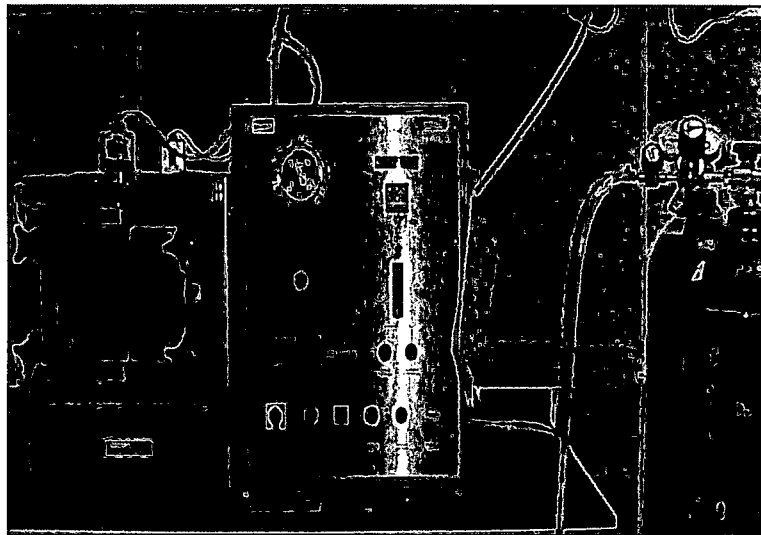


Figure 3.9: Lynx Gas Furnace

3.3.1.4 Sintered Density

Bonding of the particles together results in an increase in the density of the part and lead to the process that is called densification. Density measurement to asses sintering behaviour was carried out by lacquer-coating the sample to seal surface porosity. Metler Toledo weighing machine was used for this purpose (refer to Appx. H).

3.3.1.5 Grinding and Polishing

Standard metallographic examination procedure was carried out in this study. Sample was mounted, grinded using 400, 600, 800 and 1200 grid of silicon carbide paper and polished using 6 μ m and 3 μ m diamond paste sized. Once the sample achieved mirror finish surface etching was done using Nital solution to reveal the metal structure. The study of the structure and the properties of metals and alloys require a perfect grinding and polishing of the specimen. A good interpretation needs an excellent image quality and the quality of the observation shall depend on those stages. Figure 3.10 shows the grinder and polisher machine.

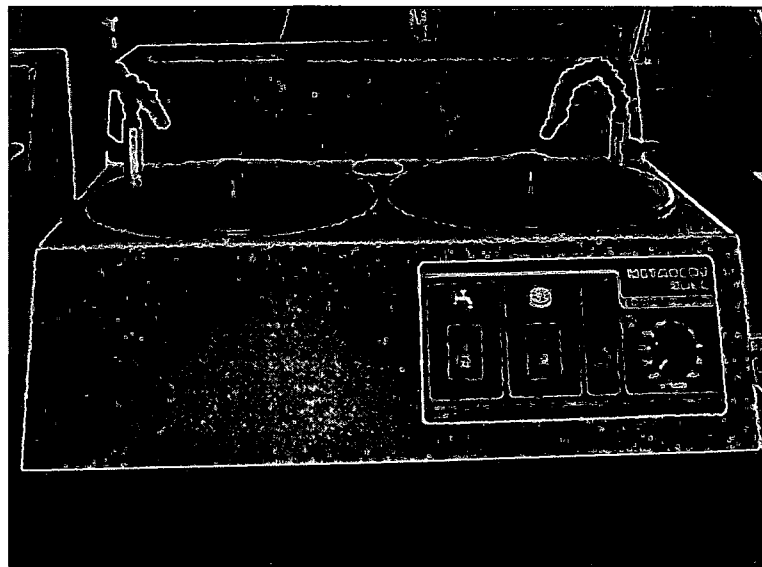


Figure 3.10: Grinder and Polisher

3.3.1.6 Metallographic Examinations

Metallographic evidence was used to support results from the densification and hardness tests. Optical microscope JVC Model (as shown in Fig. 3.11) was used throughout this metallographic study. The changes of the grain size, pores shape and distribution of copper and phosphorus was observed. In order to further investigate the influence of the substituents on microstructure evolution, sintered samples microstructure was also examined using SEM. Cast iron microstructure also being observed using OM in order to identify the matrix existed.

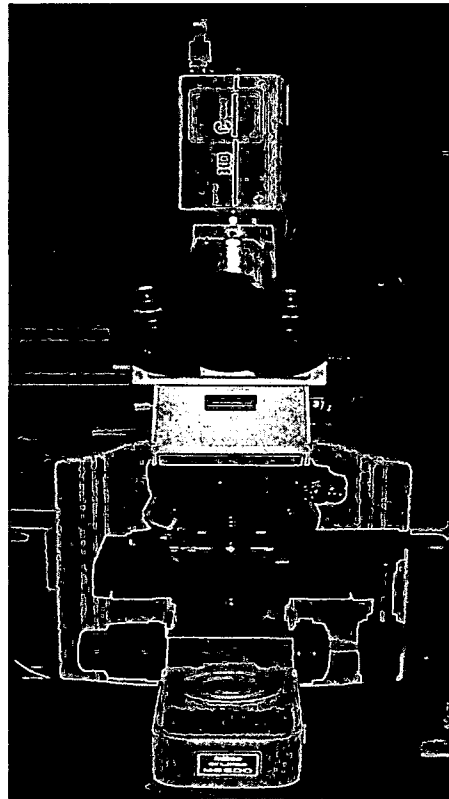


Figure 3.11: Optical Microscope

3.3.1.7 Microhardness

Hardness is the resistance of the material to indentation, which is a qualitative indication of its strength. The hardness values obtained are useful as an indicator of materials properties and expected service behavior. In this study, all hardness testing for the sintered compact was done using Vickers Microhardness Indentec Model (refer to Fig.3.12). The term microhardness testing usually refers to static indentations made with loads not exceeding 10N. The indenter is the Vickers diamond pyramid.

The surface being tested generally a metallographic finish (taken from the metallographic study samples) because in microhardness testing the smaller the load used, the higher the surface finish required. In this case, 300g load being applied on the matrix. The size of the diamond indentions was measured using the microscope attached. Correlating hardness with depth of penetration allows the hardness number to be conveniently shown on a digital display.

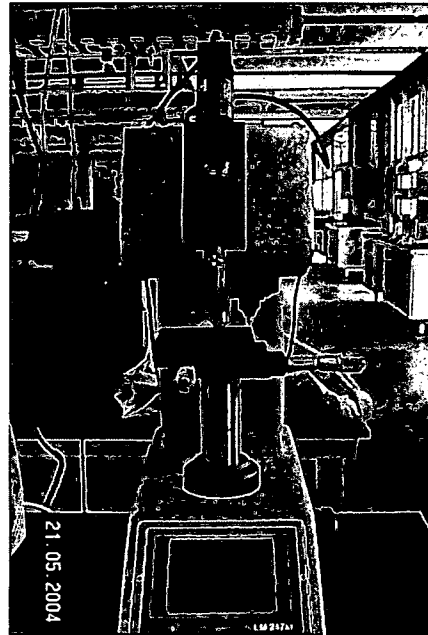


Figure 3.12: Vickers Microhardness Machine

3.3.2 Cast Iron Sample

3.3.2.1 Machining

The solid cast iron camshaft was cut using the Abraser Model cutter into small pieces sized of 10mm length, 4mm width and 2mm height for sintered bonding attempt. The same cutter also used to cut the sintered compacts before proceed with mounting process. Figure 3.13 shows the abrasive cutter used.

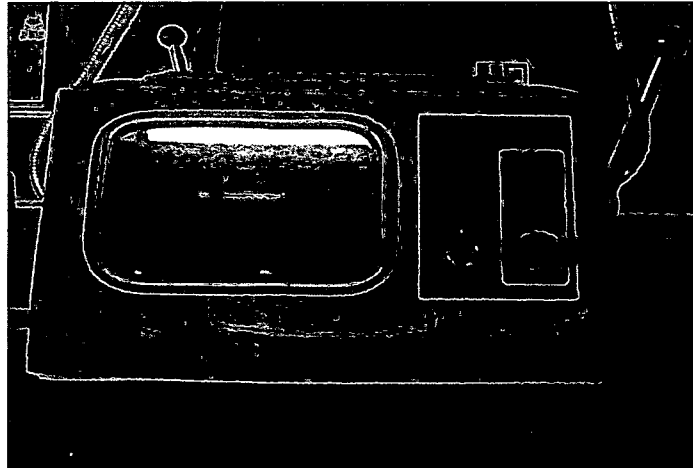


Figure 3.13: Abrasive Cutter

3.3.2.2 Polishing

The machined CI sample was polished using $6\mu\text{m}$ and $3\mu\text{m}$ diamond paste size in order to remove the any oxide or contamination. This polishing process would able to reduce the surface roughness of the CI sample from the machining action.

3.3.2.3 Composition

The polished CI sample was analyzed using the SEM assisted with EDX (SEM/EDX) machine in order to get the element composition. The chemical composition of the CI sample was analyzed by using the SEM/EDX machine.

3.3.2.4 Surface Roughness

After the machining process and again after the polishing, the surface roughness of the cast iron piece was checked using the Perthometer Surface Profiler (see Fig. 3.14) Roughness of the cast iron is significant interest because it is the roughness of a surface (given reasonable waviness and form error) that determines its friction in contact with another surface. The roughness of a surface defines how that surfaces feels, how it behaves in a contact with another surface and how well it will retain lubricant (liquid phase).

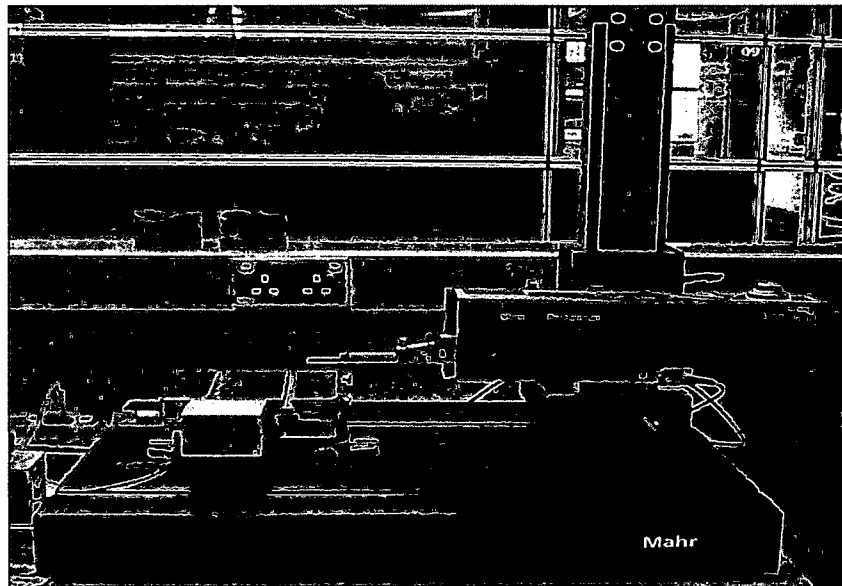


Figure 3.14: Surface Profiler

3.4 Sintered Bonding

Cast iron sample was placed at the bottom of the mould before it is compacted together with the mixture of M3/II HSS-9wt.%Cu-1wt.%P powder at 350 MPa. Then the compact was sintered at 1100°C in argon gas atmosphere (held for 30 minutes) and followed by furnace natural cooling. The sintering temperature of 1100°C was chosen as the bonding temperature due to occurrence of various liquid phase which can promote the sintered bonding. Identification of possible sintered bonding formed was performed by using SEM.

CHAPTER FOUR

RESULTS AND DISCUSSION

4.1 Powder Characterization

4.1.1 Powder Particle Shape

Powder particle shape of M3/II HSS base powder and P is in irregular and rounded irregular with rough surface (see Fig. 4.1 (a) and (c)). Based on these micrograph results it can be depicted that those powder were produced by the water atomization process. Whereas the rounded and angular shape powders are normally produced from gas atomization (see Fig. 4.1(b)).

The irregular and rough surface particle normally influence significant agglomeration problems for alloying elements with large different in size range, that could resulting in poor dispersion. The spherical copper in the other hand is effective in deagglomerating and smoothing the powder surface and subsequently will help the powder to attain a high packing density.

Figure 4.1(d) shows the powder segregation M3/II HSS base alloy while Fig. 4.1(e) showing the homogenous distribution of elements in M3/II HSS with 9wt%Cu-1wt%P loose powder mixture after milling process.

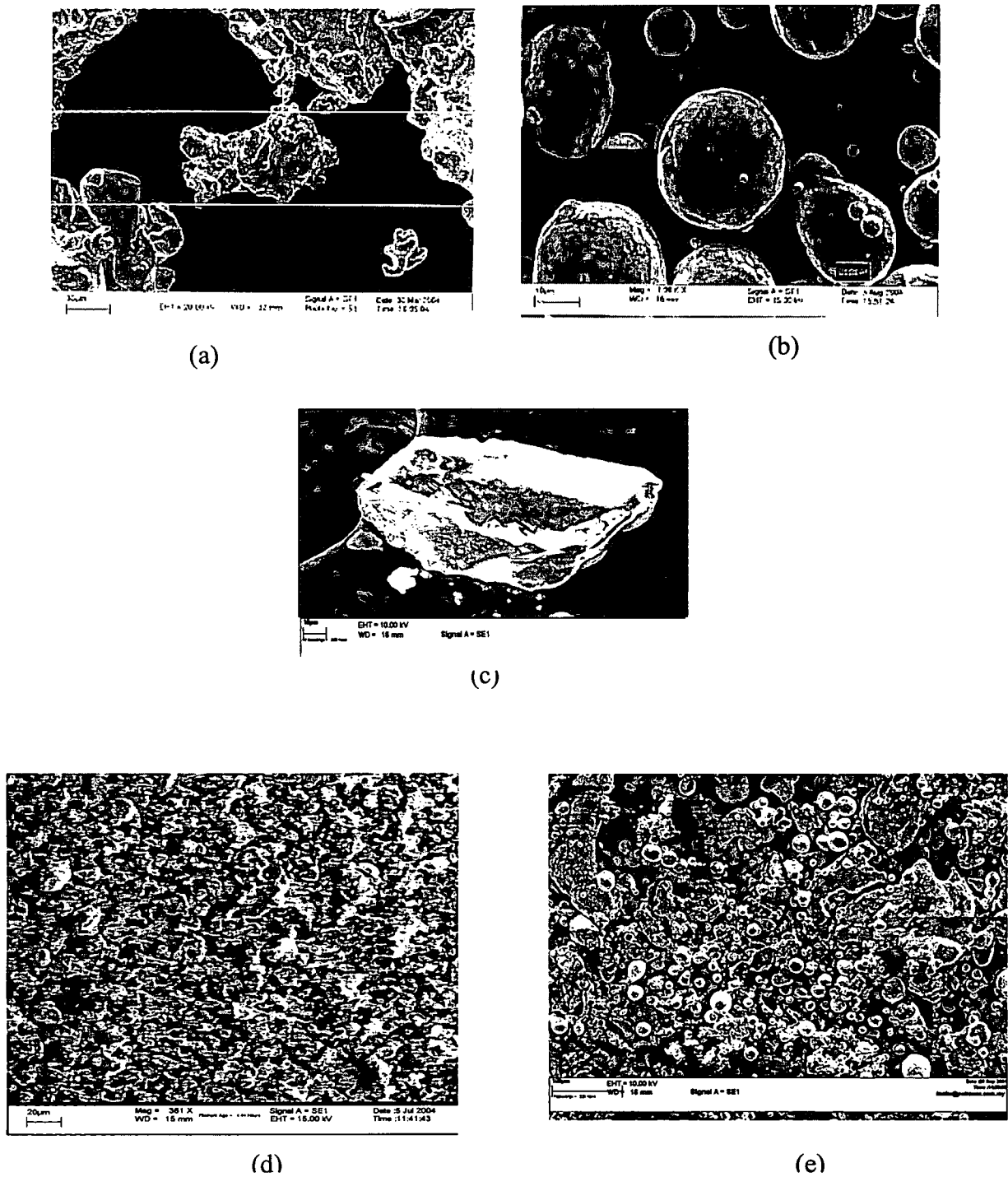


Figure 4.1: Scanning Electron Micrograph of (a) M3/II HSS base powder (Magnification 1.04kX); (b) Copper powder (Magnification 1.08kX); (c) Phosphorus powder (Magnification 1.3kX); (d) M3/II HSS loose powder (Magnification 351X); (e) Mixture of M3/II HSS with 9wt%Cu and 1wt%P powder (Magnification 500X)

4.1.2 Powder Particle Size

Particle size analysis was carried out on a Honeywell Microtrac-x100. Figure 4.2 shows the particle size distribution for M3/II HSS after 30 seconds of analysis. From the cumulative plot, 50% of the particles are 74 μm in diameter and 98 μm width. It was also observed that the diameters of the smallest particle are 28 μm and the largest are 187 μm . Refer to Appx. C for more details on the result analysis.

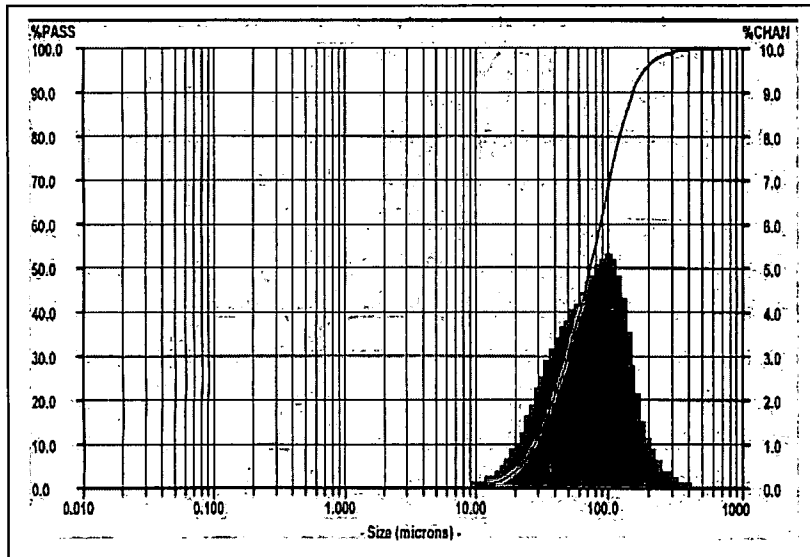


Figure 4.2: Particle size distribution of M3/II HSS powder

Referring to Certificate of Analysis given in the Material Safety Data Sheet (MSDS) in Appendix C (1) and (2), the density of the copper and phosphorus powder is 8.94 gcm^{-3} and 2.34 gcm^{-3} respectively. Table 4.1 shows summarize the size range for the copper particle resulted from sieving analysis done earlier by the manufacturer. The number of wires per inch on the screen determines the mesh size. The designation -100 +200 mesh indicates that the powder passed through a 100 mesh size opening but not a 200 mesh size opening (German, 1998). Almost 50% of the copper powder is sized below 45 μm and 99% of phosphorus smaller than 75 μm that passed through the 100 mesh size. The small size powder basically will fill the spaces or pores between the large M3/II particles. In turn, it would improve the packing density in the compact.

Table 4.1: Particle mesh size analysis for Cu

Powder	Mesh Size	Opening (μm)	% of Particle Remain
Cu	+100	150	0.0
	-100 + 200	75-150	21.2
	-200 + 325	45-75	28.9
	-325	45	49.9

4.1.2 Composition

As indicated in the Table 4.3 the M3/II HSS powder consists addition of strong carbide forming elements such as molybdenum, tungsten, vanadium and chromium which effective in providing abrasion and wear resistance. Molybdenum is the major alloying elements followed by tungsten. Both elements are strong carbide formers and the principal carbide is M_6C which is good for wear resistance. Vanadium in other hand will produce extremely hard particles of MC type. Chromium is likely to form carbides such as M_{23}C_6 and M_7C_3 and beneficial in improving the hardness and the scaling resistance (Llwellyn and Hudel, 1998). Refer to Appx. E for more details on the XRF result analysis.

Table 4.2: M3/II HSS base powder composition from XRF analysis

Element	Weight %
Iron (Fe)	75.4
Molybdenum (Mo)	7.69
Tungsten (W)	6.76
Chromium(Cr)	4.32
Vanadium (V)	3.77
Cobalt (Co)	0.415
Silocon (Si)	0.257
Nickel (Ni)	0.186
Copper (Cu)	0.180

4.1.4 Phase Constitution

The XRD patterns in Appx. F shows the differences in the relative concentration of the observed base powder that was analyzed at room temperature (27°C). Referring to the diffraction lines pronounced, M3/II HSS base powder comprised a dominant concentration of Fe in ferrite phase. Among other phases obtained by the XRD analysis are Nickel Molybdenum carbide ($\text{Ni}_3\text{Mo}_3\text{C}$), Chromium Iron Nickel (Cr-Fe-Ni) and Vanadium Carbide (V_4C_3) which fall under complex carbides group that usually present in the M3/II HSS powder. Respective intensity diffraction line for $\text{Ni}_3\text{Mo}_3\text{C}$ exceeded the measured ones for Ni-Cr-Fe and $\text{V}_4\text{C}_3\text{MC}$ phase. High concentration of $\text{Ni}_3\text{Mo}_3\text{C}$ supported the XRF result that indicates Mo as the major alloying element in the base powder. Both $\text{Ni}_3\text{Mo}_3\text{C}$ and V_4C_3 carbides were fcc that is capable of dissolving in the sintering temperature either in solid or liquid phase.

4.1.5 Thermal Analysis

During the DTA analysis, the endothermic and exothermic reaction due to the heat transformation experienced by the sample can be detected. The material phase change from ferritic to austenitic phase as the temperature increased. Melting of one elements in the sample absorb the heat where the thermal energy is used to promote the phase transformation.

Referring to the Fig.4.3, a sharp endothermic peak at 614 °C indicate the dehydration of the M3/II HSS powder where the water are evaporate or lost from the surface of the powder. The second obvious endothermic peak at 856 °C showing the dehydroxylation, that is loss of lattice water. The endothermic peaks also indicate the burnout of impurities in the sample.

The exothermic peak corresponding to the melting of the crystalline phase and also indicate the heat release due to phase transformation in the sample. A significant exothermic reaction started around 1050°C due to the formation of liquid phase which

will lead to rapid densification. Referring to the M2 HSS base metal phase diagram (refer Appx.G), large amount of liquid will continue to appear at temperature higher than 1200°C and above 1400°C the sintered sample will be distorted due to excessive of liquids. This trend corresponds to the solid state and liquid state sintering reaction in the base powder. Table 4.3, summarize the DTA peaks and possible phases occurred during the analysis.

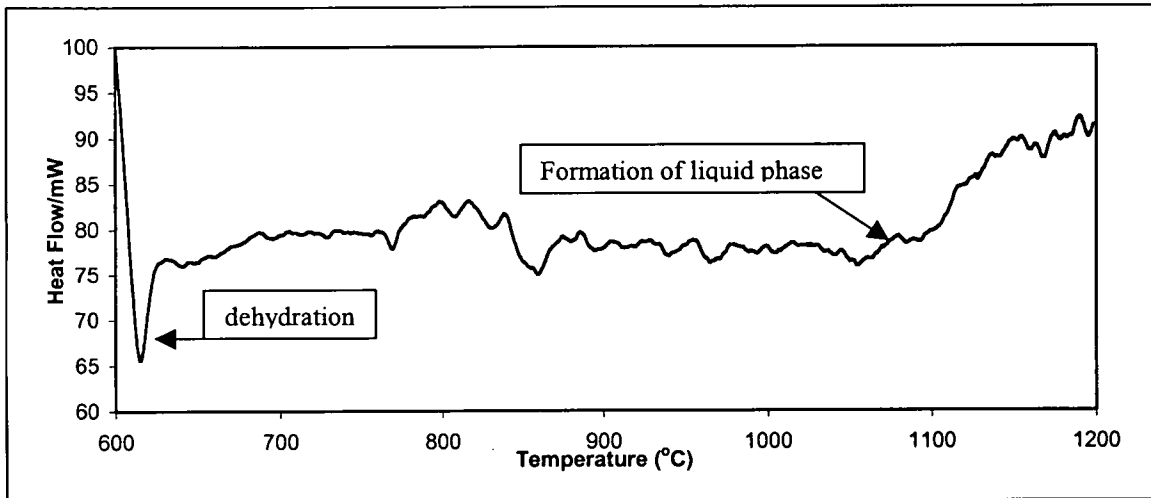


Figure 4.3: DTA peaks of M3/II HSS base powder

Table 4.3: Possible phases for DTA peaks

Peak	Temperature (°C)	Possible Phase
Endothermic	614.5	Ferrite + M
Endothermic	856	Ferrite+ M
Exothermic	1050.4	Austenite + M + Liquid
Exothermic	1175.4	Austenite + M + Liquid
Exothermic	1191	Austenite + M + Liquid
Exothermic	1198	Austenite + M + Liquid

*M refer to the complex carbides

Result from TGA (see Fig. 4.4) show (0.35 to 0.65 %) weight loss for the powder during sintering in the temperature range between 1000 to 1200°C. The accelerating weight loss in TGA similar to the phase changes as indicated in DTA plot. This weight loss can be related to deoxidation of surface oxides by carbon and due to the phase changes in the powder from solid phase to solid-liquid phase. Melting of few elements in the powder could also contribute to the weight lost.

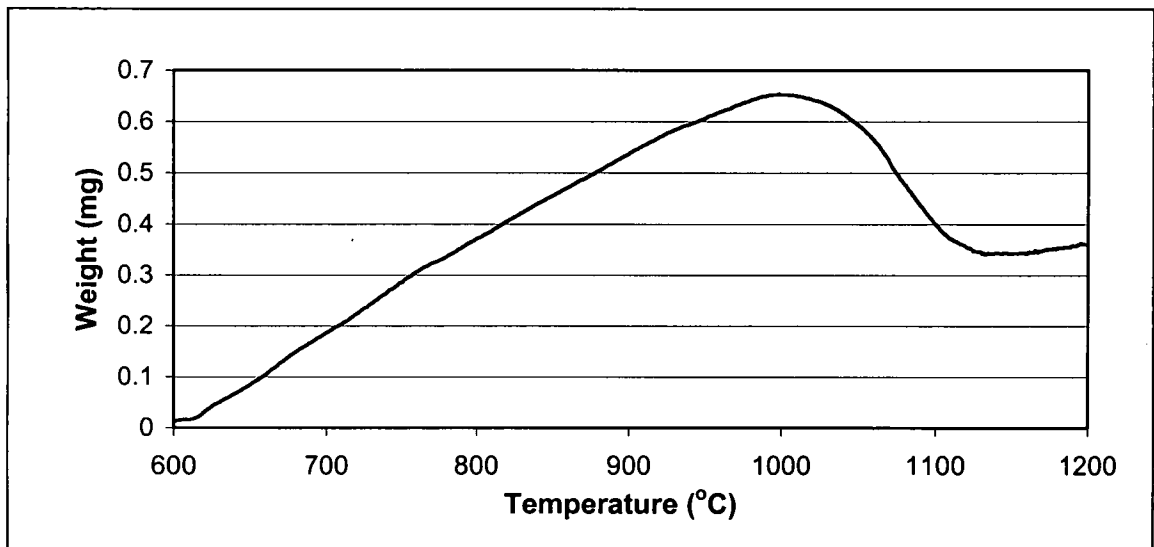


Figure 4.4: TGA Curve of M3/II HSS base powder

4.2 Sintering Evaluation

Figure 4.5 shows the sample heated under argon gas and furnace atmosphere. Compact that sintered in furnace atmosphere has a layer of oxide surrounding the steel whereas none in gas atmosphere compact. This is due to high affinity of oxygen by the alloying elements such as Cr, V and W in the base powder. The oxidation during sintering process also lead to swelling and decrease the compact sintered properties.

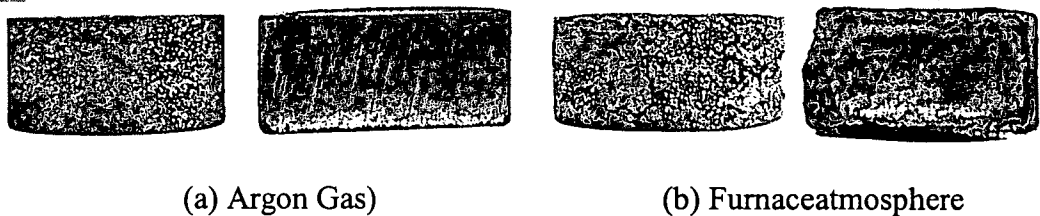


Figure 4.5: Sintered compacts in different atmosphere at 1100°C

4.2.1 Sintered Density

4.2.1.1 M3/II HSS Base Powder

The density increases as the temperature increased (see Fig.4.6). Solid state sintering played a major role in enhancing the grain growth and interparticle contact area. At 800 to 900°C, sufficient liquids phase was not present during the sintering to enhance the densification. The significant increment starts at 1000°C as the temperature moves closer to the liquidus phase (1050°C) as obtained from DTA result (refer to Appx. H for sintered density calculations example).

The green density was 4.67gcm^{-3} and the highest sintered density reached only 5.17gcm^{-3} . Density is naturally influenced by the compaction pressure. Higher density can be achieved with higher compaction pressure. During compaction, the particles slide past one another, deform and increase the surface contacts as well as minimize the pore size (German, 1994).

However, internal friction between the rough powder surface, sintering temperature and environment also influenced the low density achieved (Liu et al., 2001). An alternative to increase the density is by adding smaller size alloying elements to smoothen the rough surface and increase the interparticle contact area.

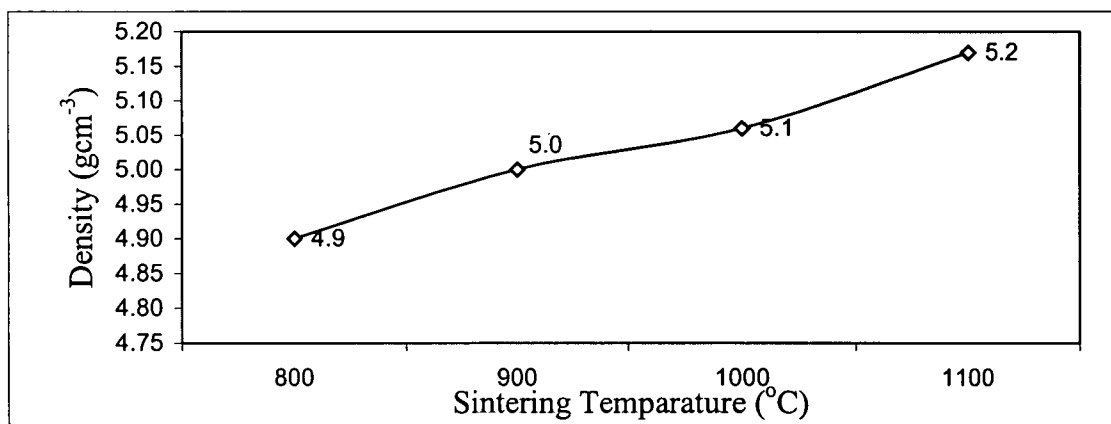


Figure 4.6: Densification of sintered M3/II HSS base powder

4.2.1.2 M3/II HSS with Cu Addition

In the densification process, microstructure development and composition controls are important. The copper particle basically filled the pores between M3/II particles and improved the packing density before and after sintering process.

During the sintering process closer to 1100°C, the alloy powders are heated to a temperature between the liquidus and the solidus. The positive influence of the Cu addition on the densification kinetics of M3/II HSS was also confirmed by the sintering experiments. Copper melting point is at 1083°C (refer to Appx. D(1)) and at 1100 °C various amount of liquid copper are present at the grain boundaries resulting in capillary forces acting on semi solid particles thereby enhancing the densification.

As the Cu composition increased from 5wt% to 9wt%, more pores are filled with Cu liquid phase, reducing the pore shape, size as well as its quantity. However, at 10 and 15wt.% addition, a different phenomena happened where the density start to decrease. Referring to Fig. 4.7, optimal composition for copper is at 9wt%, where maximum point contact between M3/II powder with one another and all of the interstitial voids are filled with small Cu particles (see Fig. 4.8). Further addition of Cu, promote agglomeration which known to decrease packing density which is a common phenomena in fine powders Zhang and German, (2001). Excess addition of Cu also lead to swelling of the compact and lower the density.

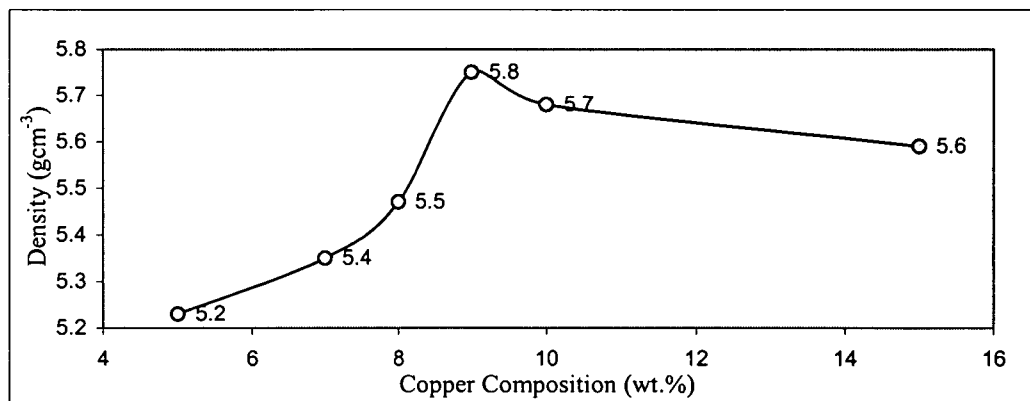


Figure 4.7: Densification of sintered M3/II HSS with Cu addition

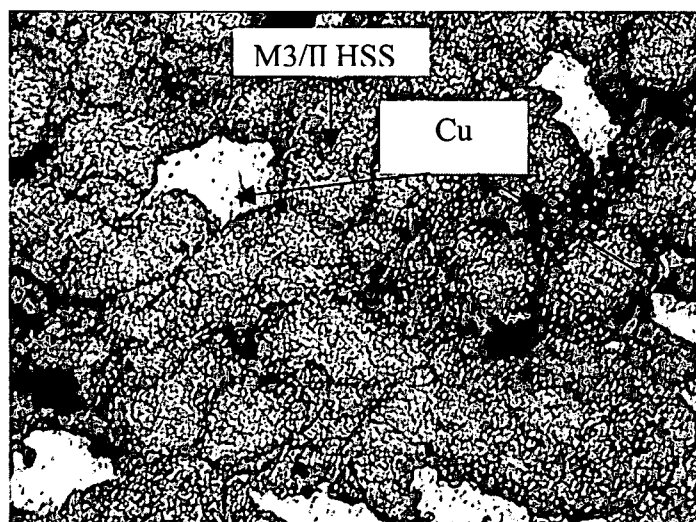


Figure 4.8: Optical Micrograph of M3/II with 9wt.%Cu (Magnification 200X)

4.2.1.3 M3/II HSS with 9wt.%Cu and 1wt.%P

Figure 4.9 shows sharp increases of densification occurred in M3/II HSS powder mixture with Cu and P. Prior to sintering process the compacts green density was 5.0gcm^{-3} . Compacts density increased up to 6.20gcm^{-3} after sintering process. The low melting point of phosphorus at 416°C (refer to Appx. D(2)) increased the densification at much lower temperature than with Cu alone.

Generally with the addition of P, it will lead to formation of an iron rich phosphide compound. Phosphorus diffuses into the iron forming a liquid phase which assists liquid phase sintering. Pools of copper were left as residual product as Cu has a limited solubility in iron and provide sufficient liquid phase at the grain boundaries that act as a medium for the metallic diffusion take place.

The secondary rearrangement of particles starts because of the high capillary forces and the densification controlled by viscous flow occurs very quickly. Liquid phase from the base metal reactions were involved especially at 1050°C as indicated in the DTA result and mixed with the liquid phase from Cu and P.

The liquid phase provides faster atomic diffusion compared to solid state sintering. The capillary pressure due to a wetting liquid gives rapid compaction densification without the need for an external pressure.

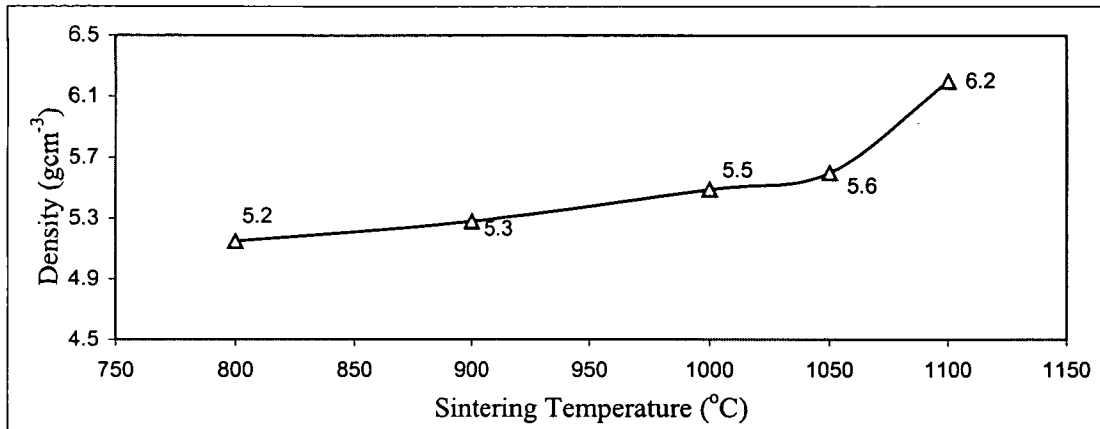


Figure 4.9: Densification of sintered M3/II HSS with 9 wt.%Cu and 1wt.%P

4.2.2 Microhardness of Sintered Sample

4.2.2.1 M3/II HSS Base Powder

Figure 4.10 shows increased hardness of sintered M3/II HSS with the increment of temperature. This result also indicated that the strength of the compact are increased. Porosity has a major affect on the hardness behavior. High stress concentration during indentation near pores location is responsible for localized slip leading to crack initiation (refer to Appx.I for hardness calculations example).

The increasing hardness from 138 to 466Hv is due to the growth of interparticle necks during sintering. The grain growth would reduce the porosity as the temperature increased and strengthening the compact.

Carbides influence mostly on the physical properties and in coherence with the matrix. The rates of carbon penetration into Fe also become more dependent on the solid state diffusion with the decreasing of porosity. Fe goes through the ferrite phase to austenite

phase transformation from 900°C to 1100°C. The transformation of Fe phase will allow more carbon and other alloying elements dissolve into the steel and hardened it (Carter, 1979).

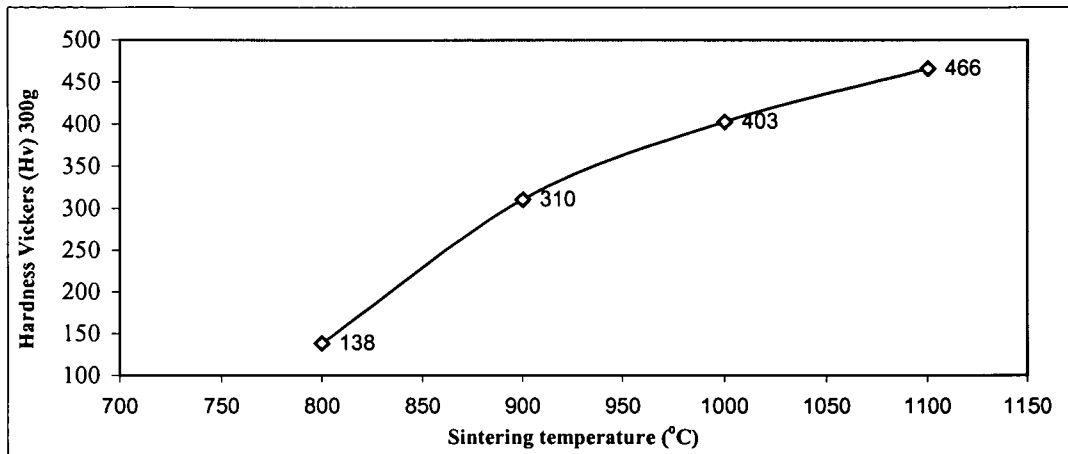
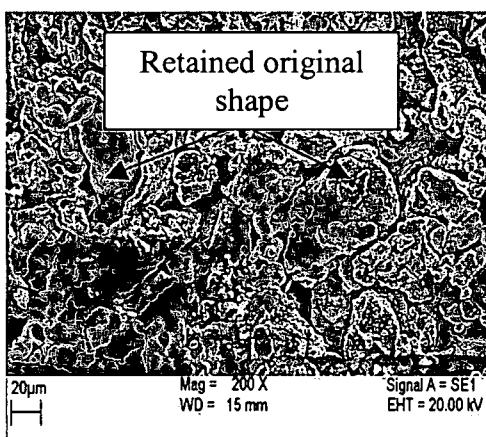
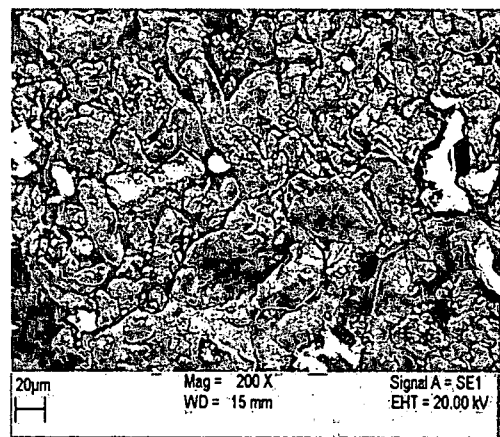


Fig. 4.10: Hardness Vickers of sintered M3/II HSS base powder

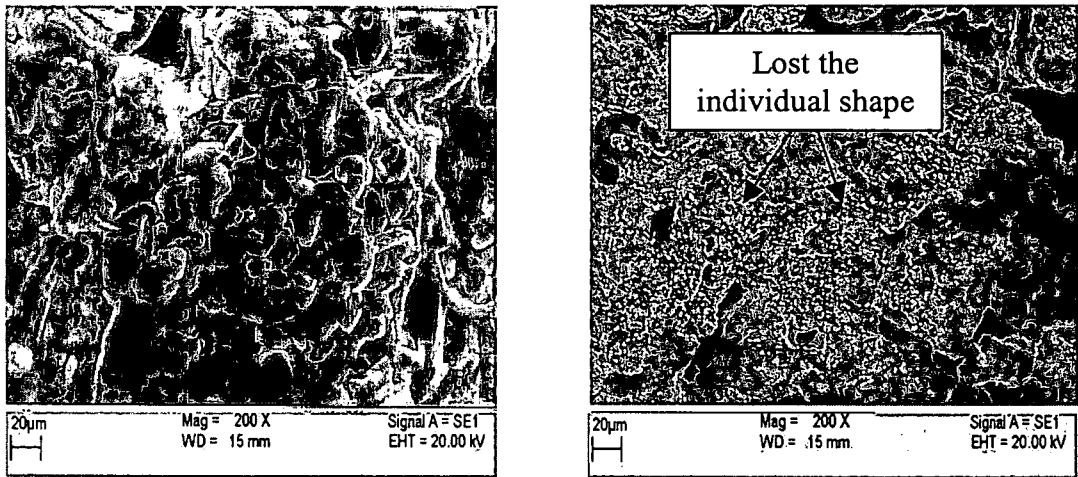
Figure 4.11 (a) shows at 800°C a large amount of pore still exist in the compact. Most of the powder particle still retains as individual particle and its original shape. Irregular and rough surface lead to low packing density because of the interparticle friction (Smith and Midha, 1997). As the sintering temperature increased the particles start to lose its rigidity and begin to increase the interparticle contact. At 1100°C, most of the particles lost its original shape and bonded together. However small amounts of residual pores still exist (see Fig. 4.11 (d)).



(a) 800°C



(b) 900°C



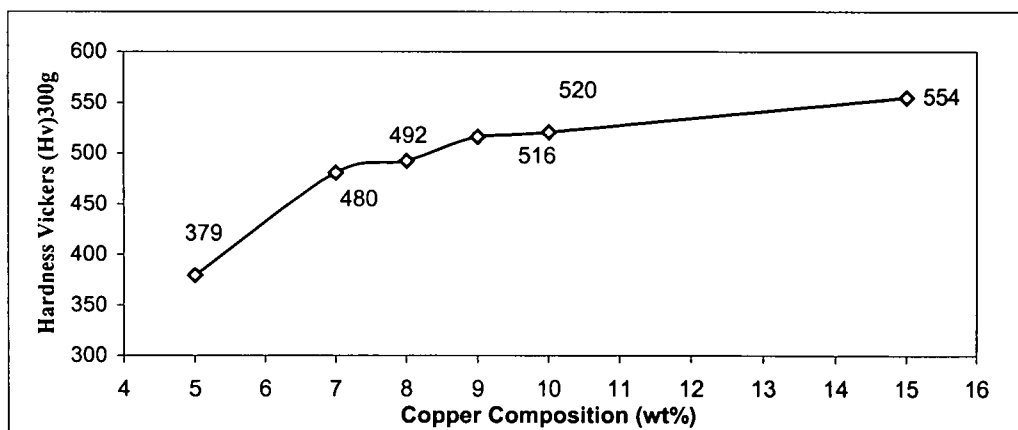
(c) 1000°C

(d) 1100 °C

Figure 4.11: Scanning Electron Micrograph of Sintered M3/II HSS Surface (200X)

4.2.2.2 M3/II HSS with Cu Addition

The effect of the copper is based on hardening the matrix. Although the sintered density start to decrease with increasing copper content (see previous Fig.4.7), the hardness still continuously increase as shown in Fig.4.12. At 1100°C, the melted of residual copper filling the pores and dissolved into the matrix. The dissolution of copper into the steel will enhance the grain growth and hardened the matrix. Although at 15wt.%Cu addition gives the highest hardness, but at 9wt.% of copper gives the highest density and it was chosen to proceed with P addition.

**Figure 4.12:** Hardness Vickers of M3/II with Cu addition

4.2.2.3 M3/II HSS with 9wt.%Cu and 1wt.%P

The plot in Fig.4.13 showing the highest microhardness value compare to the previous powder compositions. The addition of Cu and P obviously improved the microhardness and influence the accumulated strength of sintered compacts. This phenomenon is related to the strengthening of bonds between particles, softening and recrystallization of the Cu and P.

At 800°C, Cu particles begin softening but P had exhibited a liquid phase since its melting temperature is at 416°C. Phosphorus is the major particle rearrangements agent at early stage of sintering (below 800°C). The melted P would lead to the formation of a liquid film that spreads by capillary action through the porous M3/II HSS–Cu compact. As the temperature increased to 900°C, the hardness also increased from 212 to 362Hv. At this stage, the liquid acts as a transport medium for iron since iron has a greater affinity for P than Cu. Phosphorus diffuses into the steel matrix and continues to harden it (Jandeska,1982).

Copper in the other starts encounter the grain growth phase which involves the grain boundaries motion and filling the nearest pores. Grain growth of copper as well as the transformation of Fe from bcc to fcc, continuously increasing the compact hardness. The solubility of copper in iron is significantly less in the bcc phase than in the fcc phase. The Fe fcc structure with a larger interstices improve the solubility of P and Cu.

Moving from 1000 to 1050°C, closer to copper melting point, copper start to melt and the liquid would penetrate to fill pores around M3/II HSS powder. The formation of this liquid phase will wet iron particles and at the same time act as strengthening system and improved hardness to 495Hv.

As the temperature reached 1100°C, the Cu liquid film would enhance hardness in the compact by smoothing the pores and reinforcing the neck regions formed between iron

particles and blunting the sharp cusps (refer Fig. 4.14). The highest hardness achieved was 619Hv.

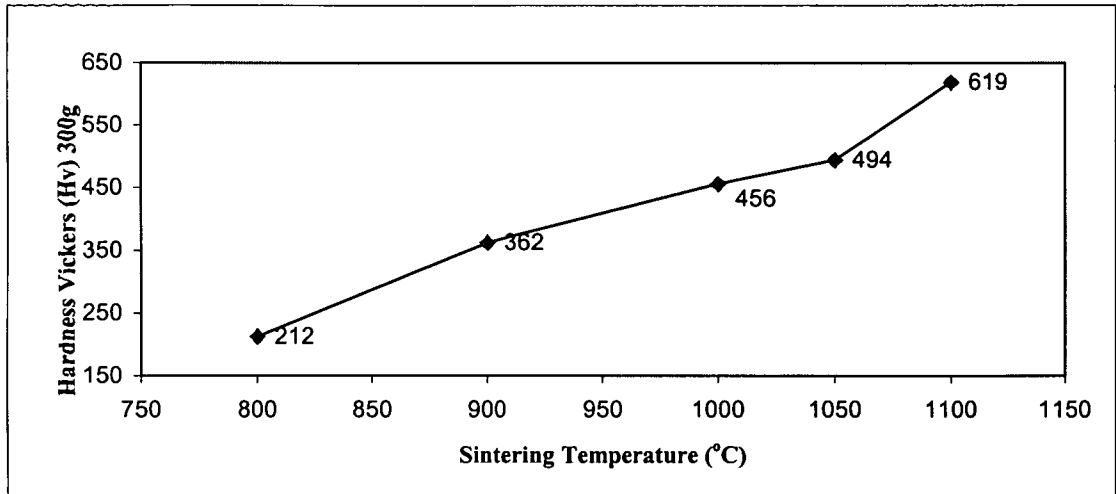


Figure 4.13: Hardness Vickers of M3/II HSS with addition 9wt.% Cu and 1wt.%P

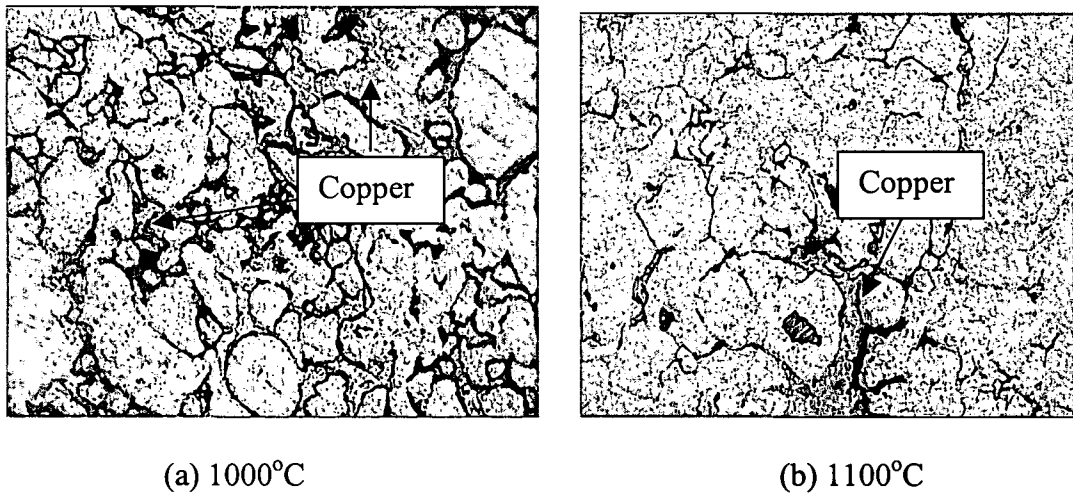


Figure 4.14: Optical Micrograph of Cu liquid phase at the grain boundaries (200X)

4.2.3 Microstructure Development of Sintered Powder

4.2.3.1 M3/II HSS Base Powder

Microstructural development analysis of the M3/II HSS alloy shows that the powder compact sintered at 800°C still preserves its pores as shown in Fig.4.15 (a). Although certain amount of it were eliminated but the pores are still in form of continuous phase (black or dark areas).

As the sintering temperature increased the pores tend to isolate and form an island as shown in Fig. 4.15 (b) and (c). Most of the sharp edges and continuous pores were rounded and separated to pore islands. At the same time, the grains become more visible and bigger especially when Fe goes through the ferrite to austenite transformation from (austenite phase starts around 900°C).

It is clear to note that sintering M3/II HSS base powder without additives even at 1100°C, could not provide enough liquid phase in the system. At this point, all events involved in the development are taking place in the solid state and below the eutectic temperature (1200°C) of the M3/II HSS.

Therefore in the sintering of M3/II HSS base powder the microstructure characteristic are dependent on the continuous carbide phase formed at the grain boundaries.

Interparticle bonds developments are more rapid at higher temperature. The mechanism of surface diffusion, which dominates at the initial stage of sintering, does not cause any significant shrinkage of the samples and can be neglected (Zhang and German,2001).

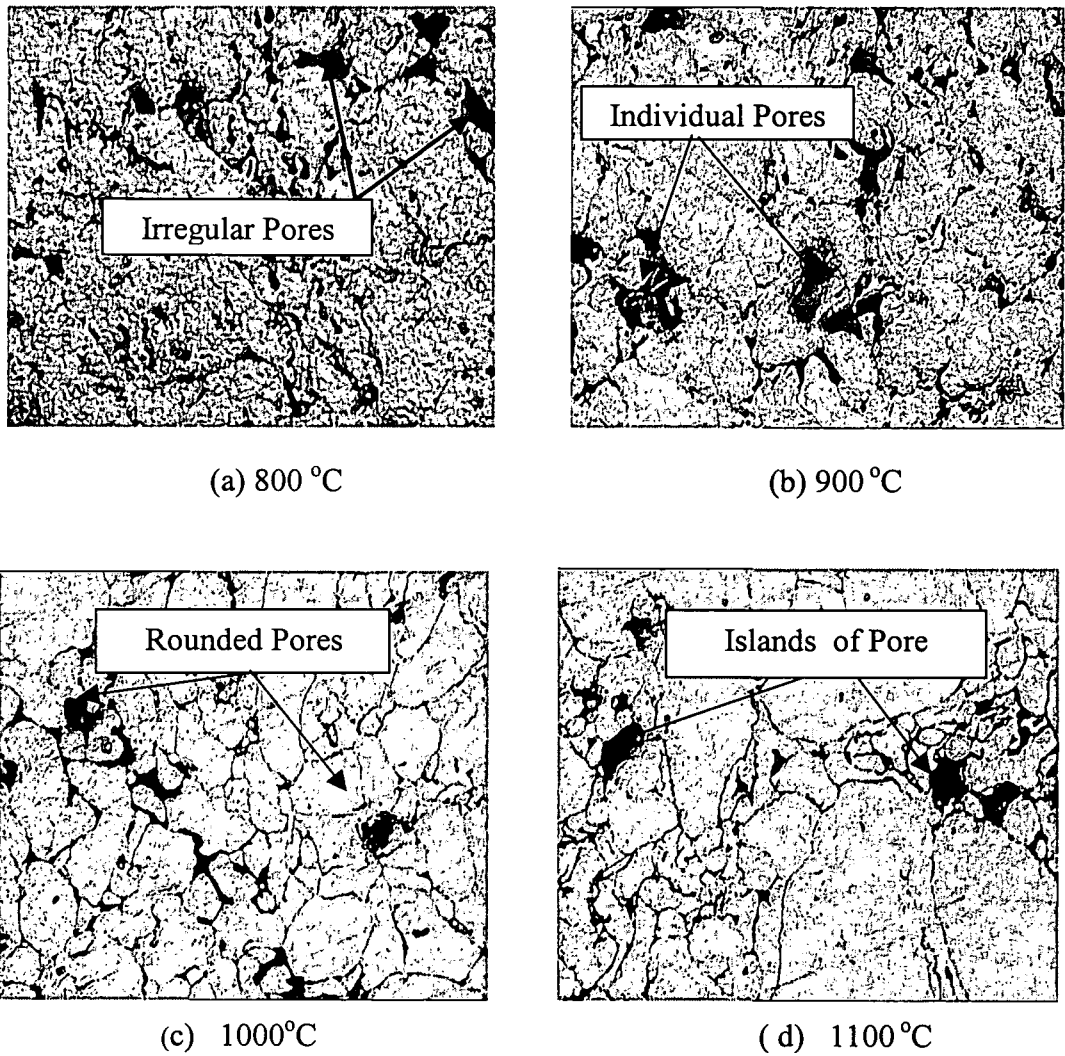


Figure 4.15: Optical Micrograph of sintered M3/II base powder (Magnification 200X)

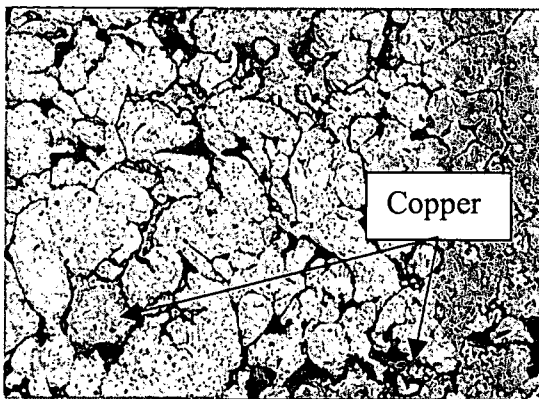
4.2.3.2 M3/II HSS with Cu Addition

The copper is present in irregular spots, which are distributed uniformly over the structure. The microstructural observation clearly identified existence of the liquid phase from the melting copper as the pore shapes become more rounded during sintering (refer to the relevant figures in 4.16 (a) to (f)).

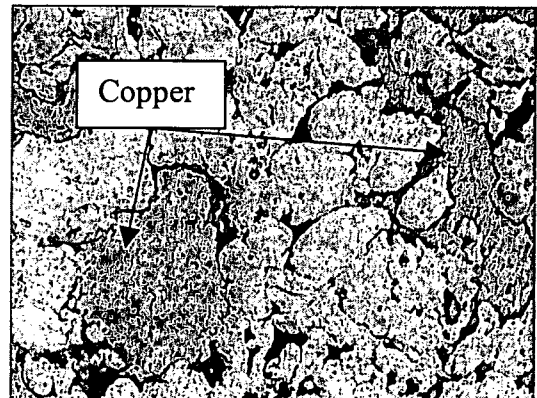
The dissolution of copper inside and reprecipitation leads to a microstructure showing larger grains with shape accommodation. Since copper may partially dissolve in the iron,

so that the proportion of free elementary copper in the structured is lowered. At 5-7 wt.% of copper addition (see Fig. 4.16 (a) and (b)), there are still large amount of pores existed in the compacts. This could be because of limited amount of liquid phase to penetrate and filling all the pores.

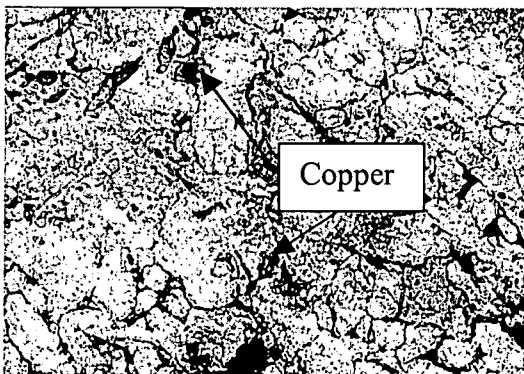
The addition of 8 to 9wt.% of copper, see Fig. 4.16 (c) and (d), were obviously seen reduce large amount of pores. The decreasing of pores amount contribute increasing the mechanical properties as discussed earlier. The liquid phase continuously appear to minimize the pores although there are still some residual pores left, see Fig. 4.16 (e) and (f).



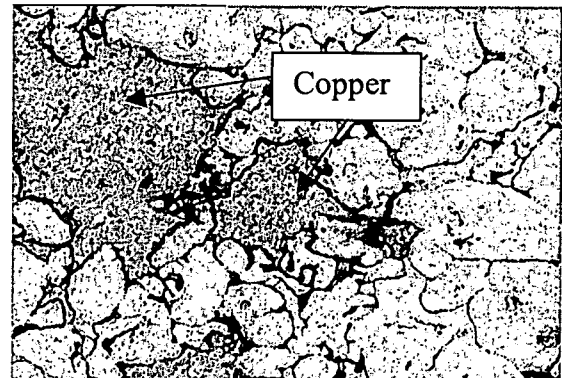
(a) 5 wt.%



(b) 7 wt.%



(c) 8 wt.%



(d) 9 wt.%

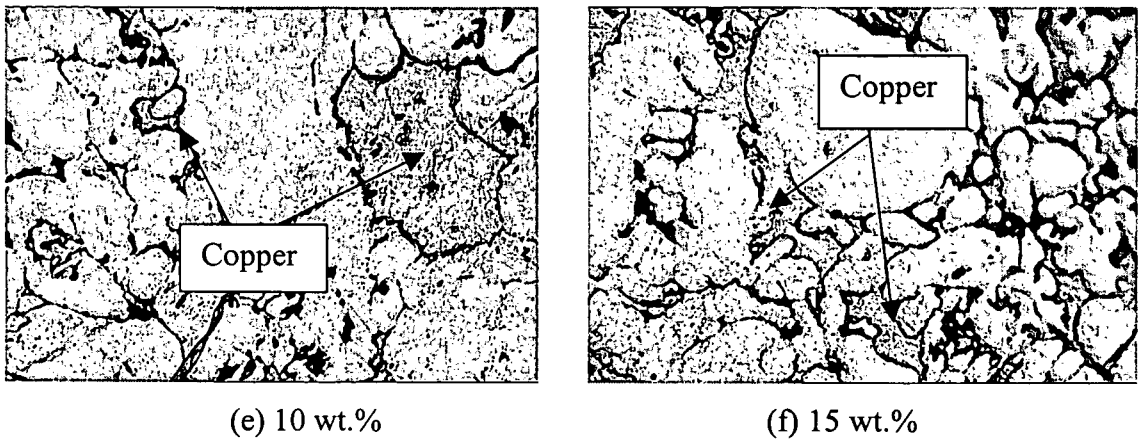


Figure 4.16: Optical Micrograph of M3/II HSS with addition of Cu in different composition sintered at 1100°C (Magnification 200X)

4.2.3.3 M3/II HSS with 9 wt.%Cu and 1wt.%P

At 800°C, there are no traces of phosphorus as phosphorus has already diffused to the steel matrix whereas copper is still remain in the interstitial pore areas. However a certain amount of copper element may present as a coating to the steels particles as resulted from solid state surface diffusion. Pool of copper is seen at the steel's grain boundaries and distributed uniformly over the structure.

Copper starts to move to other interconnected pore as the temperature reached 900°C. Comparing with the previous microstructure of M3/II HSS, the addition of copper and phosphorus that promote liquid phase had reduced the pore structure (shape and size) in the sample even at 800 and 900°C.

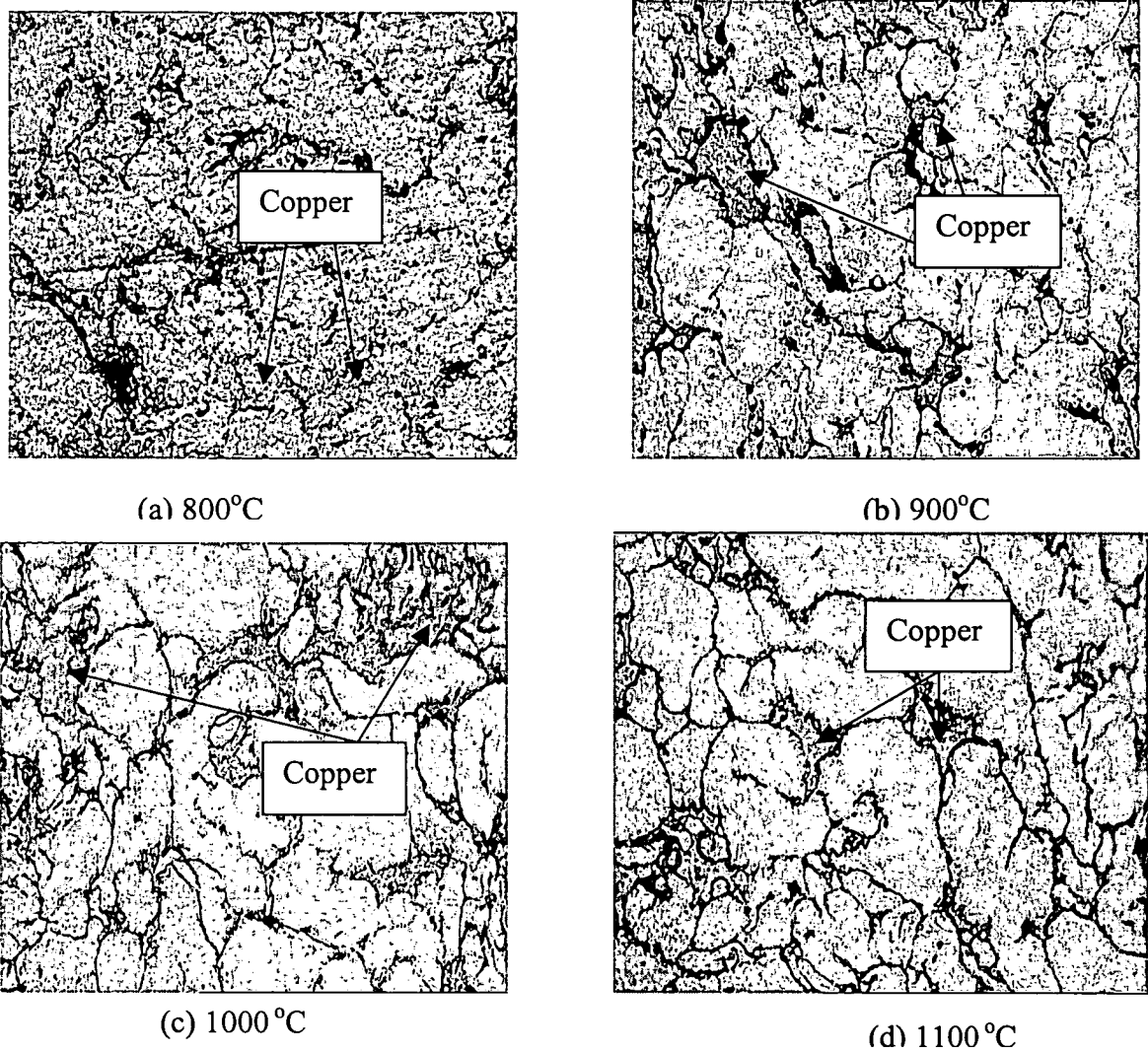


Figure 4.17: Optical Micrograph of Sintered M3/II with 9wt.%Cu and 1wt.%P. (Magnification 200X)

4.2.4 Scanning Electron Microscope (SEM) Analysis

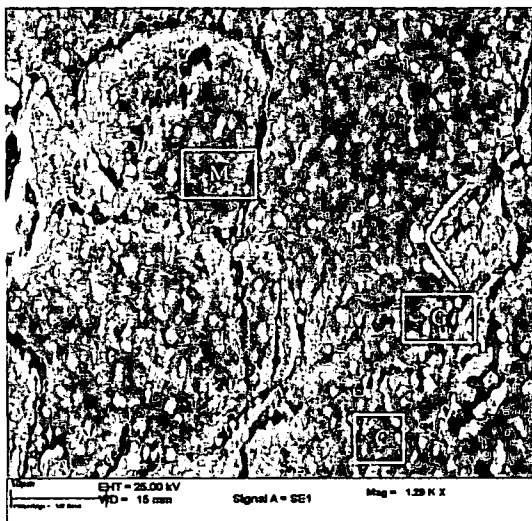
In order to gain a better understanding on the microstructure development of mixed M3/II HSS powder performance, SEM analysis was conducted on the sample with copper and phosphorus. The evidence from the SEM micrographs (refer to Fig. 4.18 (c) and (d)) indicate the formation of grey phases are seen in all sintering temperature which is the mixed phase between the solid and liquidus phase. The existence of white carbides found

scattered on the compact surface. The observed carbides are basically the primary carbides that existed in the prealloyed M3/II HSS base powder.

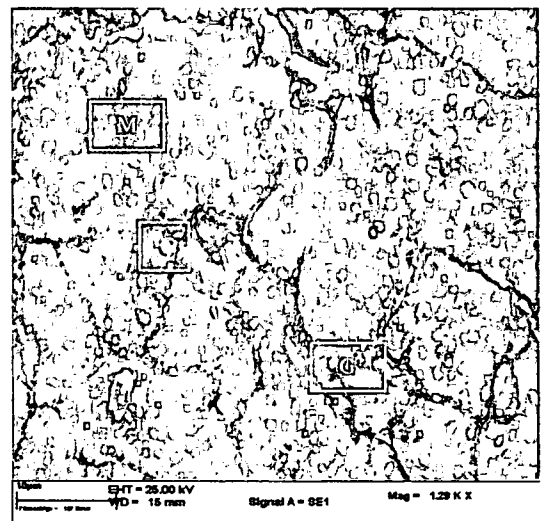
The white carbides also found at grain boundaries, see Fig. 4.18 (a) to (d). Those carbides were picked up by the penetration of liquid phase around particle boundaries. The evidence also suggested that, solution of the steel matrix into the copper rich liquid followed by the reprecipitation of alloying elements on the carbides.

Cluster of white carbide found at the 1100°C microstructure, refer Fig.4.18 (d). The carbides were dissolved into the pore zone which lay between prior particles by the liquid phase. The clustered group will act as nuclei for growth of carbide particle (Bochnowski et.al.,2003).

Metallographic observations were unable to produce an evidence of any eutectic structure. However, there was a clear evidence that clustered groups of undissolved M_6C carbides, which were dissolved by the liquid phase into pore zones which lay between prior particles. This clustered group would act as nuclei for growth of larger carbides.



(a) 800°C



(b) 900°C

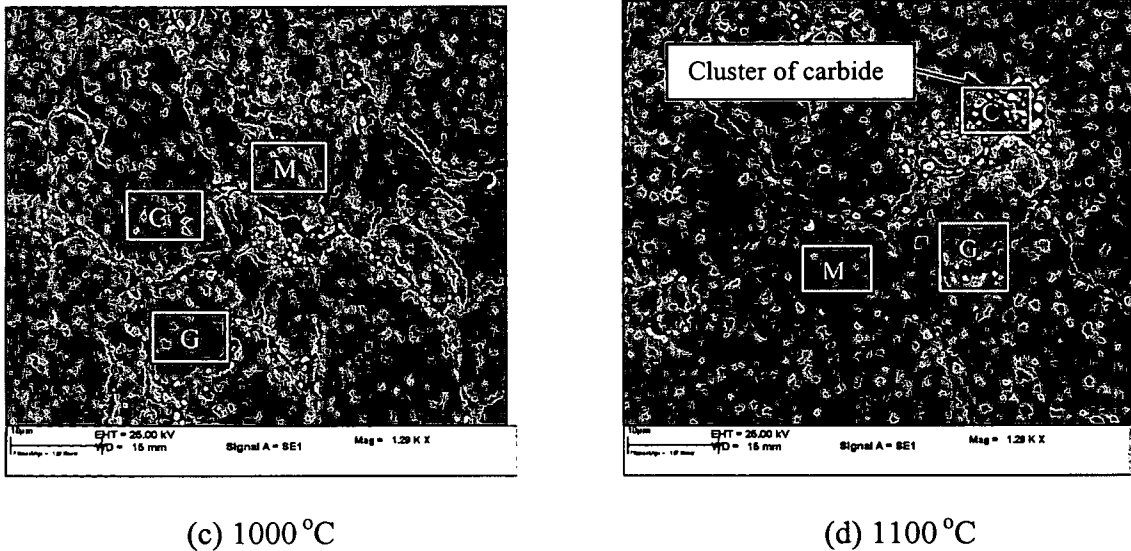


Figure 4.18: Scanning Electron Micrograph of as sintered M3/II-9wt.%-1wt.%Cu (Magnification 1.29kX)

Energy Dispersive X-ray analysis was done to analyze the composition of the matrix, white carbides, grain boundaries and the residual copper. Individual microstructural elements were investigated by the profile and mapping EDX analyses. It can be seen that composition of sintered compacts varies with the temperature. The EDX results showed that most of the carbides are mainly rich in Fe, Cr, V, Mo and W.

As the temperature decrease (cooling) from 1100°C to room temperature, the matrix phase also changes from $\gamma + M_xC$ to $\alpha + M_xC$ where the M_xC address to the complex carbide (refer the Appx.G for the M2HSS phase diagram).

Energy Dispersive X-ray result for matrix carbides composition revealed high Fe, W, Mo and Cr. Copper elements are not detected in the matrix due the presence of P with high affinity of Fe than Cu. Referring to (Jandeska, 1982), P will remain fluid before 1000°C, and after that temperature composition will reduced into half and hardly detected (refer to Appx. J) . This could be the reason of absences of P element in the EDX analysis. Chromium element also found in the matrix as the M_6C able to dissolves moderate amount of Cr, V and Co. Results from EDX analysis (refer Table 4.4) showed that the

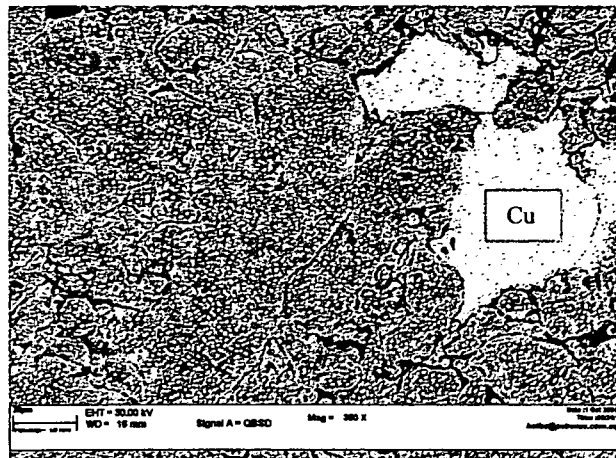
grain boundary contain high content of V and Mo which is a characteristic of MC carbide in HSS. While the white carbides in the matrix are the M_6C that contain rich W.

M_6C carbides can be easily detected at higher resolution due their high phase contrast resulting in high brightness, whereas the MC is characterized by lower brightness (refer to backscattered image Fig. 4.19). This differences in contrast were mainly due to major different element exist in the carbides.

There was obvious evidence of liquid phase at the grain boundary. From the EDX result for sintered sample at 1100°C (see Fig. 4.15) the liquid phase are from the M3/II base and Cu powder that turn into grey MC phase at the grain boundary. This is consistent with the DTA result showing the formation of liquidus start around 1050°C for the M3/II powder.

Table 4.4: EDX composition of sintered M3/II HSS with ,9wt.%Cu and 1wt.%P

Location in Figure 4.18	Element wt.%					
	Fe	Cr	V	Mo	W	Cu
(a) 800°C						
Matrix (M)	79	6	4	7	4	–
White carbides (C)	75	7	–	3	15	–
Grain Boundary (G)	74	5	4	6	6	5
(b) 900°C						
Matrix (M)	77	9	4	5	5	–
White carbides (C)	69	8	–	2	21	–
Grain Boundary (G)	73	7	6	5	4	5
(c) 1000°C						
Matrix (M)	75	5	6	7	7	–
White carbides (C)	70	7	–	1	22	–
Grain Boundary (G)	68	4	7	8	5	8
(d) 1100°C						
Matrix (M)	77	4	5	6	8	–
White Carbides (C)	69	7	–	–	24	–
Grain Boundary (G)	68	3	7	9	3	10

**Figure 4.19:** Backscattered Electron Micrograph of M3/II with 9wt.%Cu and 1wt.%P at 1100°C (Magnification 350X)

4.3 Cast Iron Characterization

4.3.1 Composition

In practice, additional alloying elements are introduced to enhance the desired characteristics. The transformation of austenite to ferrite and graphite during the cooling process is favored by silicon and aluminum. Silicon also refines the graphite distribution and increasing impact transition temperature, decrease thermal conductivity, increases ferrite strength particularly in annealed state (Elliott, 1988).

Aluminum is added in order to deoxidize the molten iron. This will ensure a low oxides content during solidification. Aluminum oxide (Al_2O_3) is very stable and will not react with carbon. Aluminum is also a strong graphitizer which promotes ferrite and graphite formation and influence the tensile properties.

Other alloying elements such as manganese (Mn), Cr and Mo will promote transformation of austenite to pearlite by stabilizes austenite by increasing the C solubility and moderately refines pearlite. Manganese addition is limited because its moderately a strong carbide promoter and also affect nucleation adversely. The higher level of Mo are for alloying purposes and are usually balanced by lower Mn additions. Magnesium is used to produce spheroidal graphite and also as deoxidizer. Consequently it will modify the graphite morphology when oxygen gas is low (Elliott, 1988). Cast iron normally contains more than 2 wt.% C. However, it was not detected through the conducted EDX analysis. Table 4.5 shows the composition found in the CI used in this research.

Table 4.5: CI elements composition (without C composition)

Element	Weight%
Iron (Fe)	96.10
Silicon(Si)	2.50
Manganese (Mn)	0.30
Aluminum (Al)	1.06
Magnesium(Mg)	0.04

4.3.2 Metallography Examination

Microstructure shows that the austenite matrix has transformed to ferrite and pearlite (see Fig. 4.20 (a) and (b)). Ferrite is a Fe-C solid solution in which relatively soft, ductile, poor wear resistance, good fracture and relatively good thermal conductivity. Pearlite is a mixture of ferrite and Fe_3C , which forms from austenite by a eutectoid reaction. This kind of matrix is relatively hard, with moderate toughness, low thermal conductivity than ferrite. This mixed structure is often used to obtain properties intermediate between the extremes properties of both phase. This mixed microstructure with its alternate black and white circular appearances (Elliott, 1988).

Figures 4.20 (a) shows the spherical morphology of graphite nodules on the CI surface. It can be noted clearly the presence of the graphite nodules in envelopes of free ferrite in the pearlite matrix. Ferrite forms around graphite nodules and growth proceeds until pearlite nucleates and consumes the remaining austenite. Consequently, there are only a small relative ferrite content after the pearlite has nucleated.

The nodular graphite indicated that the cast iron has a good strength, good ductility and shock resistance. The flakes graphite probably occurs due to low content spheroidizer to change the flakes to spherical graphite.

The microstructure shown in Fig. 4.20 (b) also consists of the eutectic phase that mainly controlled by the diffusion of carbon from the liquid to graphite through the austenite shell. The eutectic solidification is a nucleation and growth process that fills the space between the dendrite arms. This eutectic phase could influence the bonding mechanism later due to the high content of solidified liquid phase. This solidified liquid would enhance the wettability during the bonding later.

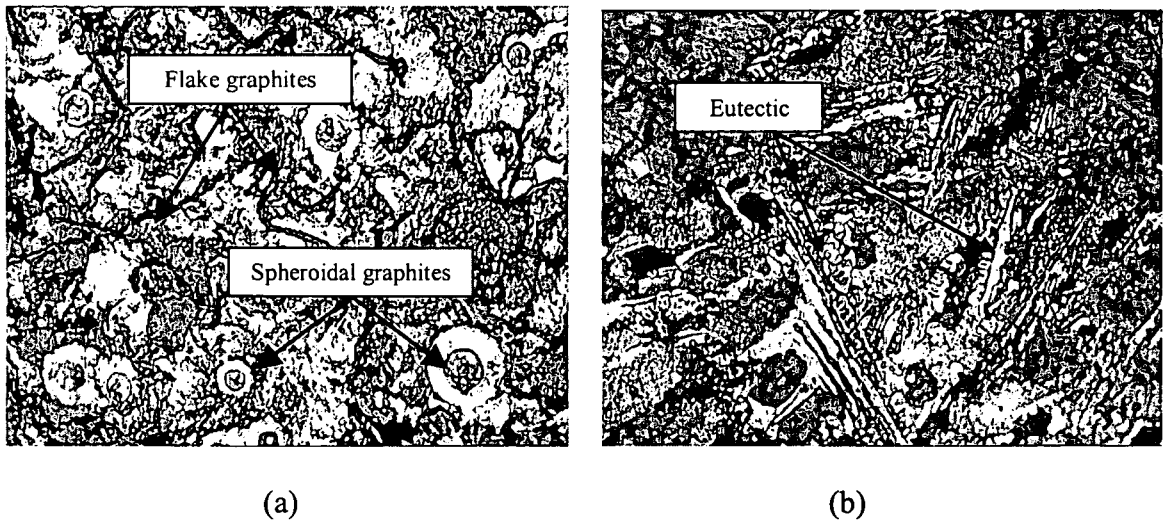


Figure 4.20: Optical Micrograph of CI (Magnification 200X)

4.3.3 Surface Roughness

Surface roughness will give a significant effect on the wetting process. From the surface profiler results, the average surface roughness (R_a) for CI after machining is $0.20\mu\text{m}$ (refer Appx. K). Although the rough peaks or grooves increase the contact area and promote wetting by pulling the liquid phase into the channels by the capillary forces, high roughness peak will cause but wetting might be incomplete leaving regions of free surface on the high spot peaks.

The polished CI surface in the other hand, have an average roughness (R_a) of $0.13\mu\text{m}$. Polishing the surface had reduced the roughness of the affected area and also removed any contamination on the affected area. This will increase the wetting area and dissolving any contamination (oxide) film on the surface as well as holding the liquid phase from the compact.

4.4 Sintered Bonding

Figure 4.21 shows the result of the attempt which focused onto the interface between M3/II and CI. Time joint formation for 30 minutes was the typical time frame used to encourage interdiffusion between the two materials. The expected formation of migration layer caused by the liquid phase between the powder mixture and the cast iron was not found under the SEM.

Although the real sintered bonding layer cannot be produced but few observations from the attempt can be crystallized. One of the primary factors is the presence of chemically stable and physically tenacious oxide layer on the cast iron surface due to the chemical composition and graphite that impedes the liquid phase to produce an intimate contact with the cast iron even though polishing was done earlier on the cast iron. The plastic flow of the liquid phase was not able to scour and remove the oxide layer.

The remaining pores in the compact powder can be factor wicking the liquid phase away from the joint and weakened it. Although the liquid phase is likely to penetrate to the interface due to the gravity force and the higher heat affected zone, the liquid phase draw back to again the former interstitials or grain boundaries. This is due to the low solubility or wetting of the cast iron surface plus higher capillary force from the compact powder attracting the liquid phase than the cast iron.

The heat transmitted through the material dependent on the amount of porosity. Greater amounts of porosity change the heat transfer mechanism and ultimately the joining parameters. Since the sintered compact only reached 76% of its full density, the retain porosity had contributed to the heat dissipation through the compact. Pores act as thermal insulators, which slow the transfer of heat making the powder compact less hardenable than the cast iron.

The presence of carbides in the joint area also gives a negative effect since carbide is a very hard material, its presence cause the joint to become brittle. The possibility of carbides transformation during cooling of the powder could promote cracks initiation at the joint (Nicholas, 1998).

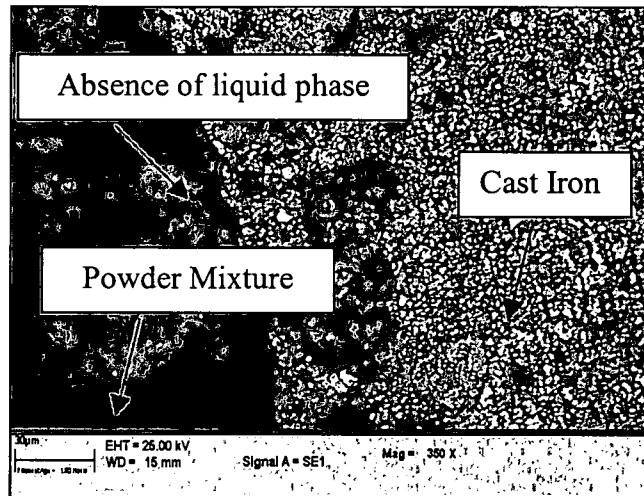


Figure 4.21: Scanning Electron Micrograph of Sintered Bonding Attempt (Magnification 350X)

CHAPTER FIVE

CONCLUSION AND RECOMMENDATION

5.1 Conclusion

The present research has successfully characterized M3/II HSS alloy particle size, element composition, phase existed, thermal properties, density, hardness and the resultant microstructure for M3/II HSS alloy with sintering temperature.

The particle size analysis shows the average M3/II HSS particles size 74 μm in diameter and 98 μm width with irregular shape and rough surface. In the other hand, the addition of other alloying element especially copper powder with spherical shape will effectively smoothed the M3/II HSS particle surface and prevented agglomeration.

The XRF result indicated the presence of strong carbide former element such as Mo, W, V and Cr. Molybdenum is the major alloying element that helps strengthening the matrix and enhancing the hardenability. The XRD result confirmed the existence of the complex carbides such as the M_6C and MC as detected through the respective diffraction line.

The DTA peaks of M3/II HSS show a significant exothermic reaction started around 1050 $^{\circ}\text{C}$ which is due to formation of liquid phase in the base powder. The phase transformation accelerates the densification and the weight loss as indicated in TGA curve. M3/II type high speed steel base powder alone was not able to be the only source providing the liquid phase during the sintered bonding mechanism that brings to the addition of copper and phosphorus.

Higher density and hardness achieved as the sintering temperature increased in the all compacts. It has been established that the addition of copper and phosphorus that promote the liquid phase improves the densification and hardenability of the compacts. This liquid phase accelerated particle rearrangement and diffusion, thereby aiding densification and pore elimination in the compact. Highest density and hardness achieved was 6.2 gcm^{-3} (76% of HSS full density) and 619Hv respectively. The results indicated that as the sintering process continues at higher temperatures, the inherent porosity in the powder mass is reduced as pores are eliminated by bulk diffusion to grain boundaries.

As observed by the metallographic investigation, it showed the individual powder particles also lost their identity completely as grain boundaries move across prior particle boundaries. Larger grains replaced the original fine particle structure. The grain growth lead the remaining pores to lose their angular, irregular nature and become smaller, smooth, tending toward perfect spheres as the sintering temperature increased. The micrographs also showed the copper present in irregular spots, which are distributed uniformly over the structure and filling the pores at the interstitial.

The conducted SEM analysis showed the existence of white carbides scattered on the sintered compact surface. From the EDX results, the elements composition showed that the presence of complex carbide that are corresponds to M_6C and MC .

Optical Microscope observation on the CI revealed the mixture of ferrite and pearlite matrix with the graphite nodules is in envelopes of free ferrite. The CI also consists of eutectic phase, which have a high content of solidified liquid phase. The CI surface was polished in order to reduce the surface roughness and contamination. From the EDX analysis done on the CI, a few elements was detected such as Fe, Si, Mn, Al and Mg. The exact group of the CI may differ from what have been assumed although most casting alloy are specified by composition. Consequently, this is not possible as many the compositions of the various types of iron overlapping each other and the properties of a particular type depend on the solidification conditions that in this case are not known.

The expected formation of migration layer of liquid phase was not found due to the presence of chemically stable and physically tenacious oxide film as those formed by the Al and Cr from the CI alloying elements and graphites. The film impedes an intimate contact between CI and the liquid phase. Conventional chemical methods such as polishing did not remove the oxides.

The material characteristic such as mutual solubility between the solid and the liquid, wettability, absence of surface contaminates and adequate surface finish play important role during liquid phase sintering. Furthermore the ability of at least one component to undergo sufficient plastic flow, in order to develop complete contact across the interface between the two component are also critical. The influence of the processing parameters; time, temperature and pressure, are being assessed in terms of the strength and quality of the bond and the mechanics of bond formation.

5.2 Recommendation

Due to the time constraints of this research, further works is required to make the findings more reliable to use. Base on the results and learning obtained from this research several recommendations are made.

Binder such as zinc streate can be added to enhance interparticle bonding in preliminary compression and act as a wetting film on the powder and also reduce the friction between particle that will increase the densification and hardness.

Sintering in a vacuum atmosphere will reduce the porosity caused by the trapped gas in the pores and allowing full density to be achieved and preventing the liquid phase beings wick away from the joint and increase the heat transfer through the material.

A chemical treatment is possible to disturb and disperse the stable oxides layers on the surface. A pretreatment for CI is by immersing the CI for several minutes in a salt bath at 400°C that contains a mixture of sodium and potassium nitrides. The chemical treatment

will completely removes any exposed graphitic phase from the surface and leaves an iron rich surface that is readily wetted by many filler alloys.

Another alternative is using very reactive brazing materials or filler such as titanium that can be added to the Cu alloy base fillers. This would help the liquid phase to penetrate beneath to the metal substrate.

Appropriate mechanical testing procedures such as the tensile test, impact and fatigue can be done to assess the bonding properties and qualities, taking account the unique features of the joint.

This research identifies the characteristic and physical differences between PM parts and cast iron as it pertains to joining. The results constitute a set point to obtain tailored M3/II HSS alloy properties through the PM technique and with the saving of raw material derived from the use of proposed method. However, further work to optimize the joining procedure and to understand the fusion zone for improving the bonding still represents a considerable challenge.

In conclusion, it is hope that joining dissimilar materials such as PM and other conventional materials could be transferred through the research development program own either by the government or private sectors especially those related with PM or metal based industries. This will embark and expand the commercialization of PM in Malaysia

REFERENCES

1. Amador D.R. and Torralba J.M., Morphological and microstructural characterization of low alloying Fe powder obtained by mechanical attrition, *Materials Processing Technology*, pp. 776-780, 2003.
2. Badisch E. and Mitterer C., Abrasive wear of high speed steels: Influence of abrasive particles and primary carbides on wear resistance, *Tribology International*, vol. 36, no. 10, pp. 765-770, 2003.
3. Boccalini M. and Goldenstein H., Solidification of high speed steels, *International Materials Reviews*, vol. 46, no.2, pp.92-102, 2001.
3. Bochnowski W. et.al., Primary and secondary carbides in high-speed steels after conventional heat treatment and laser modification, *Materials Chemistry and Physics*, vol. 81, no. 2-3, pp.503-506, 2003.
4. Boettinger W.J and Kattner U.R, On DTA Curves for the melting and Freezing of alloys, *Metallurgy Material Transactions*, vol. 33A, pp.1779-1794, 2002.
5. Bolton J.D. and Gant A.J., Liquid phase Sintering of MMC containing solid lubricants, *Journal of Material processing Technology*, vol. 56, pp.136-147, 1996.
6. Bolton, J.D. et. al., Liquid-phase sintering of high-speed steels, *Journal of Material Science*, vol. 26, pp. 5203-5211, 1991.
7. Cam G. and Kocak M., Progress in joining of advanced materials, *International Materials Reviews*, vol. 43, no.1, 1998.
8. Capus Joe, Fuel miser technology carries off two awards, www.metal-powder.net/jan03hitachifeat.html, January edition, 2003.
9. Carter F. Giles, *Principles of Physical and Chemical Metallurgy*, American Society for Metals, ch. 13, pp. 346, United State of America, 1979.
10. Chisamera M. and Riposan I, *Advanced Materials Research vol. 4-5*, Scitec Publications, pp. 293-300, Switzerland, 1997.
11. Elliot Roy, *Cast Iron Technology*, Butterworth & Co.(Publisher) Ltd., ch.1,6, pp. 1-5, 229, Great Britain,1988.
12. German, M. Randall, A status report on liquid phase sintering, *Progress in Powder metallurgy*, MPIF, vol 42, pp. 85,1985.
13. German, M. Randall, *Powder Metallurgy of Iron and Steel*, John Wiley & Sons Inc. New York , ch 1-13, 1998.

14. German, Randall M., *Powder Metallurgy Science*, Metal Powder Industries Federation, USA, ch1-11, 1994.
15. Hamill Jack A. Jr., *P/M Joining Process Materials and Techniques*, Hoeganaes Corporation, Riverton, 2000.
16. Hoyle G., *High Speed Steels*, Butterworth and Co. Ltd., Kent England, ch.1-3, 1988.
17. Humpston Giles and Jacobson David M., *Principles of soldering and brazing*, The Materials Information Society, USA, ch 1, pp.5,1993.
18. Jandeska William F., *Strength and ductility enhancement of low temperature sintered iron powder structures*, MPR, September edition, 1982.
19. Kauly T. et. al., Highly filled particulate thermoplastic composites, Part 1 Packing density of irregularly shaped particles, *Journal of Material Science*, pp.693-699,1997.
20. Key to Steel, Classification of cast iron, *www.Key-to-Steel.com*, Key to Metal Task Force & INI International, 2003.
21. Leithner Karl , Method for producing cam, *United States patent*, no. 629 230, 1990.
22. Liu Z. Y. et. al. , Microstructure evolution during sintering of injection molded M2 high speed steel, *Material Science and Engineering A*, vol. 293, no. 1-2, pp. 46-55, 2000.
16. Liu Z. Y. et. al., Mechanical alloying of TiC/M2 high speed steel composite powders and sintering investigation, *Material Science Engineering A*, vol. 311, no.1-2, pp. 13-21, 2001.
17. Llwellyn D.T and Hudel R.C., *Steel: Metallurgy and application. Third Edition.* ch. 3, pp. 254-258, Great Britain, 1998.
18. Maki S. et. al., Sinter-joining of different metal powder compacts using resistance heating, *Journal of Material Processing Technology*, vol.143-144, pp.561-566, 2003.
19. Metal Powder Report, Assembled camshaft using sintered components, May edition, *Elsevier Advanced Technology*, pp.286, 1983
20. Metler Toledo, Thermal Analysis, *www.mt.com*, visited on 14 April 2005.

21. Michalski J. et. al., An experimental study of diesel engine cam and follower wear with particular reference to the properties of the materials, *Wear*, vol. 240, Issues 1-2, pp.168-179, 2000.
22. Narasimham K.S, Sintering of powder mixtures and the growth of ferrous powder metallurgy, *Materials Chemistry Physics*, pp.56-65, 2001.
23. Nicholas M.G, *Joining Process (Introduction to brazing and diffusion bonding)*, Kluwer Academic Publishers, ch. 1, 7,8, pp.22,227-230,298, Netherland, 1998
22. Othman Mamat, Development and design of PM alloys based on ternary Fe- Mo- C and quaternary Fe-Mo-C-Cr System with Copper Phosphorus addition, pp.59, *PhD thesis*, University of Bradford, United Kingdom, 1998.
24. Parmigiani J.P. and Kosco J.C., *Joining of P/M components*, Society of Automotive Engineers Inc. no. 1999-01-0889,1999
25. Porter D.A and Easterling K.E., *Phase transformation in metals and alloys*. Chapman and Hall, ch.4, pp.251-253, 1997.
26. R.B. Gupta, *Automobile Engineering*, Satya Prakashan, ch. 7, pp. 149-148, New Delhi, 2001.
27. Ruiz-Navas E. M. et. al., Development and charaterisation of high-speed steel matrix composites gradient materials, *Journal of Materials Processing Technology*, vol. 143-144, pp. 769-775, 2003.
28. Shackelford James F, *Materials Science for Engineers*, Prentice Hall Inc. New Jersey , USA, ch.11, pp. 408, 2000.
29. Shigley Joseph E. and Mischke Charles R., *Mechanical Engineering Design*, ch.2, pp. 274, 281, McGraw Hill International Edition, New York, 2001.
30. Smith William F., *Structure and properties of engineering alloys. Material Science and Engineering Series*, ch.9, pp. 414-427, Mcgraw Hill, USA, 1993.
31. Smith L.N. and Midha P.S., *Computer simulation of morphology and packing behaviour of irregular particles for predicting apparent powder densities*, Computational Materials Science, pp 377-383, 1997.
32. Suganuma et. al., Antiwear sintered alloy and manufacturing process thereof, *UK Patent*, no. 4491477, 1985.
33. Suganuma Tetsuya and Kazuoka Koji, A method for manufacturing a slide member, *UK Patent*, no. 8218929,1981.

34. Sustarsic B. et. al., The characteristic of vacuum sintered M3/2 type HSS with MoS₂ addition, *Journal of Material Processing Technology*, vol. 143-144, pp. 98-104, 2003.
35. Suzuki, M., Application of P/M joining in Japan, *Japan society of powder and powder metallurgy* , pp. 457-462, 1993.
36. Swift K.G. and Booker J.D., *Process selection, From design to manufacture*, Arnold, ch.1-3, pp. 21-90, London 1997.
37. Upadhyaya G.S., *Sintering Metallic and Ceramic Materials, Preparation, Properties an Application*, *John Wiley and Sons Ltd.* USA, 2000.
38. Wright C.S et. al., Development of robust processing routes for powder metallurgy High Speed Steels, *Journal of Material Science and Technology*, vol. 14, pp. 945-956, 1998.
39. Zhang Haorong and German Randall M., Homogeneity and properties of injection moulded Fe-Ni alloys, July Issues, *Metal Powder Report*, pp. 18-22, 2001.

PUBLICATION

1. Wan Nursheila Wan Jusoh and Othman Mamat, **“The Development of Powder Metallurgy Sintered Bonding M3/II High Speed Steel with Cast Iron”** 3rd National Technical Postgraduate Symposium, Kuala Lumpur, Malaysia, 15-16 December 2004.

APPENDIX A: Pellet Preparation

M_P	=	Pellet mass	$\rho_{M3/II}$	=	M3/II density
$M_{M3/II}$	=	M3/II HSS mass	ρ_{Cu}	=	Cu density
M_{Cu}	=	Cu mass	ρ_P	=	P density
M_P	=	P mass	V_P	=	Pellet volume
V_{Cu}	=	Cu volume	V_P	=	P volume
$V_{M3/II}$	=	M3/II HSS volume	$F_{M3/II}$	=	M3/II fraction
F_{Cu}	=	Cu fraction			
F_P	=	P fraction			

Referring to M3/II HSS with 9wt.%Cu and 1wt.%P, the calculations are as follows:

Green compact diameter = 13mm; Green compact height = 4mm; $\rho_{M3/II} = 8.2\text{gcm}^{-3}$;
 $\rho_{Cu} = 8.92\text{gcm}^{-3}$; $\rho_P = 2.32\text{gcm}^{-3}$

$$\begin{aligned}
 M_{M3/II} &= V_{M3/II} \times \rho_{M3/II} \\
 &= [F_{M3/II} \times V_P] \times \rho_{M3/II} \\
 &= [0.90 \times (\pi \times 0.65 \times 0.65 \times 0.4)] \times 8.2 \\
 &= 3.92\text{g}
 \end{aligned}$$

$$\begin{aligned}
 M_{Cu} &= V_{Cu} \times \rho_{Cu} \\
 &= [F_{Cu} \times V_P] \times \rho_{Cu} \\
 &= [0.09 \times (\pi \times 0.65 \times 0.65 \times 0.4)] \times 8.9 \\
 &= 0.43\text{g}
 \end{aligned}$$

$$\begin{aligned}
 M_P &= V_P \times \rho_P \\
 &= [F_P \times V_P] \times \rho_P \\
 &= [0.01 \times (\pi \times 0.65 \times 0.65 \times 0.4)] \times 2.3 \\
 &= 0.01\text{g}
 \end{aligned}$$

$$\begin{aligned}
 M_P &= M_{M3/II} + M_{Cu} + M_P \\
 &= 3.91 + 0.42 + 0.01 \\
 &= 4.36\text{g}
 \end{aligned}$$

APPENDIX B: Compaction Pressure Calculations

Pressure= Force/Area

Force used = 10,000 lbf

Pellet Diameter =1.3cm

=0.25 inch

Pellet Area = $\pi \times 0.25 \times 0.25$

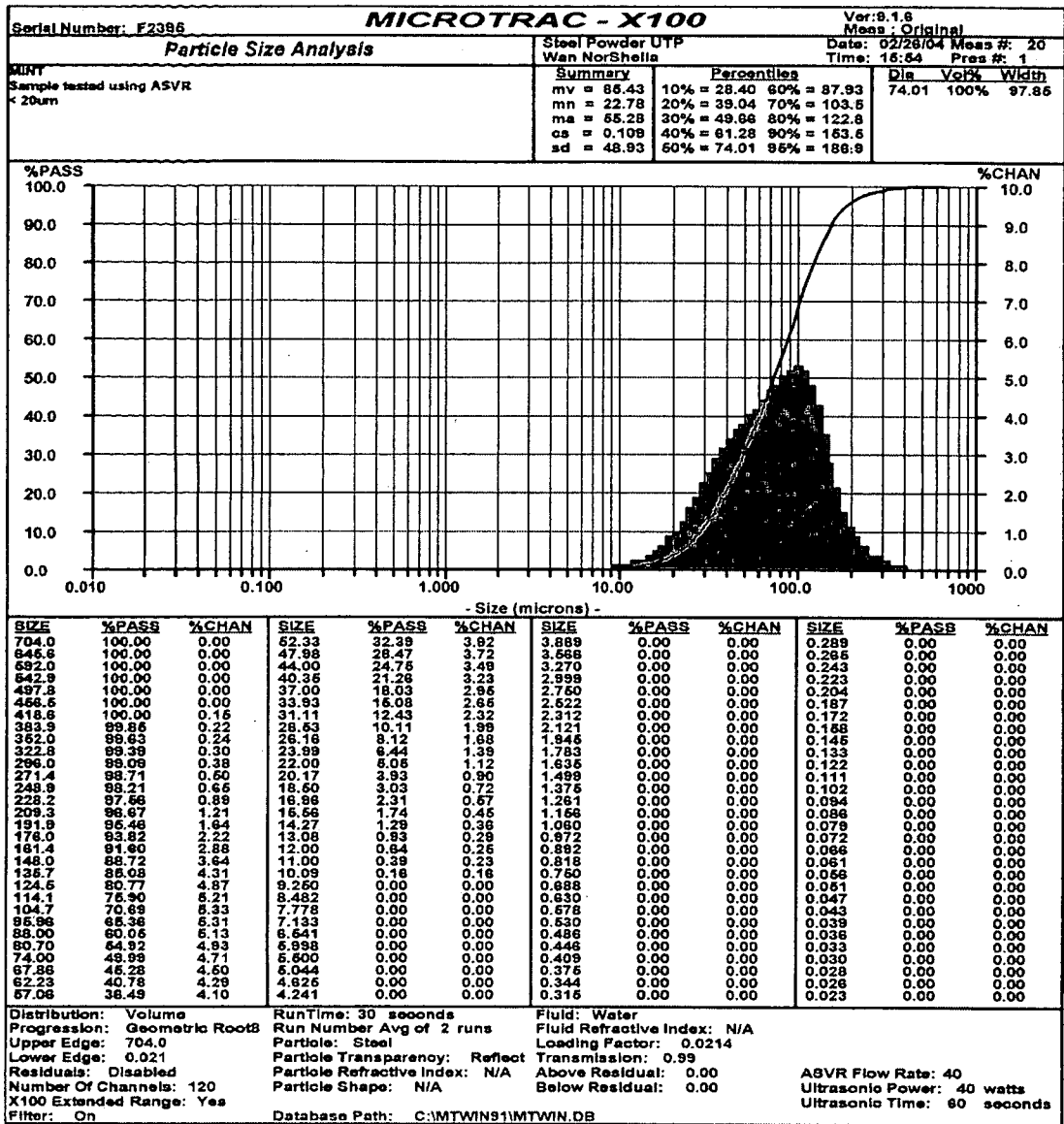
= 0.20 inch²

Pressure=10 000/0.20

=50 000lbf/inch² (10 lbf/inch²= 0.07 MPa)

= 350MPa

APPENDIX C: Particle Size Analysis Result



APPENDIX D: Certificate of Analysis

(1) Copper

Material Safety Data Sheet

acc. to OSHA and ANSI

printing date 07/15/2004

Reviewed on 05/27/2004

Product name: Copper powder

(Contd. of page 3)

Body protection: Protective work clothing.

9 Physical and chemical properties:

General Information	
Form:	Powder
Color:	Copper colored
Odor:	Odorless
Change in condition	
Melting point/Melting range:	1083°C (1981°F)
Boiling point/Boiling range:	2595°C (4703°F)
Sublimation temperature / start:	Not determined
Flash point:	Not applicable
Flammability (solid, gaseous)	Highly flammable.
Ignition temperature:	Not determined
Decomposition temperature:	Not determined
Explosion limits:	
Lower:	Not determined
Upper:	Not determined
Vapor pressure:	Not determined
Density at 20°C (68°F):	8.94 g/cm ³
Solubility in / Miscibility with	
Water:	Not determined

(2) Phosphorus

Material Safety Data Sheet acc. to OSHA and ANSI

Printing date 07/15/2004

Reviewed on 06/23/2004

Product name: Phosphorus powder

(Contd. of page 3)

Body protection: Protective work clothing.

9 Physical and chemical properties:

General Information	
Form:	Powder
Color:	Red
Odor:	Not determined
Change in condition	
Melting point/Melting range:	416°C (781°F)
Boiling point/Boiling range:	Not determined
Sublimation temperature / start:	416°C (781°F)
Flash point:	Not applicable
Flammability (solid, gaseous)	Highly flammable.
Ignition temperature:	259°C (498°F)
Decomposition temperature:	Not determined
Danger of explosion:	Explosive when mixed with oxidizing substances.
Explosion limits:	
Lower:	Not determined
Upper:	Not determined
Vapor pressure:	Not determined
Density at 20°C (68°F):	2.34 g/cm ³
Solubility in / Miscibility with water:	Insoluble

APPENDIX E: X-Ray Florescence Result

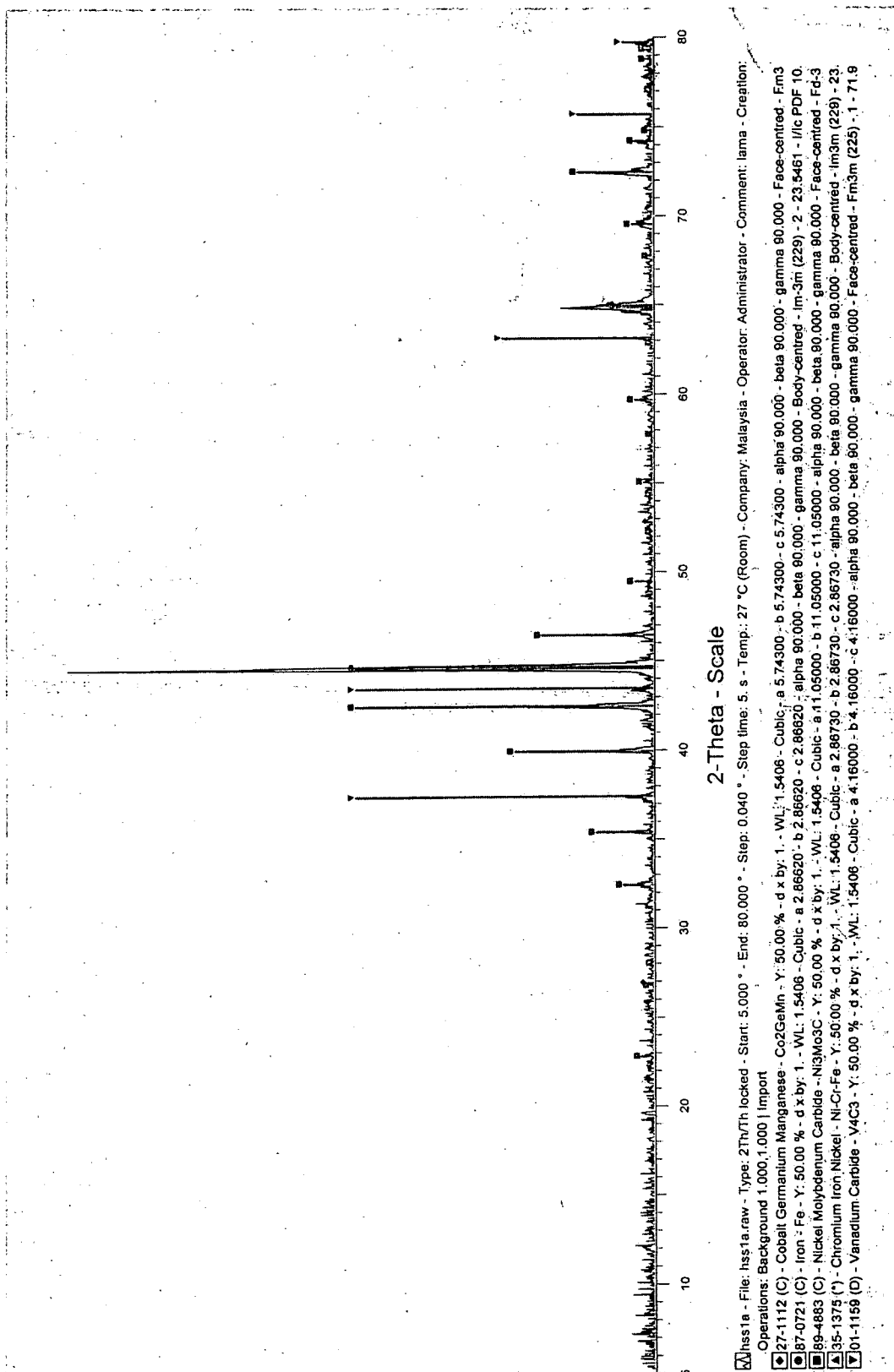
Sample measured on 15-Jan-2004 15:39:03

Si	V	Cr	Mn	Fe	Co	Ni
2.9 KCps	163.6 KCps	290.7 KCps	20.1 KCps	5215.3 KCps	58.7 KCps	10.6 KCps
0.257 %	3.77 %	4.32 %	0.229 %	75.4 %	0.415 %	0.186 %

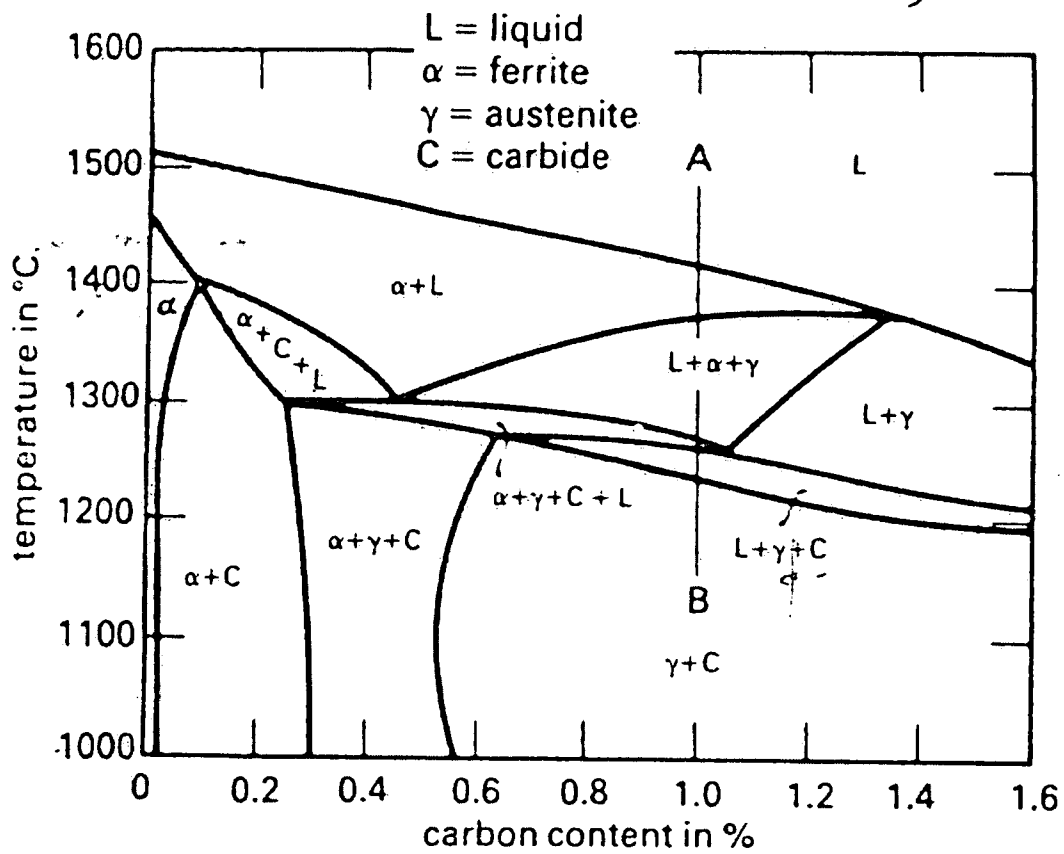
Cu	Mo	Ho	Yb	W	Re	Compton
10.3 KCps	1473.5 KCps	5.0 KCps	151.4 KCps	128.0 KCps	35.9 KCps	
0.180 %	7.69 %	0.0118 %	0.605 %	6.76 %	0.0961 %	0.27

Rayleigh	Norm.
0.98	100.00 %

APPENDIX F: X-ray Diffraction Pattern



APPENDIX G: M2 High Speed Steel Phase Diagram



Appendix H : Sintered Density Calculations

$$\text{Density} = \frac{M}{\frac{[M_L - M_{LW}]}{W} - \frac{[M_L - M]}{L}}$$

- M = Weight in air (uncoated)
- M_L = Weight in air (coated sample)
- M_{LW} = Weight in water (coated sample)
- W = Water density (1.0gcc)
- L = Lacquer density (0.9gcc)

Referring to M3/II+9wt.%+1wt.P sintered at 1100°C sample

- M = 4.36g
- M_L = 4.37g
- M_{LW} = 3.66g
- L = 0.9gcc
- W = 1.0gcc

$$\begin{aligned} \text{Sintered density} &= \frac{4.36}{\frac{[4.37-3.66]}{1} - \frac{[4.37-4.36]}{0.9}} \\ &= \frac{4.36}{0.71 - 0.01} \\ &= 6.23\text{gcm}^{-3} \end{aligned}$$

APPENDIX I : Sintered Hardness Calculations

M3/II HSS Base Powder

Sintering Temp.°C	Reading			Average (Hv)
	1	2	3	
800	136.7	137.4	139.6	137.9
900	269.4	361.9	299.8	310.4
1000	354.8	449.4	405.6	403.3
1100	509	455	434.8	466.2

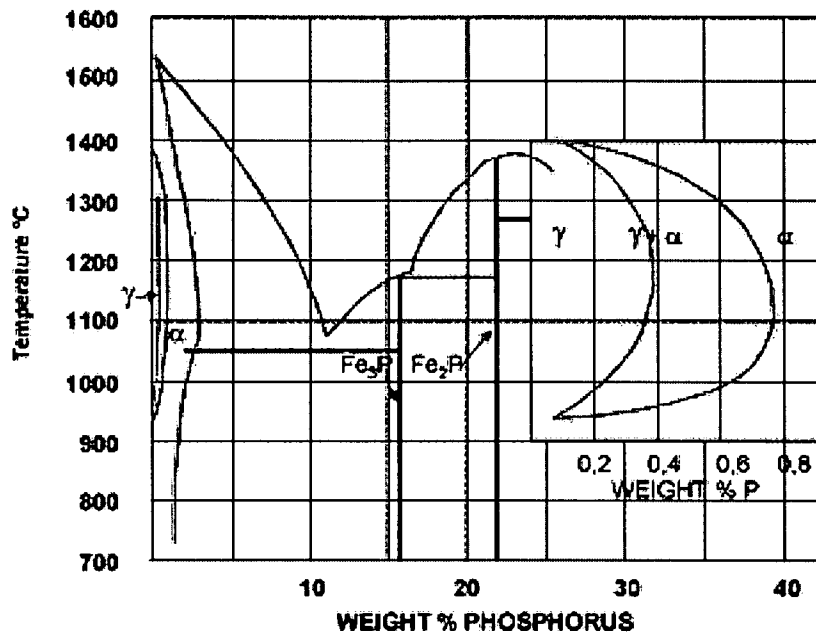
M3/II HSS with Cu Addition

Weight % of Cu	Reading			Average (Hv)
	1	2	3	
5	308.1	399.7	430.3	379
7	371.3	400	470.5	480.6
8	533	475.6	468.4	492.3
9	525	490.1	533.3	516.1
10	512.6	545.7	503.5	520.6
15	490	580.7	593.8	554.8

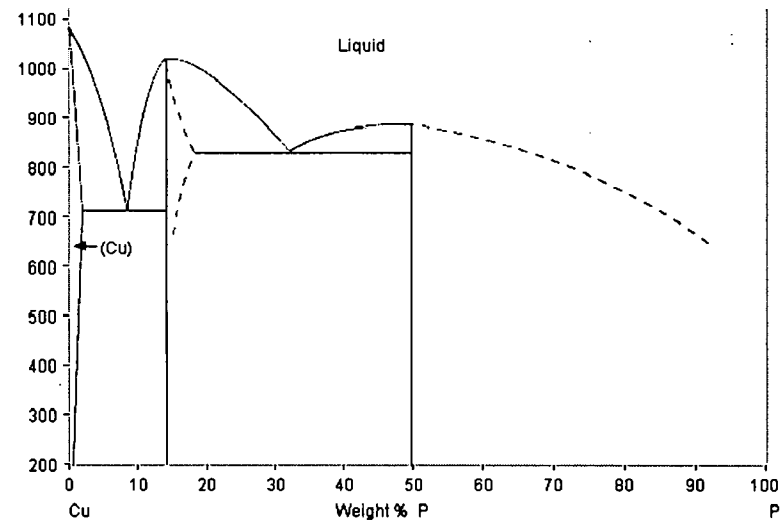
M3/II HSS with 9wt.%Cu and 1wt.%P

Sintering Temp.°C	Reading			Average (Hv)
	1	2	3	
800	261.9	221.7	152.6	212.1
900	378.7	303.5	405	362.4
1000	455	434	480	456.3
1100	732.7	534	590.7	619.1

APPENDIX J: Fe-P and Cu-P Phase Diagram



Fe-P System



Cu-P System

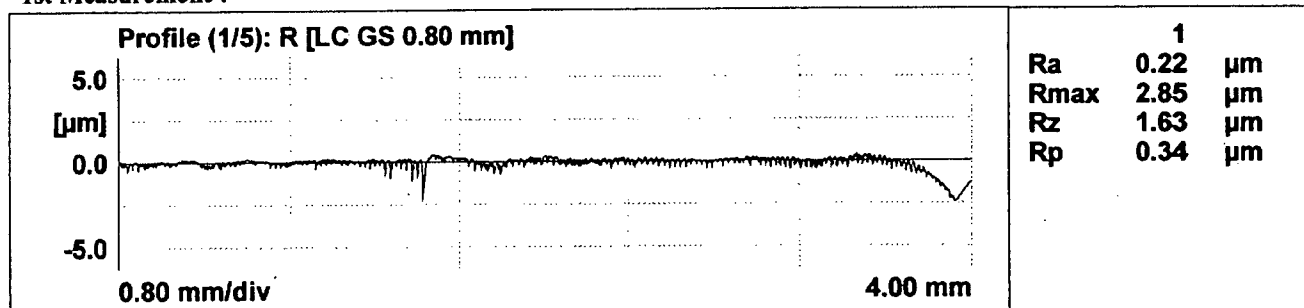
APPENDIX K: Surface Roughness Result

(1) Before Polishing Process

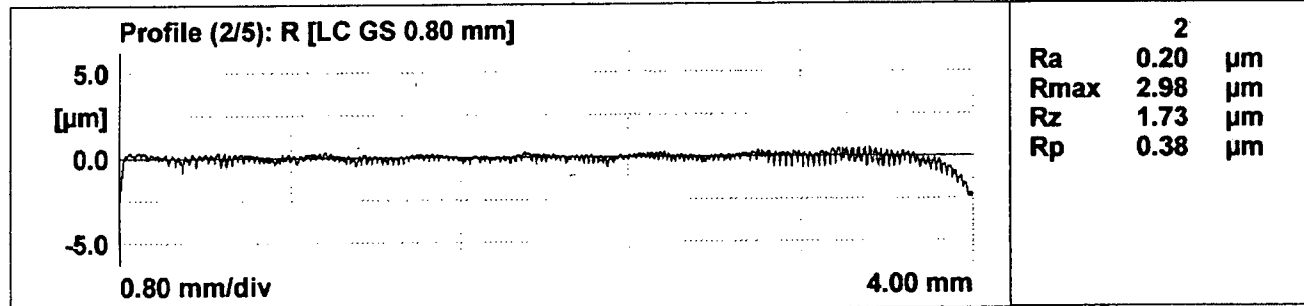


UNIVERSITI TEKNOLOGI PETRONAS Bandar Seri Iskandar, 31750 Tronoh, Perak, Darul Ridzuan.	Perthometer Concept	
Object: cast iron Number: test no 1	Remark: Pick-up: MFW-250 #2799 23,S-CAL	Inspector: sheila Date, time: 13.07.2004, 11:46

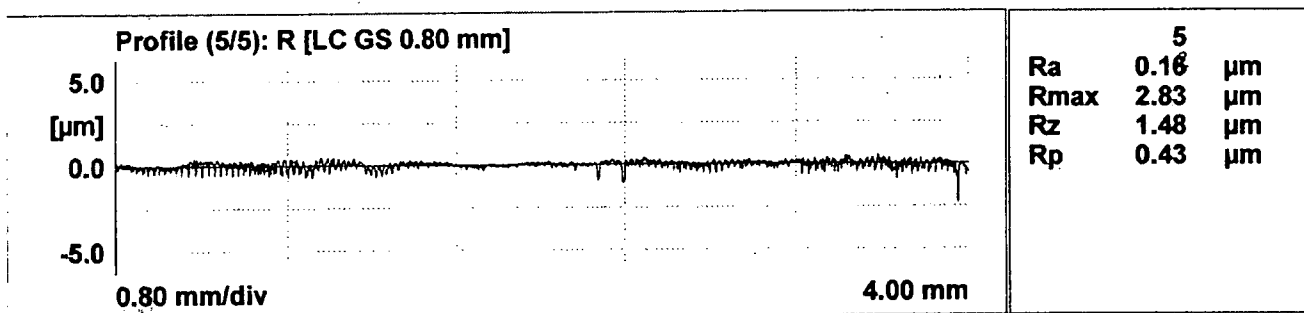
1st Measurement :



2nd Measurement :



3rd Measurement :

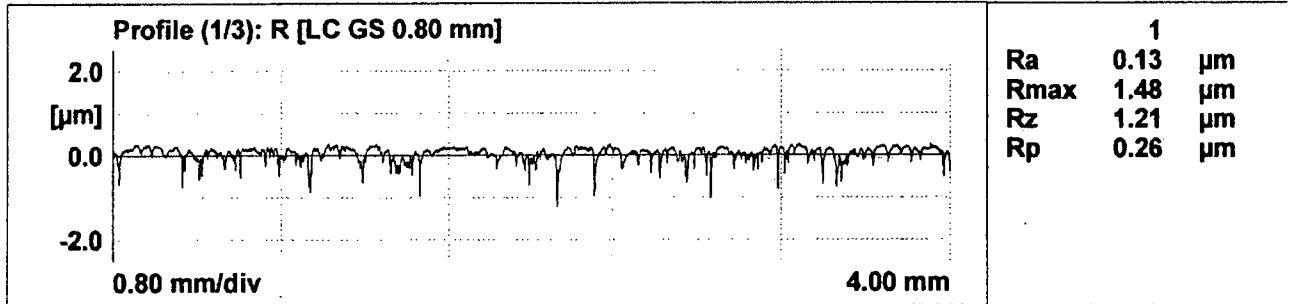


(2) After Polishing Process

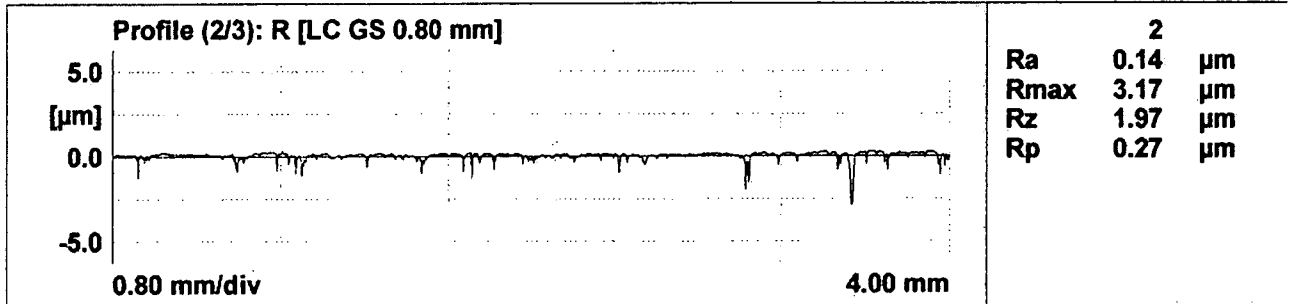


UNIVERSITI TEKNOLOGI PETRONAS Bandar Seri Iskandar, 31750 Tronoh, Perak, Darul Ridzuan.	Perthometer Concept	
Object: cast iron Number: test no 1	Remark: Pick-up: MFW-250 #2799 23,S-CAL	Inspector: sheila Date, time: 02.12.2004, 11:07

1st Measurement :



2nd Measurement :



3rd Measurement :

